Neuroanatomical Scaling, Neurotopography of Gene Expression, and Sex Chromosome Aneuploidy



P. K. Reardon
Lincoln College
University of Oxford

A thesis submitted for the degree of
Doctor of Philosophy

Trinity 2019

P. K. Reardon: *Neuroanatomical Scaling, Neurotopography of Gene Expression, and Sex Chromosome Aneuploidy*

Abstract

The publication of topographically-defined, whole-transcriptome quantifications in the human brain has created the opportunity to mine the association of imaging findings with genetic data. An increasingly popular analysis is to connect groupwise anatomical differences in imaging space with differential expression of genes as defined by their topographical expression across the cortical mantle.

This thesis uses this approach to address two problems in neuroimaging: 1) total brain size normalization and 2) association of anatomical changes with gene expression in health.

The thesis begins by examining surface area scaling in the cortex and subcortex. It describes the regions of non-linear surface area scaling in both compartments — and claims those foci of non-linear scaling may pose challenges for the analysis of disease.

Next, the thesis considers the biological meaning of surface area scaling in the cortex by comparing regions of non-linear scaling to known maps of developmental and evolutionary expansion — among others. A spatially sensitive bootstrapping procedure is introduced to quantify similarity or disimilarity amongst cortical maps.

Lastly, this thesis applies a scaling-sensitive normalization framework for total brain size differences in the analysis of a neurogenetic disease cohort. In particular, scaling-sensitive analysis of the striatum, thalamus, and globus pallidus in Sex Chromosome Aneuploidy results in increased specificity for disease specific anatomical changes in both nucleus volume and shape.

Publications

Chapters 2, 3, and 4 are published as

> *Reardon, P. K., Jakob Seidlitz, Simon Vandekar, Siyuan Liu, Raihaan Patel, Min Tae M. Park, Aaron Alexander-Bloch, et al. "Normative Brain Size Variation and Brain Shape Diversity in Humans." Science 360, no. 6394 (June 15, 2018): 1222–27.* `https://doi.org/10.1126/science.aar2578`.

and

> *Reardon, Paul K., Simon N. Vandekar, Siyuan Liu, Raihaan Patel, Min Tae M. Park, Aaron Alexander-Bloch, Jakob Seidlitz, et al. "Normative Brain Size Variation and the Remodeling of Brain Shape in Humans." BioRxiv, October 19, 2017, 205930.* `https://doi.org/10.1101/205930`.

Chapters 2, 5, 6 are published as

> *Reardon, Paul Kirkpatrick, Liv Clasen, Jay N. Giedd, Jonathan Blumenthal, Jason P. Lerch, M. Mallar Chakravarty, and Armin Raznahan. "An Allometric Analysis of Sex and Sex Chromosome Dosage Effects on Subcortical Anatomy in Humans." The Journal of Neuroscience 36, no. 8 (February 24, 2016): 2438–48.* `https://doi.org/10.1523/JNEUROSCI.3195-15.2016`.

Contents

1 Introduction **10**

1.1 Scope and Aims 10
1.2 Neuroanatomy and Brain Parcellation: Historical Antecedents 15
1.3 sMRI Data Acquisition and Brain Parcellation 16
1.4 Linear Registration, Single Atlas and Multi-atlas Nonlinear Registration, and Groupwise Statistical Analysis of sMRI Data 19
1.5 Normative Scaling of the Cortex 20
1.6 Normative Scaling of the Subcortex: Application to Neuroanatomical Sex Differences and Biomarkers 22
1.7 Testing for Brain Size Effects in Neurogenetic Disorders: Scaling as Normalization Strategy 25
1.8 Roadmap 26

2 Materials and Methods **28**

2.1 Participant Recruitment and Acquisition of Brain Structural Magnetic Resonance Images 28
2.2 Cortical Morphometry of PNC and NIH Data in CIVET . . . 38
2.3 Subcortical Morphometry for SCA, PNC, and NIH Cohorts in MAGeT Brain 40
2.4 Deriving Vertex-Level Estimates of Cortical Area Scaling by Log-Log Regression 43
2.5 Deriving Estimates of Subcortical Structure Volumetric Scaling by Log-Log Regression 46
2.6 Disruption of the PNC Cortical Scaling Map by Sample Permutation 48
2.7 Reproducibility of Cortical Scaling in a Third Cohort Using Different Imaging Processing Software 49
2.8 Aligning Cortical Maps to the CIVET Template Surface . . . 50

2.9 Cortical Area Expansion in Evolution 50
2.10 Cortical Area Expansion in Development 52
2.11 Cortical Parcellation into 7 and 17 Functional Connectivity Networks Based on Resting State Functional MRI (rsFMRI) . 52
2.12 Cortical Parcellation into the 7 Cytoarchitectonically Distinct "Types" of von Economo 53
2.13 Arterial Spin Labeling (ASL) Map of Resting State Blood Flow 53
2.14 Positron Emission Tomography (PET) Map of Resting State Glucose Utilization 54
2.15 Spatial Permutation Tests for Alignment Between Comparison Cortical Maps and Scaling Maps in PNC and NIH Samples . . 54
2.16 Categorical Comparison Maps 56
2.17 Comparison of Scaling Maps to Gradients of Cortical Gene Expression in the Adult Human Brain 57
2.17.1 Preprocessing of Allen Institute Gene Expression Data from Human Brain Tissue 57
2.17.2 Assigning Scaling Indices to Allen Atlas Brain Samples 58
2.17.3 Quantifying Associations Between Gene Expression and Neuroanatomical Scaling 58
2.18 Gene Ontology Enrichment Analyses 61
2.19 Deriving Vertex-Level Estimates of Subcortical Area Scaling . 62

3 Normative Areal Scaling 64
3.1 Abstract 64
3.2 Discovery/Replication Study Design 65
3.3 Surface Area Scaling in the Cortex 71
3.4 Surface Area Scaling Across 5 Subcortical Nuclei 80

4 Significance of Areal Scaling 83
4.1 Abstract 83
4.2 Scaling and Evolution and Development 84
4.3 Scaling and Functional Networks and Cytoarchitecture 84
4.4 Scaling, Genetics, and Metabolism 92

5 Scaling, Sex Differences, and Sex Chromosome Aneuploidy: Subcortical Volumes 99
5.1 Abstract 99
5.2 Sample Characteristics 100
5.3 Statistical Modeling of Scaling, Sex, and Chromosome Dosage Effects on Subcortical Structure Volume 103
5.4 Allometry of Subcortical Volumes 111

6 Scaling, Sex Differences, and Sex Chromosome Aneuploidy: Subcortical Surface Area 118
6.1 Abstract . . . 118
6.2 Statistical Modeling of Scaling, Sex, and Chromosome Dosage Effects on Subcortical Structure Shape . . . 119
6.2.1 Allometry of Subcortical Shape . . . 121
6.3 Sex and Sex Chromosome Dosage Effects on Subcortical Shape 122
6.4 Allometry of Subcortical Shape . . . 128
6.5 Sex and Sex Chromosome Effects on Local Subcortical Anatomy . . . 130

7 Limitations and Future Directions for Imaging-Genetics in Neuroimaging 135
7.1 Cortical Scaling . . . 137
7.2 Subcortical Scaling in Disease . . . 139
7.2.1 Subcortical Surface Area in Disease . . . 142
7.2.2 Allometry of Subcortical Shape in Sex Chromosome Aneuploidy . . . 144
7.3 Last Thoughts . . . 145

List of Figures

1.1 Citation of Brodmann's Collective Work 17

2.1 Histogram of Participant Age in the Philadelphia Neurodevelopmental Cohort 31
2.2 Dot and Line Plot of sMRI Scan Distribution for Each Participant in the NIH Cohort 34

3.1 Histogram of Participant Age in the Philadelphia Neurodevelopmental Cohort 67
3.2 Dot and Line Plot of sMRI Scan Distribution for Each Participant in the NIH Cohort 69
3.3 Cortical Map of Surface Area Scaling 72
3.4 Permutation Test for Spatial Similarity of Scaling between NIH and PNC cohorts 75
3.5 Regions of Categorical Positive and Negative Surface Area Scaling in the Human Brain 76
3.6 Overlap between Maps 77
3.7 Scaling in Human Connectome Project 78
3.8 Permutation Test for Spatial Similarity of Scaling between HCP Cohort at Different Smoothing Kernels and NIH and PNC cohorts 79
3.9 Subcortical Scaling in Amygdala, Globus Pallidus, Hippocampus, Striatum, and Thalamus 82

4.1 Positive Scaling vs Evolutionary Surface Area Changes 85
4.2 Permutation Testing for Overlap Between Positive Scaling and Evolutionary Expansion 86
4.3 Positive Scaling vs Developmental Surface Area Changes . . . 87
4.4 Permutation Testing for Overlap Between Positive Scaling and Developmental Expansion 88
4.5 Positive and Negative Scaling Overlap with Functional Regions 90

4.6 Positive and Negative Scaling Overlap with Cytoarchitectonic Classes . . . 91
4.7 Computational Linking of Scaling Metrics with Gene Expression in the Allan Institute for Brain Science Microarray Gene Expression Atlas . . . 93
4.8 Semantic Plot of GO Cellular Component Terms Enriched amongst Genes Differentially Expressed in regions of Positive Scaling . . . 94
4.9 Overlap of Positive Scaling with Blood Flow and Glucose Uptake 95
4.10 Permutation Testing for Overlap Between Positive Scaling and Blood Flow . . . 96
4.11 Permutation Testing for Overlap Between Positive Scaling and Glucose Uptake . . . 97

5.1 Nucleus Volumes In Core Sample . . . 107
5.2 Subcortical Nuclei Volumes across Aneuploidy Karyotypes vs Individuals with XY 23^{rd} Comment Chromosome Complement 108
5.3 Subcortical Nuclei Volumes across Aneuploidy Karyotypes vs Individuals with XX 23^{rd} Comment Chromosome Complement 109
5.4 Normative Globus Pallidus Scaling and the Effect of Sex Chromosome Aneuploidy . . . 113
5.5 Normative Striatum Scaling and the Effect of Sex Chromosome Aneuploidy . . . 114
5.6 Normative Thalamus Scaling and the Effect of Sex Chromosome Aneuploidy . . . 115

6.1 Normative Sex Differences in Striatal, Pallidal and Thalamic Shape . . . 123
6.2 Normative Sex Differences Accounting for Allometry . . . 125
6.3 Sex Chromosome Dosage Effects on Striatal, Pallidal and Thalamic Shape . . . 126
6.4 Point Range Plot of Surface Area for Each Domain by SCA Group . . . 127
6.5 Regional Allometry of Subcortical Shape by K-means Clusters 132

List of Tables

1.1 Volumetric Normalization for Subcortical Volumes 24

2.1 Demographics of Philadelphia Neurodevelopmental Cohort . . 30
2.2 Demographics of National Institutes of Health Cohort 33
2.3 Demographics of the Human Connectome Project 36
2.4 Demographics of AIBS Gene Expression Cohort 60

3.1 Demographics of Philadelphia Neurodevelopmental Cohort . . 66
3.2 Demographics of National Institutes of Health Cohort 68
3.3 Demographics of the Human Connectome Project 70
3.4 Cortical Asymmetry of Area Scaling Across Cohorts 73
3.5 Scaling Correlation Across Datasets and Permutations 74

5.1 Demographics of Sex Chromosome Aneuploidy Cohort, Age Matched Controls, and Independent Normative Scaling Cohort 101
5.2 Tanner-Marshall Sexual Maturity Stages 102
5.3 Normative scaling of subcortical volumes in health 112
5.4 Comparing different methods of controlling for brain size in analysis of subcortical volume 117

6.1 Standardized Residuals for Vertex Counts in Each Pairing of Structure and K-means Cluster 129
6.2 Scaling of Regional Subcortical Area with Overall Structure Size in Health 131

Chapter 1

Introduction

1.1 Scope and Aims

To identify a biomarker of a disease or a phenotype, a robust normative framework for biological variation must first be established. In the case of developmental neuropsychiatric disease, structural MRI (sMRI) has emerged as one of the key modalities for establishing the normative framework for evaluating for the growth and maturation of neuroanatomy. sMRI is uniquely amenable to wide application in adult and pediatric cohorts because it enables the non-invasive acquisition of 3D neuroanatomical data without exposing research participants to harmful radiation. Since its wide adoption by neuroscientists in the late 1980s, structural MRI has revived the study of brain parcellation, a prerequisite for the localization and quantification of the size and shape of brain regions with respect to their role in normative behavior and in neuropsychiatric disease. In the endeavor to identify a neuroanatomical biomarker that could allow clinicians to predict disease

onset or treatment response, neuroimaging researchers have begun to pose questions about whether and by what means the relative shape and size of neuroanatomical regions may serve as suitable biomarkers for disease or developmental stage. Such questions about the role that the relative size and shape of a particular neuroanatomical compartment may play in behavior were first posed by evolutionary biologists at the turn of the twentieth century. It is no surprise then that many of the foundational assumptions of neuroimaging work may actually be traced back to anatomists and cytologists working in England, France and Germany at the turn of the twentieth century. This thesis argues that the identification of a suitably specific and robust anatomical biomarker from sMRI data requires the revival of an idea crucial to the work of these earlier biologists predating the development of molecular biology: allometry or non-linear scaling.

Consequently, this introduction briefly introduces the intellectual environment from which the concept of allometry arose before situating it in its modern context by sketching a brief history of anatomic and cytoarchitectonic brain parcellation by histological examination and homology inference. This will also set the stage to approach the technical considerations underpinning current sMRI data acquisition and analysis strategies, which give rise to the first of many questions of quantitative neuroanatomical data normalization that motivate this work. While sMRI data acquisition relies on the magnetic resonance of hydrogen atoms in mixed tissues, it is really only the processed signal generated from magnetic resonance that neuroanatomical biomarkers may be derived from. This signal is used to refine the anatomical parcellations first introduced by Korbinian Broadmann and Constantin Von

Economo (among others) from the turn of the twentieth century by detecting imaging-based signatures of connectivity, microstructure and function that divide cortical areas into biologically meaningful units. It is in the context of our capability to identify and compare brains in an abstracted imaging space that allows practitioners in the field to attempt a more granular dissection of the differential microstructure, connectivity, and differential metabolic and hemodynamic activity of the human brain.

Equipped with the analytical tools to identify brain regions within an sMRI scan and compare brain regions across many subjects, neuroimagers have generated normative trajectories of cortical and subcortical development. Most strikingly, it has emerged that neurodevelopment of the cortex proceeds in two stages: the growth of grey matter (a term from gross anatomy denoting those tissues comprised primarily by non-myelinated cells and cell bodies) in childhood followed by pruning and reduction in grey matter in adolescence through early adulthood [1]. Moreover, it is becoming clear that typical males and females exhibit different neurodevelopmental trajectories and proportional subcortical structure size. At first blush, this is an encouraging place for the field of anatomical neuroimaging to be. The epidemiology of neurodevelopmental disease differs strikingly between males and females, and the identification of robust and replicable neuroanatomical sex differences in development could presage the identification of anatomical biomarkers for conditions such as autism or specific language impairment. Since there are sex differences in neurological disease incidence, two premises underlying population-based studies of neuroanatomical sex difference are that 1) testing for and identifying sexually divergent sources of variation in

brain anatomy will enable the identification of a more bespoke neuroanatomical biomarker accounting for sex and 2) there is an underlying neurobiological difference predisposing individuals with an XY 23^{rd} chromosomal pair to diseases with an increased incidence among study participants with similar sex chromosome complements and vice versa. Many questions necessarily and appropriately should dampen enthusiasm for the second of these two. Most importantly, it is unclear to what extent different environmental factors may contribute to these anatomical differences such as rearing, socialization practices, and socioeconomic status — among others. But even bracketing the diverse questions that fall under that remit, there remains a striking lack of scholarly consensus on sex differences in neuroanatomy — particularly in subcortical nuclei, such as the striatum, which play a pivotal role in diverse neuropsychiatric diseases from Attention Deficit Hyperactivity Disorder to Schizophrenia.

This thesis claims that this lack of consensus is due to the fact that there is no robust normative framework for assessing the relative size of subcortical nuclei and cortical areas that adequately allows for their quantitative comparison unaffected by other anatomical confounders. To pose the question at the heart of this work directly, how much does the variation in overall brain volume between demographic or clinical groups constrain the variation of neuroanatomical regions? For example, the normative 20% size difference between individuals with a 23^{rd} chromosome complement of XY and XX distorts the identification of replicable demographic regionally defined neuroanatomical biomarkers of sex chromosome complement. This source of distortion is also present in comparisons between clinical cohorts who pre-

dictably exhibit reductions in overall brain volume.

To address and remove this distortion obscuring potential neuroanatomical biomarker identification, the relationship between overall brain volume and its regional parcellation in the cortex and subcortex is examined in this thesis through the analytic framework of structural scaling. In particular, this thesis argues that regions where nonlinear scaling — allometry for short — is evident will be uniquely difficult candidates for the reproducible identification of disease biomarkers. Of historical note, the concept of allometry was first introduced to the analysis of biological form by Galileo Gallilei in the first of his *Dialogues Concerning the Two New Sciences*. It is a quirk of history that his second new science was the study of objects falling through space [2]. The roadmap to come is this: first the galileian framework of allometry is leveraged to address the most fundamental question of this thesis: how certain areas of the cortical sheet and subcortical nuclei shift as total brain size varies. Second, this non-linear scaling informed normative framework will be used to show how accounting for such global size variation enables better normalization in the context of volumetric and morphometric analysis of striatal, pallidal, and thalamic nuclei in a neurogenetic disorder to increase specificity in the identification of potential neuroanatomical sex differences and disease-specific biomarkers.

1.2 Neuroanatomy and Brain Parcellation: Historical Antecedents

To localize a functional component of the brain, a map of its regions must first be established. A territory cannot be identified unless its borders are drawn. At the turn of the 20th century and in the wake of German Idealism and Darwin, psychologists in Berlin and Jena were dedicated to describing a purported common anatomical archetype that the mammalian brain instantiates — what was later termed the *Bauplan* [3]. This research program attempted to identify functional constituents of anatomy with reference to an idealized form or shape of the anatomy of a species, which under the influence of Erns Haeckel in Jena focused on the relationship between the development of an individual *in utero* and the evolution of a species' form — leading to the striking, though subsequently disproved *biogenetic law*: ontogeny recapitulates phylogeny [4, 5, 6].

This environment gave rise to the first modern anatomical brain parcellation, created by one of Haeckel's students, Korbinian Brodmann, who drew the boundaries for cortical regions and layers based on these ideas of the shared idealistic anatomical blueprint guiding the evolution and development of the mammalian brain, which were later fromalized on the more palatable and Darwinian notion of anatomical and evolutionary homology [6, 7, 8, 9]. Brodmann's work encompassed histological comparison of 64 vertebrate species and yielded the modern heuristic that the human cortex consists of 6 histologically and hodologically defined layers with unique cellular composition and connectivity. The 52 territories or regional areas

that he identified in the cortex were defined by the distribution of cell types across homologous regions amongst the species included in his study. The Brodmann map, consequently, synthesized both histological and evolutionary data to infer meaningful biological compartments, regions, and layers in the cortical sheet. These Brodmann areas are still used in functional and structural MRI studies in human. His evolutionarily informed cytological approach to identifying cortical regions was later further refined by Constantin von Economo [10, 11], which parcellated the cortex into lobes, regions, and layers, defined by their cytological appearance and histologically-assayed cell type composition.

1.3 sMRI Data Acquisition and Brain Parcellation

The cortical areas and subcortical nuclei identified by Brodmann, von Economo, amongst others, were used to create reference atlases defining the regional anatomy of the cortex that would later guide neuropathologists in the identification and pathological examination of patient brains *post mortem*. Later with the broad adoption of imaging modalities to visualize neuroanatomy, these parcellations were used to identify, compare, and evaluate brain anatomy in research and clinical contexts *in vivo*. Citations of Brodmann and von Economo's work spikes drastically with the introduction of these imaging modalities to neuroscience, Fig 1.1.

Their work serves as the bedrock for understanding the images produced

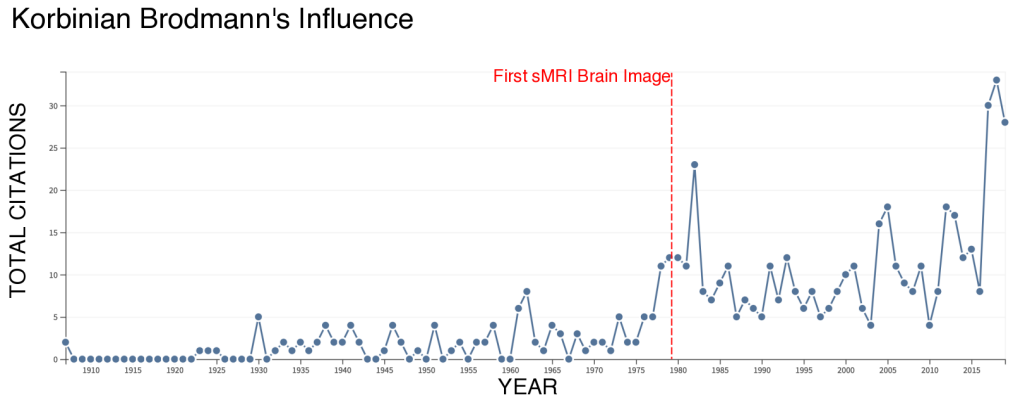


Figure 1.1: **Citation of Brodmann's Collective Work**. Annual total sum of citation of Korbinian Brodmann's work. Source: Web of Science

by sMRI; however, many cortical areas defined by these initial efforts do not follow the large scale features produced by an sMRI scan. Magnetic Resonance Imaging developed out of the discovery of nuclear magnetic resonance. When this technique is applied to tissue classification for brain imaging, the relative molecular environment of hydrogen atoms determines a unique signal that may be associated with a tissue type such as blood, fat, or brain parenchyma [12].

The quantification of regional neuroanatomical structure volume or shape within a single MRI image requires that the region assessed be identified reliably. The gold standard for region identification in structural MRI is manual delineation by trained expert neuroanatomists or neuroradiologists [13, 14, 15, 16]. However, this method has three drawbacks. First, it is labor intensive and not tractable for the analysis of large cohorts. It is estimated that manual segmentation of an unlabeled structural magnetic resonance image of a single human brain at 1mm cubed resolution may normally take between two days to three weeks [14, 17]. Second, each anatomist brings a unique set of biases based on his or her unique training to the task, and thus the manual annotation of an sMRI image will result in inconsistent borders of a region of interest being hand drawn in serial imaging sections by reference to these atlases. Lastly, a given manual annotator will not label every scan consistently as a result of normal human error. Nevertheless, should a hypothesis-driven imaging study of a region be undertaken, the reliability of labels generated by an anatomist tasked with identifying the study's region of interest in all MRI scans is best validated against both the labelling practices of other anatomists and against labels generated by the

first anatomist at several time points [18].

1.4 Linear Registration, Single Atlas and Multi-atlas Nonlinear Registration, and Group-wise Statistical Analysis of sMRI Data

Once the reliability of anatomical annotations for regions identified within participant scans is established, the volume or surface area of the region may be quantified with reference to the expert label linking an anatomical structure from sMRI data to the established anatomical feature in a reference atlas. Linking the features in an sMRI scan with a label in a neuroanatomical atlas requires that the raw scan be situated in the same orientation and with the same coordinates as that atlas. There are several basic factors that need to be corrected for to align sMRI scans with an atlas, which are addressed through a set of computational steps referred to as linear registration. In the process of sMRI data acquisition, the raw brain scan may contain inter-subject differences in the angular orientation of the brain in the axial plane of the scan (more colloquially referred to as head tilt) and differences in the brain's coordinate location or placement within the volume captured by the scan [15, 19].

Comparing the anatomy of multiple participants in a groupwise analysis of demographic or clinical characteristics in this regime depends not only on aligning these scans with an atlas but also on ensuring that each brain is suitably aligned with each other. This is a two step process of image reg-

istration. Large population level and consortia-based MRI studies leverage data gathered from patient and demographic cohorts based on thousands of scans. Manual annotation in this context would be prohibitive and potentially misleading due to inconsistent labeling. Thus, large scale studies of anatomy have turned to software-based registration and parcellation algorithms for the automatic identification and normalization of neuroanatomy. For the data presented in this thesis, collected by the Children's Hospital of Pennsylvania and the National Institute of Mental Health, sMRI brain images were registered and parcellated using two distinct automated methods, which represent the vanguard in this field. Cortical anatomy was automatically processed using Civet 1.1.0, which uses a single atlas for linear registration and a sample pool derived average for the non-linear registration template. Subcortical anatomy from 5 subcortical nuclei were processed using MAGeT, which relies on a multi-atlas model and a sample pool derived label-fusion method for the non-linear registration.

1.5 Normative Scaling of the Cortex

Allometry as a conceptual tool was first appreciated and applied by comparative anatomists. The variation in mean brain volume amongst animal species allows for the description of scaling relationships between brain regions and total brain structure. This framework was adopted in comparative morphology at the beginning of the 20th century to describe the non-linear proportional dynamics of regional structure size in evolution [20, 21, 22]. The brain's component parts may scale with global brain size across species

in three ways [23]. In the simplest relationship, total and focal brain size increase in lockstep with each other at a ratio of one-to-one. However, constituent parts of the brain may also outstrip total expansion — resulting in proportional size expansion relative to total brain size — or regions may fail to increase in proportion to global brain size — resulting in proportional size reduction. While these scaling norms have been observed across animals with varying evolutionary relationships, it is unclear whether similar scaling laws hold amongst humans as brain size varies in health and disease.

Beginning the analysis of human brain scaling with the cortex, it is unknown how an increase in total cortical surface area accrues from focal areal changes. This open question in brain morphology has profound consequences for neuroimaging practice. In demographic studies of development or sex differences in anatomy, neuroimaging practice commonly ascribes a uniform contribution of regional areal size to total brain structure [24, 25, 26, 27]. Consequently, the first step in assessing scaling relationships in the cortex is to test for sex-specific, dynamic, and nonlinear relationships between focal and total surface area in adulthood and throughout the development of the human cortex.

This thesis shows that the relationships amongst local cortical regions and total cortical surface area emerges by 5 years of age, remains stable throughout development and maturity, and holds similarly for both sexes. In the cortex, the distribution of focal regions that outstrip or fall behind global expansion overlap with regions of established functional identity, uniquely high blood flow and glucose metabolism, and evolutionary expansion within primates. The overlap of this distribution is quantified using a novel spa-

tially sensitive permutation based approach. But beyond similarity to neuroanatomical maps of diverse physiological phenomenon, this thesis also attempts to identify the molecular identity of non-linearly expanding cortical regions with reference to publicly available topographically defined gene expression data. To investigate the genetic associations of regional surface area expansion, this map of cortical scaling is linked to gene expression samples from the Allen Institute for Brain Science human microarray data set [28]. In a computational context, this thesis inadvertently recapitulates a strategy initiated by Brodmann at a molecular level — define regions based on their evolutionary significance and differential gene expression defined by topography.

1.6 Normative Scaling of the Subcortex: Application to Neuroanatomical Sex Differences and Biomarkers

Humans display replicable sex-differences in multiple domains of behavior, cognition, and psychopathology [29, 30, 31]. Several of these domains are subserved by distributed neural systems involving both cortical and subcortical structures [32, 33, 34]. Although advances in structural neuroimaging have been leveraged to map sex differences in human cortical anatomy at high spatio-temporal resolution [35, 36, 37], most studies of sex differences in subcortical anatomy have examined bulk volumes rather than fine-mapping anatomical variation within each nucleus [38, 39, 40, 41, 42, 43].

The mean volume of the brain differs by 20% between men and women [1]. Consequently, scaling would dramatically affect focal neuroanatomical contrasts. This emphasis on scaling — and appreciation of its nonlinear features — is a departure from the current neuroimaging practice. An unstated null hypothesis in the field is that regional structure size contributes uniformly to total brain size and current normalization strategies are guided by this assumption. For example, the practice in studies of pathology is to identify focal cortical contrasts between subjects or groups only after uniform correction for their total brain size differences through linear regression or by normalization by expressing regional measurements as a proportion of brain size [24, 25, 26, 27]. Differentiating and elucidating disease-specific biomarkers requires a robust descriptive understanding of the interdependence between focal and global neuroanatomy. To date, no consensus guidance exists as to whether regression or normalization by proportion is the best way to account for global brain size on regional morphology in disease or demographic studies. Furthermore, the current normalization methods assume the relationship between global and local morphology remains stable between groups with frank differences in overall size in both demographic cohorts (e.g. males and females) and clinical cohorts (patients and controls).

We show that the globus pallidus, thalamus, and striatum scale sublinearly with total brain volume — mirroring known relationships between subcortical volume and total brain volume amongst species [23]. Traditional correction or normalization methods for normative differences in total brain volume assume linear scaling and can therefore invert or exaggerate sex effects on subcortical anatomy for these three structures 1.1.

	XY vs XX
	XY
STRIATUM	
Proportionalization	↓
"Nuisance"	=
Allometry	=
THALAMUS	
Proportionalization	↓
"Nuisance"	=
Allometry	=
PALLIDUM	
Proportionalization	↓
"Nuisance"	↑
Allometry	↑

Table 1.1: **Volumetric Normalization** Normalizing for total brain size with different methods will yield contradictory results for subcortical volumetric sex differences

1.7 Testing for Brain Size Effects in Neurogenetic Disorders: Scaling as Normalization Strategy

Sex chromosome complement variations represent an opportunity to address observationally the dose effect of sex chromosome genes on neuroanatomy. This provides one window in to potential biological etiologies of sex difference. In transgenic mouse studies where gonadal status and sex chromosome complement have been dissociated by relocating the *SRY* gene to a different chromosome, the presence of gonad-independent sex chromosome dosage effects on both cortical and subcortical anatomy have been detected [44, 45]. Second, neuroimaging studies in human sex chromosome aneuploidies (SCA) have established that changes in X-and Y- chromosome count can modify the anatomy of cortical regions with known subcortical projections [46, 47, 48]. To date however, it is not known if and how supernumerary sex chromosome dosage influences subcortical morphology in humans. Addressing these questions provides a preliminary foothold on our mechanistic understanding of normative sex-differences in subcortical organization, and identifies potential subcortical biomarkers for the cognitive-behavioral alterations that are associated with SCA [49]

Thus far in the field, structural neuroimaging of humans with typical and atypical sex chromosome complements has established the marked influence of sex-chromosome dosage on total brain volume and identified potential cortical substrates for the psychiatric phenotypes associated with sex chro-

mosome aneuploidy. Allometric analysis of sex chromosome aneuploidy in this thesis reveals that supernumerary X- and Y-chromosomes both cause disproportionate reductions in pallidal volume. This thesis provides a novel understanding of sex chromosome dosage effects on subcortical volumes by using normative scaling rules to normalize for overall differences in brain size. Focusing on the striatum, globus pallidus, and thalamus, large effect-size differences in the volume of all three structures are detected as a function of aneuploidy. Total brain volume effects on subcortical size are corrected for by leveraging normative scaling rules for subcortical nucleus volumes in humans, which are derive here for the first time.

The volumetric scaling laws for this analysis of subcortical volumes in sex chromosome aneuploidy are derived here with a sample of youth and adolescents with a 23^{rd} chromosome complement of either XY or XX. Because brain regions can vary in their scaling relationships with overall brain size [50], and sex chromosome aneuploidy robustly alters overall brain size [45], allometric norms are required to distinguish whether regionally-specific effects of aneuploidy on brain anatomy arise as a consequence of regional differences in scaling, or actually represent focal anatomical deviations from the norm given overall brain size differences.

1.8 Roadmap

Global brain size variation inscribes a heretofore undetected parcellation of non-linear scaling in cortical and subcortical regions. This has the consequence of inhibiting the reproducibility of putative biomarker discovery in

cases where this non-linear relationship has not been appropriately corrected for in statistical analysis. As this thesis shows, many putative biomarkers of sex difference and disease status in the samples and structures analyzed here are in fact the result of normative variations in regional structures in the context of reduced global brain size. This thesis shows this by first detecting the areas of nonlinear scaling in the cortex and subcortical structures to establish the first map of the patterning of areal scaling in the human brain. Next, this thesis applies this map to evaluate volumetric sex differences previously reported in the literature and to isolate biomarkers that distinguish the individuals with XX and XY 23^{rd} chromosome complements in the context of normative total brain volume variation. Lastly, this thesis shows that normative scaling laws are radically reorganized in subcortical areas in the context of supernumerary sex chromosome dosage.

Chapter 2

Materials and Methods

2.1 Participant Recruitment and Acquisition of Brain Structural Magnetic Resonance Images

Data from the four neuroimaging studies presented below are either publicly available or has been generously provided by collaborators.

Philadelphia Neurodevelopmental Cohort (PNC)

All participants were selected for neuroimaging plus psychiatric and cognitive assessments from a previously identified group of 50,000 subjects from the Center for Applied Genomics at the Children's Hospital of Philadelphia [51]. Participants were recruited first by mail and then by a follow-up telephone call to screen for exclusion criteria. Subjects were only enrolled in the neuroimaging study if they did not have medical problems that could impact

brain function or compromise the ability to complete the neuroimaging tasks, or implanted ferrous metal. Subject scans were excluded from this analysis if medical history additionally indicated a history of psychoactive medication or a history of psychiatric hospitalization. A T1-weighted structural magnetic resonance imaging brain scan was acquired from all participants using the same 3T Siemens TIM Trio whole-body scanner located in the Hospital of the University of Pennsylvania. Brain structural imaging was obtained using a magnetization prepared, rapid-acquisition gradient-echo (MPRAGE) sequence with echo time, 3.5 ms; repetition time, 1810 ms; inversion time, 1100 ms; flip angle 9 (DEG); acquisition matrix 192 256 160; and field of view, 180 mm. Receive coil shading was reduced by selecting the Siemens prescan normalize option, which corrects for B1 inhomogeneity based on a body coil reference scan. Scans were included in the analysis if upon visual inspection there was no evidence of motion. Sample characteristics are detailed in Table 2.1, and the associated distribution of scans by age can be seen in Figure 2.1. The institutional review boards of both the University of Pennsylvania and the Children's Hospital of Philadelphia approved all study procedures and signed informed consent and/or assent to participate in this study were obtained from the adult participants or the parents of pediatric participants respectively.

National Institutes of Health (NIH)

All participants were typically-developing individuals recruited through local advertisement. The absence of neurological or psychiatric illness was

Characteristic	All	Male	Female
Number of Individuals	1373	645	728
Race, No			
Caucasian	603	314	289
African-American	601	253	348
Other	169	78	91
Age Distribution of Scans (years)			
Mean (SD)	14.83 (3.66)	14.56 (3.67)	15.06 (3.64)
Range	8.08—23.08	8.17—23.00	8.08—23.08

Table 2.1: **Demographics of Philadelphia Neurodevelopmental Cohort**. Crossectional Cohort.

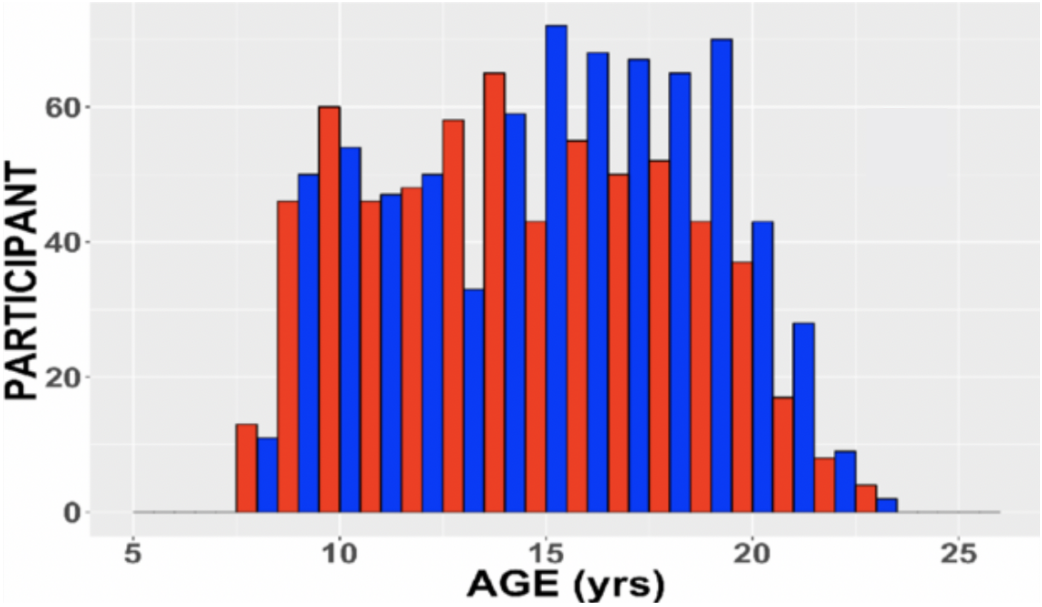


Figure 2.1: **PNC**. Histogram of Participant Age. Female participants are labeled red and male participants blue.

established through completion of a screening questionnaire (Child Behavior Checklist) [52] and clinical interview by a child psychiatrist [1]. Handedness was assessed by physical and neurological examination. All participants had a full-scale intelligence quotient (IQ) greater than 80 as estimated by age-appropriate Wechsler Intelligence Scales [53]. Socioeconomic status was quantified using Hollingshead scales [54]. Participants were invited to return at approximately 2 year intervals, resulting in an unbalanced longitudinal dataset of 792 individuals seen and scanned at a total of 1531 visits between ages 5 and 25 years. The number of scans per participant ranged from 1 to 6, with 51% of participants having 2 or more scans. At each visit T1-weighted structural magnetic resonance imaging brain scans were acquired using the same 1.5T General Electric (Milwaukee, WI) Signa scanner and a 3D spoiled gradient recalled echo sequence with echo time, 5 ms; repetition time, 24 ms; flip angle 45 (DEG); acquisition matrix, 256 x 192; axial slices, 124 x 1.5 mm and field of view, 240 mm. Scans were included in the analysis if upon visual inspection there was no evidence of motion. Sample characteristics are detailed in Table 2.2, and the associated distribution of scans by age as seen in Fig 2.2. The institutional review board of the National Institutes of Health approved the research protocol employed in this study (Clinical trial reg. no. NCT00001246, clinicaltrials.gov; NIH Annual Report Number, ZIA MH002794) and written informed consent and assent to participate in the study were obtained from parents/adult participants and children respectively.

Characteristic	All	Male	Female
Number of Individuals	792	403	389
Singleton	493	256	237
Member of twin pair	299	147	152
Right handed	673	343	330
Race, self-reported No.			
Caucasian	673	341	332
African-American	54	27	27
Asian	17	10	7
Hispanic	26	11	15
Other	22	14	8
IQ			
Mean (SD)	114.2 (12.52)	114.7 (12.90)	113.7 (12.10)
SES			
Mean (SD)	42.04 (18.93)	41.78 (19.34)	42.33 (18.59)
Number of Scans per Person			
1 scan	386	191	195
2 scans	200	103	97
3 scans	116	54	62
4 scans	59	37	22
5 scans	25	14	11
6 scans	6	4	2
Total Number of Scans	1531	801	730
Age Distribution of Scans (years)			
Mean (SD)	13.58 (4.75)	13.90 (4.75)	13.22 (4.72)
Range	5.14—25.79	5.24—25.79	5.14—25.65

Table 2.2: **National Institutes of Health Cohort**. Longitudinal Cohort.

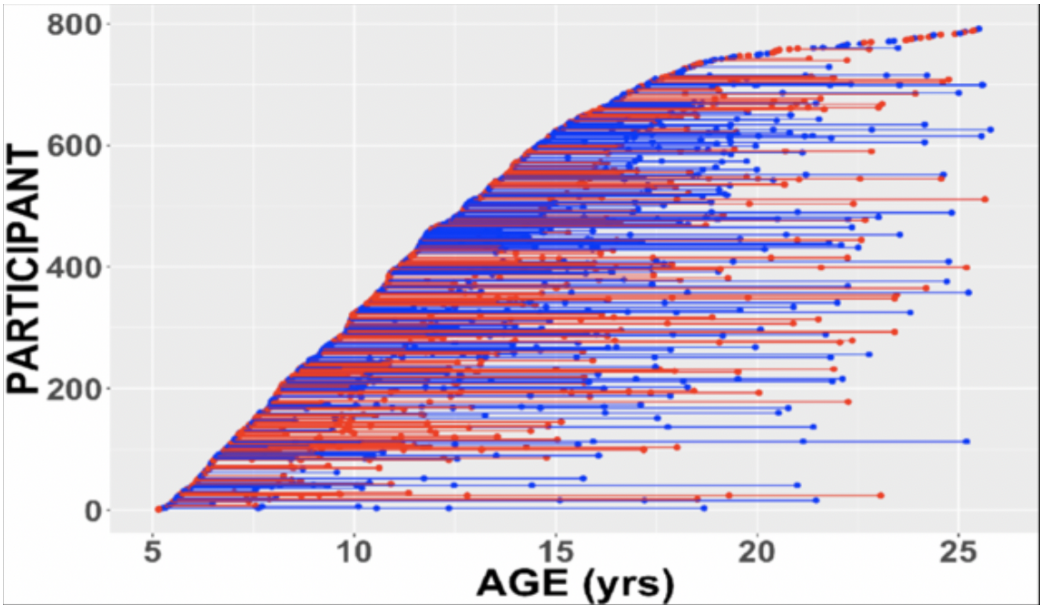


Figure 2.2: **NIH**. Dot and line plot of distribution of scans of each participant by age and sex. Female participants are labeled red and male participants blue.

Human Connectome Project (HCP)

The scans were drawn from the HCP12000 dataset (March, 2017 release). The participant pool was comprised of individuals within the Missouri Department of Health and Senior Services Bureau of Vital records who had been born in Missouri to families that included twins (Table 2.3). The absence of neurological or psychiatric illness was established through the Semi-Structured Assessment for the Genetics of Alcoholism [55].

T1-weighted structural magnetic resonance imaging brain scans were acquired from all participants using the same customized Siemens 3T 'Connectome Skyra' scanner at Washington University in St. Louis. Complete hardware and imaging protocol details can be found online at `https://www.humanconnectome.org/storage/app/media/documentation/s1200/HCP_S1200_Release_Reference_Manual.pdf`. To summarize, the scanner is equipped with a standard 32-channel Siemens receive head coil and a customized SC72 gradient insert and a body transmitter coil with 56 cm bore size (*diffusion*: Gmax= 100mTm/m, max slew rate = 91 mT/m/ms; *readout/imaging*: Gmaz = 42 mT/m, max slew rate = 200 mT/m/ms). The Skyra used to collect this data employed the standard set of Siemens shim coils. The customized Skyra included a gradient coil and gradient power amplifiers that together increase the maximum gradient strength from 40 mT/m to 100 mT/m. The T1-weighted structural scan was acquired using a magnetization prepared, rapid-acquisition gradient echo (MPRAGE) sequence with echo time, 2.14 ms; repetition time, 2400 ms; inversion time 1000 ms; flip angle 8 (DEG); field of view 224mm; acquisition matrix 320,

Characteristic	All	Male	Female
Number of Individuals	1113	507	606
Age Bins (years)			
22 — 25	231	147	84
26 — 30	486	221	265
31 — 35	383	135	248
36 and above	13	4	9

Table 2.3: **Human Connectome Project**. Adult Crossectional Cohort.

with 256 sagittal slices in a single slab.

Sex Chromosome Aneuploidy Sample

Sex chromosome aneuploidy groups were recruited through advertisements via the NIH Web site and parent-support groups across North America. To be included in the study, participants must have had an X-/Y- aneuploidy and not have ever had a head injury or condition that would result in gross brain abnormalities. All participants with aneuploidy were non-mosaic as assessed through peripheral blood smear and metaphase spread. Typically developing participants were all singletons recruited from the United States of America and enrolled in an ongoing longitudinal study of typical brain development [36] Inclusionary criteria for healthy participants included never having required special education services, taken psychiatric medications, received mental health treatment, or having had any medical condition impacting the nervous system.

Tests for Effects of Demographic, Pubertal and Cognitive Factors in SCA Sample

For all analyses of sex chromosome dosage effects on subcortical anatomy within our core sample, additional models were used to confirm the robustness of our findings to inclusion of social economic status as a covariate. IQ was not included in analyses of sex chromosome aneuploidy effects because (i) IQ reductions are central to the sex chromosome aneuploidy phenotype, and (ii) inclusion of IQ as a nuisance variable in regression analyses assumes

the presence of a linear relationship between IQ and brain anatomy that is invariant across karyotype groups.

Within our non-overlapping normative sample, additional models were run to confirm robustness of all reported sex differences in subcortical allometry to inclusion of Tanner stage, IQ and socioeconomic status (SES) as covariates.

2.2 Cortical Morphometry of PNC and NIH Data in CIVET

Total and vertex-wise estimates of cortical surface area were generated for all PNC and NIH scans using the automated CIVET pipeline (version 1.1.10; Montreal Neurological Institute at McGill University, Montreal, Quebec, Canada) [56]. First, scans are corrected for radiofrequency intensity non-uniformities and then undergo spatial normalization and registration to the stereotaxic space defined by the ICBM 152 template [15, 57]. After these two preprocessing steps, voxels from a scan are classified as designating grey matter, white matter, and cerebrospinal fluid. After tissue segmentation, the cortical surface for each hemisphere is constructed in several iterations of deformation and subsampling of the surface. Initially, the surfaces are approximated with 320 vertices. In the last step, the mesh representing each hemisphere contains 40,962 vertices. At this vertex density, intervertex distance is 1 mm, which is equivalent to the sampling of the image [58, 59]. While this deformation algorithm *a priori* guarantees that the ith vertex in

one scan is equivalent to the ith vertex in every other scan in the study, there is no evidence to support that there is any anatomical basis to this correspondence. The paper introducing the CIVET-CLASP algorithm ([59]) provides observational but unquantified data that the spatial registration and normalization steps preceding cortical reconstruction ([15]), 'effectively enforces [sic] a relatively consistent placement of points on the cortical surface... However, this loose homology may be useful when dealing with averages of a large number of data sets...' [59]. Potentially, a combination of blurring kernel application and re-sampling and re-registering subject level measurements on to the model surface ensures inter-subject vertex homology for group-wise statistical testing, but this should be examined and stated explicitly. This step is made explicit in the Human Connectome Project's surface area software pipeline estimation [60], whose surface area scaling estimates converge with those derived from the CIVET pipeline. The surface area for each vertex was computed by estimating the area of a triangle formed by three vertices on the surface mesh and attributing a third of this area to each vertex [61]. Note that the total vertex count of 40962 in each hemisphere includes 2357 vertices (5%) that lie within a non-cortical "medial wall", and are not included in analyses. Estimates of vertex surface area were smoothed with a 20 mm full-width-half-max (FWHM) surface kernel. This FWHM departs from the historical CIVET default value of 40 mm [61] but aligns with current standards: 20 mm is the mean FWHM smoothing kernel used for vertex-level surface area analyses across studies from the two other large scale developmental neuroimaging cohorts besides those included in our own study [62, 63]. It is important to note however that there are no univer-

sally optimal methods for selection of smoothing kernel size. In particular, while signal processing theory predicts that the ideal kernel size for signal detection should match the intrinsic smoothness of the signal to be detected, this intrinsic smoothness is typically not known a priori, and is also likely to vary across different biological questions, morphometric properties and cortical regions. Furthermore, the effective level of smoothing achieved by a given FWHM can vary across the cortical sheet for a fixed FWHM because the accuracy of inter-subject surface alignment is greater in regions of low vs. high population-level folding variability. Total cortical surface area was calculated by summation of all constituent vertices in the cortical mesh. The CIVET pipeline also provides an estimate of total brain tissue volume as the sum of gray and white matter voxel volumes, based on tissue segmentation using a validated neural net approach to voxel tissue class classification [64].

2.3 Subcortical Morphometry for SCA, PNC, and NIH Cohorts in MAGeT Brain

Total and vertex-wise estimates of surface area (SA) were generated for the thalamus, pallidum, striatum, hippocampus, and amygdala in all NIH and PNC scans using the automated MAGeT Brain Morphology pipeline (https://github.com/CobraLab/MAGeTbrain) [65, 66]. Scans are first corrected for radiofrequency intensity non-uniformities and then registered to the ICBM152 template for estimation of brain masks and data cropping to a bounding box. The mask and bounding box for the image is then transformed

back to native space. All subsequent processing is done to the corrected and masked images in native space. For the striatum, thalamus, and pallidum, the MAGeT morphology pipeline creates automated segmentations using a single atlas for 21 randomly selected participants within each sample. The single atlas was created using a three-dimensional reconstruction of serial histological data and warped to a high-resolution and contrast MRI based on the average of 27 MRIs of the same individual [67]. The 21 participants were uniformly drawn from even quartiles of the age range of the participants in the normative sample. The resulting study-specific library for the segmentation of the striatum, thalamus, and globus pallidus consists of 21 segmentations (1 atlas x 21 templates). These segmentations are used to label each scan in the final segmentation, which was determined by label fusion using a voxel-wise majority vote [65].

Separately for the hippocampus and amygdala, the MAGeT morphology pipeline creates automated segmentations using a set of 5 high-resolution in vivo atlases for 21 randomly selected participants within each sample. The same 21 participants used for the segmentation of the striatum, thalamus, and globus pallidus were used to create the study-specific library for the final hippocampus and amygdala segmentation. The 5 reference atlases for the hippocampus and amygdala segmentations were generated from high resolution and high contrast T1 and T2 weighted image volumes from 2 males and 3 females using a 3 T scanner with final super-sampled isotropic voxel dimensions of 0.3 mm. The resulting study-specific library for hippocampal and amygdalar segmentation therefore consists of 105 segmentations (5 atlases x 21 templates). With respect to the morphological quantification of

the hippocampus and amygdala, each scan within our dataset was labeled using all 105 segmentations within the study-specific library, and the final segmentation was determined by label fusion using a voxel-wise majority vote.

Surface-based representations of the striatum, thalamus, pallidum, hippocampus, and amygdala are defined on their respective input atlases and were estimated using the marching cubes algorithm. Next, the nonlinear portions of the 21 transformations mapping each subject to the 21 input templates were concatenated and averaged across the template library to minimize noise and increase accuracy. These surface representations were warped to fit each template and each of these surfaces was warped to match each subject. This procedure yields 21 possible surface representations per subject for the striatum, pallidum, and thalamus, and 105 possible surface representations for the hippocampus and amygdala, which are then merged by estimating the median coordinate representation at each location. At this point, a third of the surface area of each triangle comprising the mesh of the surface representation is assigned to each vertex within the triangle. The surface area value stored at each vertex is the sum of all such assignments from all connected triangles. Finally, surface-area values were blurred with a surface-based diffusion-smoothing kernel (5 mm for the amygdala, hippocampus, striatum and thalamus, and 3 mm for the pallidum). The measures of interest generated by this processing stream for each scan were total and vertex-wise surface estimates for left and right amygdala, hippocampus, pallidum, striatum, and thalamus at a total of 26,401 vertices across all structures (amygdala left 1473, right 1405; hippocampus left 1152, right 1215;

pallidum left 1266, right 1138; striatum right 6450, left 6178; and thalamus left 3016, right 3108).

2.4 Deriving Vertex-Level Estimates of Cortical Area Scaling by Log-Log Regression

Scaling relationships between brain size and regional cortical anatomy were modeled by estimating the regression coefficients for $\log_{10}$(total cortical surface area) as a predictor of $\log_{10}$(vertex area). Brain size effects on cortical vertex area were modeled using total cortical surface area instead of a volumetric index of brain size because (i) total cortical area is highly correlated with total brain volume (Pearson r, PNC = 0.92 , NIH = 0.93), and (ii) the resultant vertex-wise scaling coefficients could be more directly interpreted relative to the null value of 1 (denoting linear scaling between vertex area and total area). Vertex-wise areal scaling with total cortical area was estimated using a semi-parametric spline regression model that simultaneously incorporated effects of age and sex on vertex area [68, 69]. The scaling relationships presented in our results, were estimated using the following fixed-effects model:

Log_{10}(vertex area) $\approx$ s(age, by=sex) + ß$_1$[$\log_{10}$(total area)] [1]

where s(age, by=sex) denotes a fixed-effect thin plate spline basis estimated for each sex. Random effects for family and person were included in [1] for analysis of the longitudinal NIH dataset. Model [1] was selected for use in both PNC and NIH samples after systematically excluding statistically sig-

nificant higher-order effects such as potential non-linear or linear changes in scaling as a function of age, sex or interactions between these two terms. The ß$_1$ coefficient from model [1] provides an estimate of how area at each cortical vertex scales with total cortical size. ß$_1$ coefficients that are statistically indistinguishable from 1 show isometric (i.e. linear) scaling with total structure size (i.e. vertex area increasing proportionally with total structure area increases). ß$_1$ coefficients deviating from 1 denote allometric (i.e. non-linear) scaling with total structure size variation. ß$_1$ values greater than 1 denote positive allometric scaling (i.e. proportional vertex area increases with increasing cortical surface area), and values below 1 indicate negative allometric scaling (i.e. proportional vertex area decreases with increasing structure size). To visualize spatial gradients in scaling, un-thresholded ß$_1$ values were projected onto a CIVET 3D surface model for the ICBM 152 template. Domains of statistically-significant positive and negative areal scaling were defined by testing the observed ß1 value at each vertex against the null value of 1, and correcting for multiple comparisons across all vertices in each bilateral structure [using False Discovery Rate correction (18) with q, the expected proportion of false discoveries set at 0.05]. To test for statistically-significant asymmetries in cortical scaling within PNC, NIH and HCP cohorts, we calculated the t-statistics for inter-hemispheric difference in scaling at homologous vertices by subtracting the ß$_1$ coefficient of each vertex on the right hemisphere from its matched vertex on the left hemisphere and dividing by the square root of the sum of the squared standard errors for the ß$_1$ value at both vertices. The p-values associated with these t-statistics were subjected to FDR correction for multiple comparison across vertices (with

q set at 0.05) to test for cortical regions of statistically-significant scaling asymmetry. In addition to comparing thresholded scaling asymmetry maps across all three cohorts, we also compared scaling asymmetry across cohorts with 3 additional approaches. First, within regions showing statistically-significant scaling asymmetry in any one cohort, violin plots were used to visualize the distribution of scaling values in corresponding regions of the left and right hemisphere in the other two cohorts. Second, the observed cross-vertex correlation in scaling asymmetry was compared between cohorts with the distribution of null correlations generated with rotational permutation on PNC and NIH scaling asymmetry maps. This addressed if the topography of scaling lateralization was similar between cohorts. Third, given a region of statistically-significant scaling asymmetry in any one cohort, the mean scaling asymmetry was calculated within this mask for the other two cohorts, and then in each of these two cohorts, and compared this observed scaling symmetry value to the distribution of scaling coefficient symmetry values associated with 1000 random spatial rotations of the scaling mask. This addressed if regions with a significantly lateralized scaling in one cohort showed a similar lateralization of scaling in other cohorts relative to other facets of the cortical sheet.

2.5 Deriving Estimates of Subcortical Structure Volumetric Scaling by Log-Log Regression

Scaling relationships between brain size and regional subcortical nucleus volumes were modeled by estimating the regression coefficients for $\log_{10}$(total brain volume) as a predictor of $\log_{10}$(nucleus volume). For each subcortical structure, normative scaling laws were estimated using the following equation (using thalamic volume as an example):

$\log_{10}$ (Bilateral Thalamic Volume) $\sim$ ß$_0$(Intercept) + ß$_1$($\log_{10}$(TBV)) [1]

Here, ß$_1$ provides the estimated scaling coefficient linking variation in thalamic volume to variation in total brain volume. A ß$_1$ value of 1 indicates linear scaling (i.e. proportional thalamic volume remains unchanged with variations in brain size). A ß$_1$ values less than 1 denotes hypoallometric scaling (i.e. proportional thalamic volume becomes smaller with increasing brain size). Lastly, ß$_1$ values greater than 1 indicate hyperallometric scaling (i.e. proportional thalamic volume becomes larger with increasing brain size). For all three structures examined, the linear model design summarized by [1] was used after first establishing the absence of significant interactions between sex and logarithmically normalized total brain volume measurements for explaining the variance of subcortical structure volume in the study sample. Next, having estimated these normative scaling laws for the striatum, thalamus, and globus pallidus, a test was performed to see if the subcortical volumes observed in each sex chromosome aneuploidy group fell within the normative

range. The normative framework derived from typical scaling of subcortical volumes with total brain volume was also leveraged to test if subcortical volumes in individuals with non XX and XY 23^{rd} chromosome complements in our sample represented a statistically significant disruption of the normative relationship between structure volume and total brain volume. A significant deviation from the allometrically informed normative framework was operationalized as a lack of overlap between the 95% confidence intervals for the observed and predicted mean structure volume in each karyotype group.

The log-normalized regression framework presented here is not the exclusive method for detecting and describing scaling relationships. One may also represent allometric relationships as the relative fractional change of two quantitative features (e.g. $\frac{\partial x}{x} = ß\frac{\partial y}{y}$). In the case of neuroimaging, the two features may be total brain size and any constituent anatomical compartment such as the thalamus or the globus pallidus, but the two features may be any two anatomical regions such as the thalamus **and** the globus pallidus. To generalize the allometric relationship formalized in a linear model across many features at once, it has been advocated to test for allometry using the first principle component of the covariance matrix of log normalized values of the features of interest [70]. Whereas the linear model formalism for describing allometry assumes that measurement error is included only in the predicting terms, this principal component analysis framework permits the measurement error to be included in both structures analyzed. This approach was not taken here. First, this work is concerned with total brain size correction methods in anatomical neuroimaging and consequently, the thesis only addresses proportional relationships in a linear model framework

between regions of interest (ROI) and total brain size or between vertex size in an ROI and total ROI size. A limitation of this approach is that it is limited to computing allometric relationships and evaluating their impact on prediction in well registered regions. This is the motivation for using the MaGET pipeline for volumetric and surface area measurements of the subcortical structures considered herein.

2.6 Disruption of the PNC Cortical Scaling Map by Sample Permutation

As a first test of the possibility that intrinsic aspects of CIVET-based image processing were artifactually generating agreement between scaling maps in PNC and NIH cohorts, we reproduced the log-log analysis of cortical scaling using a permuted version of the PNC cohort where links between participants and their scans had been disrupted. The resultant scaling map was visualized by projection into the CIVET surface, and compared with the scaling map in NIH data in two ways: by calculating the Pearson correlation coefficient between scaling values across vertices, and by comparing these observed correlation coefficients to distributions of correlations based on 1000 surface-based rotations of the NIH scaling map.

2.7 Reproducibility of Cortical Scaling in a Third Cohort Using Different Imaging Processing Software

To further assess if reproducibility of the observed scaling map across PNC and NIH samples could be due to our use of the CIVET pipeline for cortical morphometry in both samples, we repeated the log-log regression analysis of cortical scaling using cortical morphometry output from a different sMRI processing pipeline, FreeSurfer [71, 72]], with five different kernel sizes for surface-based smoothing of vertex area estimates (5 mm, 10 mm, 20 mm, 30 mm and 40 mm), in a third independent sample of structural MRI brain scans [Human Connectome Project [60, 73, 19]]. FreeSurfer surface reconstructions (based on 3T T1-weighted anatomical scans) were downloaded from the HCP 1200 release for 1113 subjects (606 females). For each subject, vertex-wise (mid-thickness) surface area estimates were registered to the fsaverage template using FreeSurfer's "recon-all -qcache" pipeline, with five different smoothing kernels (FWHM = 5 mm, 10 mm, 20 mm, 30 mm and 40 mm). Then, log-log regression analysis was performed at each vertex using the aligned surface area data, co-varying for sex and age. The results of these analyses were visualized after projection onto the standard CIVET surface as both un-thresholded and categorical scaling maps. Once on the CIVET surface, scaling maps based on FreeSurfer processing of HCP data were compared with the observed scaling maps based on CIVET processing of PNC and NIH data in two ways: by calculating the Pearson correlation

coefficient between scaling values across vertices for the HCP-PNC and HCP-NIH comparisons, and by comparing these observed correlation coefficients to distributions of correlations based on 1000 surface-based rotations ("spins", see below) of the PNC and NIH scaling maps (respectively).

2.8 Aligning Cortical Maps to the CIVET Template Surface

Several independent cortical maps were transferred to CIVET surface space for comparison with cortical scaling gradients. All independent maps were either publicly available, or provided by the kind cooperation of the research groups that had generated the datasets. All independent maps were transferred onto the standard CIVET ICBM 152 surface space using surface-to-surface transformations, with the exception of the alignment of the Arterial Spin Labeling map of regional blood flow (see below), which was available in ICBM 152 volumetric space and required an initial step of volume-surface projection. Details of each independent comparison map are provided below. None of the maps used were under copyright.

2.9 Cortical Area Expansion in Evolution

Hill et al, 2010, PNAS [74] Cortical Area Differences Between the Adult Human and Adult Macaque Brain: This right hemisphere map provided vertex-level estimates of surface area fold-change in a sample of adult humans compared with adult macaques. This map was converted to the fsaverage6 surface

template using standard transformations provided in the HCP Connectome Workbench (v1.2.2) software package (https://www.humanconnectome.org/software/connectome-workbench). Next, the fsaverage6-aligned map was transformed to the CIVET ICBM 152 surface space by a direct surface-to-surface transformation in which values at vertices in the target coordinate matrix were assigned to one of their nearest neighbor vertices within a 10 mm radius in the source coordinate matrix. This conversion resulted in an estimate of area expansion in humans vs. macaques for all 40962 vertices of the CIVET right hemisphere. For any bilateral analyses, this right hemisphere map was reflected to the 40962 homologous left hemisphere vertices in the ICBM 152 template used by CIVET. To visualize the conjunction between this map of "evolutionary areal expansion" and maps of areal scaling in the PNC and NIH cohorts, the evolutionary scaling estimates were binarized by splitting into different categories based on their median. Thus vertices with evolutionary area expansion values above the 50th centile were considered to show relatively "high" degrees of areal expansion. The conjunction between these vertices and red regions of statistically-significant positive areal scaling in defined cortical regions of disproportionate areal expansion with both inter-species (human vs. macaque) and intra-species (larger vs. smaller human brains) increases in total cortical size. Within these conjunction regions, the relative magnitude of inter- and intra-species areal scaling was compared by (i) dividing all vertex-level areal expansion values in the Hill map by 10 (the reported fold-change of total cortical surface area in humans relative to macaques [75]), and then (ii) calculating the difference between these scaling values and those given

by log-log regression within PNC and NIH cohorts.

2.10 Cortical Area Expansion in Development

Hill et al, 2010, PNAS [74] / Cortical Area Differences Between the Adult Human and Infant Human Brain: This right hemisphere map provided vertex-level estimates of surface area fold-change in a sample of adult humans compared with infant humans. We converted this map to the CIVET ICBM 152 surface space by the same surface-to-surface transformation described above for the evolutionary expansion map. This conversion resulted in an estimate of area expansion in adult vs. infant humans for all 40962 vertices of the CIVET right hemisphere. For any bilateral analyses, this right hemisphere map was reflected to the 40962 homologous left hemisphere vertices in CIVET. Conjunction analyses between this developmental expansion map and areal scaling maps in the NIH and PNC samples were conducted as described above for the evolutionary expansion map.

2.11 Cortical Parcellation into 7 and 17 Functional Connectivity Networks Based on Resting State Functional MRI (rsFMRI)

Yeo et al, 2011, Jnl Neurophysiology [76]: Yeo et al. used resting-state fMRI data to generate 2 bilateral surface-based parcellations of the cortex into mutually-exclusive functional connectivity networks – one defining 7 net-

works, and a finer-scale parcellation defining 17 networks (which are mostly sub-divisions of cortical divisions within the 7-network scheme). The 7 and 17 network parcellations were available in FreeSurfer ICBM 152 surface space. These parcellations were converted to CIVET ICBM 152 surface space by the same direct surface-to-surface transformation from the human connectome workbench described above.

2.12 Cortical Parcellation into the 7 Cytoarchitectonically Distinct "Types" of von Economo

Whitaker et al, PNAS, 2016 [77]: This cytoarchitectonic parcellation [10] was available in FreeSurfer ICBM 152 surface space, and transferred to the CIVET ICBM 152 surface space by the same direct surface-to-surface transformation described above.

2.13 Arterial Spin Labeling (ASL) Map of Resting State Blood Flow

Satterthwaite et al, 2014, PNAS [51]: This map was available in ICBM 152 volume space, and provided voxel-wise estimates of mean blood flow based on ASL data in the subset of PNC participants as described by Satterthwaite et al [51]. This map was projected to CIVET ICBM 152 surface grid using a voxel-vertex nearest neighbor method analogous to the vertex-to-vertex

mapping methods described above.

2.14 Positron Emission Tomography (PET) Map of Resting State Glucose Utilization

Remapped from Vishnavi et al, 2010, PNAS in Glasser et al, 2014, Neuroimage [78, 79]: This map was converted to FreeSurfer fsaverage6 surface space, and transferred to the CIVET ICBM 152 surface space by the same direct surface-to-surface transformation described above.

2.15 Spatial Permutation Tests for Alignment Between Comparison Cortical Maps and Scaling Maps in PNC and NIH Samples

Continuous Comparison Map: Several comparisons in our study involved assessing the spatial congruence between two continuous maps, including: NIH vs. PNC scaling map; and both PNC/NIH continuous scaling maps vs. (i) scaling maps in subsets of the PNC and NIH cohorts over 18 years of age, (ii) CIVET-derived scaling map after permutation of person-scan assignments in the PNC cohort, (iii) scaling maps generated using FreeSurfer in the HCP dataset at four different surface smoothing kernels, (iv) evolutionary and developmental area expansion maps, (v) ASL blood flow, and (vi) glucose

utilization from independently published PET data. All data for external comparisons was generously provided by the authors of the studies in which they were generated. For each test the original data was projected into ICBM 152 coordinate space and represented on the CIVET model surface.

For all of these comparisons, the spatial correspondence of any continuous map with the continuous PNC or NIH scaling map was assessed using a spatially aware permutation test. The observed cross-vertex Pearson correlation coefficient between scaling values in each map was calculated. This observed correlation value was compared to the distribution of correlation coefficients generated by 1000 random surface-based rotations of the spherical projection of the PNC/NIH continuous scaling map (see below). The coordinates corresponding to the vertices in the scaling maps were rotated at angles randomly chosen from a uniform distribution between zero and 360 degrees about the x, y, and z axis. This comparison generated an empirical P_{spin} value – the proportion of 1000 null correlations that had a higher value than the observed correlation. P_{spin} values <0.05 were taken to indicate statistically-significant overlap between continuous maps. The purpose of this "spin test" is to quantify how statistically unusual an observed correlation between two maps is, while controlling for the spatial autocorrelations inherent in cortical data, and arbitrariness in the number of observations (vertices) across which correlations are calculated. Each comparison of two continuous cortical maps by the spin test was conducted three times - using data across both hemispheres, and once for each hemisphere in isolation. The only exceptions were when the cortical map for scaling comparison was only available for one hemisphere (e.g. Hill et al evolutionary and developmental

expansion [74]): in these cases the spin test was run for the available hemisphere in isolation, and with a bilateral map made by mirroring the available hemisphere data.

2.16 Categorical Comparison Maps

Several cortical map comparisons in our study involved assessing the spatial congruence between regions of statistically-significant positive and negative areal scaling in PNC/NIH cohorts, and an alternative cortical parcellation, including: (i) Parcellation of the cortex into 7 and 17 resting state functional connectivity networks, and (ii) Parcellation of the cortex into 7 distinct cytoarchitectonic classes. For all these comparisons, the spatial correspondence of any categorical cortical parcellation and the categorical PNC or NIH scaling map was calculated as the number of overlapping vertices divided by the total number of vertices in each functional network or cytoarchitectonic class. This was performed separately for the positive and negative categorical scaling maps. These empirical normalized percent overlap statistics were compared to those computed from 1000 spatial permutation "spins" of the PNC/NIH categorical scaling maps.

Random Surface-Based Rotation of PNC and NIH Scaling Maps: These rotations were conducted as described by Alexander-Bloch et al [80] using a spherical representation of the CIVET cortical surface. One thousand random angular transformations were applied to the unit sphere (analogous to randomly spinning the sphere in x, y, and z directions). The permuted data was then resampled onto the original spherical surface using a nearest neigh-

bor method in order to achieve spatially resampled data that respected the spatial auto-correlation of the original data. This process can be thought of as "spinning" the observed scaling maps on the cortical surface. As described above, these resampled data were used to generate the null distribution of the statistic to quantitatively test the statistical significance of the observed spatial overlap between the scaling map and other cortical maps.

2.17 Comparison of Scaling Maps to Gradients of Cortical Gene Expression in the Adult Human Brain

2.17.1 Preprocessing of Allen Institute Gene Expression Data from Human Brain Tissue

The Allen Institute of Brain Sciences (AIBS) human microarray data [28] was downloaded from http://human.brain-map.org/static/download on January 8, 2016. It consists of the microarray datasets of six healthy brains (five males, one female, mean age: 42.5, standard deviation: 13.4). Left and right hemisphere were available for two donors, and left hemispheres only for the remaining four. This AIBS dataset contains 58,692 probe expression profiles sampled throughout the brain and normalized across all brains using both within-batch and cross-batch array normalization process. A total of 16,906 probes as selected by Richardi et al. [81] were used in the following analysis. Probe selection was primarily based on which probe has the minimum mis-

matches to the reference sequence, and the assignment of probe sequences to genes was re-annotated using Re-annotator [82] for an up-to-date mapping.

2.17.2 Assigning Scaling Indices to Allen Atlas Brain Samples

Montreal Neurological Institute stereotaxic coordinates were available for all postmortem samples from the six AIBS donor brains and every cortical vertex within our areal scaling maps. We used the nearest neighbor method to find a one-to-one match of Allen Institute brain samples to each surface vertex in our areal scaling maps, based on minimal Euclidean distance. We restrained our search to the AIBS samples annotated as lying within the cerebral cortex, and required that Allen AIBS samples fell within a 10 mm radius of the vertex to which they were assigned. This process allowed us to assign a scaling value to each of 1939 post-mortem cortical samples across the 6 AIBS donors (Table 2.4), with an average (standard deviation) Euclidean distance of 2.38 (1.74) mm.

2.17.3 Quantifying Associations Between Gene Expression and Neuroanatomical Scaling

We sought to rank genes according to the statistical significance of correlation between their spatial expression across AIBS samples and the neuroanatomical scaling map. As the number of available samples varies across AIBS donors, we conducted tests in the merged set of sample locations across all six brains rather than in each brain separately to avoid possible biases

originating from uneven sample sizes across brains. For each gene, variation in expression across samples was modeled using variation in scaling coefficient across samples as a fixed effect, plus a random intercept for donor to model variance dependence between samples from the same brains. As we tested the null hypotheses of no correlations between gene expression and scaling maps for 16906 genes, an immediate concern is that the probability that Type I error can increase sharply with the number of hypotheses tested. To correct for multiple testing, we computed adjusted p values using three well-known methods: Bonferroni correction, single-step minP [83], as well as Benjamini and Hochberg (BH) [84]. The first two methods are designed to control the family-wise error rate (FWER), defined as the probability of at least one Type I error, and the last is less stringent and is used to control the false discovery rate (FDR), that is, the expected proportion of Type I errors among the rejected hypotheses. To implement the minP method, we used 5000 permutations to estimate the distribution of null hypotheses, and positive and negative scaling labels were randomly assigned in each permutation. The adjusted p values of all genes in ascending order were plotted together to compare the performance of these three methods. As our sample size was relatively large, the most stringent Bonferroni correction was selected here and adjusted with $p < 0.05$ being set as the significance threshold. However, all three methods for p-value adjustment yielded the same order of the ranked list of expressed genes in terms of the significance level in correlations with the scaling map. These invariant ranked lists for the PNC and NIH scaling maps were used in the following gene set enrichment analysis for gene ontology annotations for biological process and cellular component.

Characteristic						
ID	Allen ID	Sex	Age (years)	Handedness	Hemispheres	Post-mortem interval (hours)
1	H0351.2001	M	24	Left	L+R	23
2	H0351.2002	M	39	Left	L+R	10
3	H0351.1009	M	57	Mixed	L	25.5
4	H0351.1012	M	31	Right	L	17.5
5	H0351.1015	F	49	Right	L	30
6	H0351.1016	M	55	Right	L	18

Table 2.4:
Allen Institute for Brain Science Gene Expression CohortDemographics and participant characteristics of the Allen Institute for Brain Science gene expression cohort. L= left hemisphere. R = right hemisphere.

High-ranking genes were those with expression profiles that showed a positive spatial correlation with areal scaling.

2.18 Gene Ontology Enrichment Analyses

Ranked gene lists for the PNC and NIH scaling maps were submitted to a rank-based analysis of Gene Ontology (GO) enrichment using GOrilla (http://cbl-gorilla.cs.technion.ac.il/) ([85]). Significant GO terms for Cellular Component were visualized using REViGO for semantic space reduction [86]. As AIBS sample locations were not uniformly distributed across the cortex and across donors, using a bootstrapping technique, we tested the effect of variation in sample location selection on ranking of genes by association with scaling. For the PNC scaling map, in each of 1000 repetitions, we randomly excluded 10% of the complete set of sample locations and recalculated the gene rankings using this subset of samples. Then we calculated the Spearman correlations of gene ranks in these 1000 observed lists and the original list calculated from the complete set of samples, and the averaged Spearman r was 0.985 (sd=0.003). In an extension of this bootstrapping test, we changed the exclusion percentage from 10% to 90% in 10% steps and completed 100 repetitions of random exclusion for each step. This procedure established that the Spearman r for gene ranks using the full vs. partial post-mortem sample sets remained above 0.9 until over 75% of samples were excluded by donor. We also conducted supplementary analyses to determine if genes associated with significant GO terms of interest in our main analyses would be also be highly ranked in gene lists generated after

1000 permutations of PNC scaling values across AIBS samples. For the 2 Cellular Component GO terms of interest in our main analyses - Mitochondrial Part (GO:0044429) and Synapse Part (GO:0044456) - the observed medial rank of associated genes was higher than observed in all 1000 lists derived by scaling permutation (empirical $p < 0.001$).

2.19 Deriving Vertex-Level Estimates of Subcortical Area Scaling

Areal scaling at each cortical vertex was modeled in relation to total bilateral cortical surface area, and areal scaling at each subcortical vertex was modeled in relation to the total bilateral surface area of all subcortical structures combined (i.e., thalamus, pallidum, striatum, amygdala and hippocampus). Thus, these subcortical coefficients can be directly compared between different subcortical structures. Several considerations motivated our analysis of subcortical scaling in a surface-based rather than volume-based manner. First, the areal approach allowed us to adopt a homogeneous statistical framework for analysis of scaling in the cortex and subcortex [ie. $\log_{10}$(local area) $\approx \log_{10}$(total area)]. Subcortical shape changes modeled as surface area shifts can also aid visualization of data along the spatial gradients that are known to organize the topography of cortico-subcortical connectivity. Modeling subcortical shape changes at the surface can further reveal the congruence of scaling across neighboring facets of different subcortical structures. Subcortical vertex scaling was modeled with reference to total subcortical

area as opposed to "total brain surface area" (TBSA – i.e. the sum of total cortical and total subcortical surface area) because the cortex accounts for over 85% of TBSA (PNC: mean (89% +/- 0.6% sd, NIH: mean 89% (+/- 0.5% sd)), and shows a very small absolute deviation from linear scaling with the cortical sheet (+0.06 above linear scaling). Use of TBSA would therefore essentially result in subcortical scaling maps reflecting the changes in the relative size of subcortical vertices relative to the cortical sheet. In line with a prior study of volumetric scaling between subcortical structure and total brain size, we find that the total surface area of each subcortical structure scales negatively with that of TBSA (average scaling coefficient – 0.4 below linear scaling) meaning that all subcortical structures examined were relatively smaller in larger brains. Use of TBSA would therefore compress the range of scaling variation across vertices in each subcortical structure.

Chapter 3

Normative Areal Scaling

3.1 Abstract

Total brain size can vary over 2-fold amongst typically-developing humans of the same age [36], but the relationship between inter-individual variation in human brain size and brain shape remains unexamined in developing and mature populations [87, 88]. In this chapter, areal scaling across the developing cortical sheet is mapped at high spatial resolution first in a cross-sectional sample of neurotypical adolescents without reference to an a priori anatomical parcellation to identify data-driven organizational shifts accompanying human brain-size variation in the developing brain and illuminate how the heterogenous patterning of linear and non-linear scaling changes cortical area topography. The resulting scaling map is then tested in an independent longitudinal sample to test for the developmental stability of the patterning of brain scaling. Last a publicly available sample of neurotypical adults is examined to show that the same scaling map is reproducible in both developing

and mature population samples. To determine if non-linear areal scaling is restricted to the cortex, morphometric data from 5 subcortical nuclei (striatum, pallidum, thalamus, amygdala, and hippocampus) from each sample of developing subjects is analyzed to detect linear and non-linear regions of scaling in surface area maps of these non-cortical structures.

3.2 Discovery/Replication Study Design

This chapter presents 2,904 structural magnetic resonance imaging brain scans from two independent cohorts of typically developing youth – (i) a Philadelphia Neurodevelopmental Cohort (PNC) sample of 1,373 cross-sectional scans from a 3 Tesla machine in youth aged 8-23 years (participant information included in methods is reproduced here for ease of reference in Table 3.1 and Fig 3.1, [89]), and (ii) a National Institutes of Health (NIH) sample of 1531 longitudinally-acquired brain scans from a 1.5 Tesla machine in 792 youth aged 5-25 years (participant information included in methods is reproduced here for ease of reference in Table 3.2, Fig 3.2). 1,113 crossectionally acquired sMRI of adults from an independent cohort processed with a separate software pipeline at various FWHM smoothing kernels are also presented to demonstrate the robustness of scaling to different processing techniques and across the human lifespan (participant information included in methods is presented here for ease of reference in Table 3.3).

Characteristic	All	Male	Female
Number of Individuals	1373	645	728
Race, No			
Caucasian	603	314	289
African-American	601	253	348
Other	169	78	91
Age Distribution of Scans (years)			
Mean (SD)	14.83 (3.66)	14.56 (3.67)	15.06 (3.64)
Range	8.08—23.08	8.17—23.00	8.08—23.08

Table 3.1: **Demographics of Philadelphia Neurodevelopmental Cohort**. Crossectional Cohort.

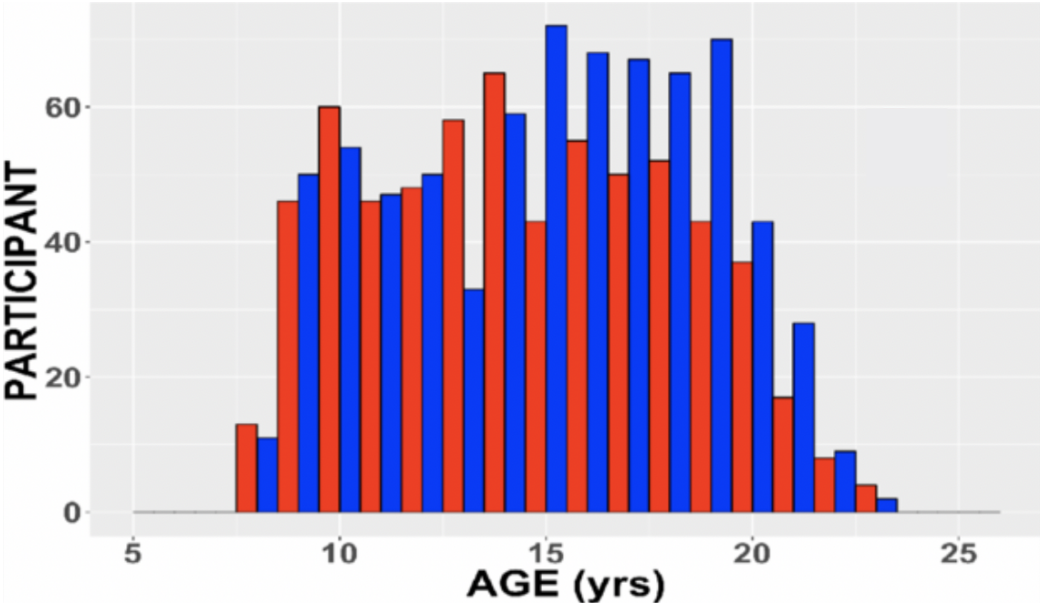


Figure 3.1: **PNC**. Histogram of Participant Age. Female participants are labeled red and male participants blue.

Characteristic	All	Male	Female
Number of Individuals	792	403	389
Singleton	493	256	237
Member of twin pair	299	147	152
Right handed	673	343	330
Race, self-reported No.			
Caucasian	673	341	332
African-American	54	27	27
Asian	17	10	7
Hispanic	26	11	15
Other	22	14	8
IQ			
Mean (SD)	114.2 (12.52)	114.7 (12.90)	113.7 (12.10)
SES			
Mean (SD)	42.04 (18.93)	41.78 (19.34)	42.33 (18.59)
Number of Scans per Person			
1 scan	386	191	195
2 scans	200	103	97
3 scans	116	54	62
4 scans	59	37	22
5 scans	25	14	11
6 scans	6	4	2
Total Number of Scans	1531	801	730
Age Distribution of Scans (years)			
Mean (SD)	13.58 (4.75)	13.90 (4.75)	13.22 (4.72)
Range	5.14—25.79	5.24—25.79	5.14—25.65

Table 3.2: **National Institutes of Health Cohort**. Longitudinal Cohort.

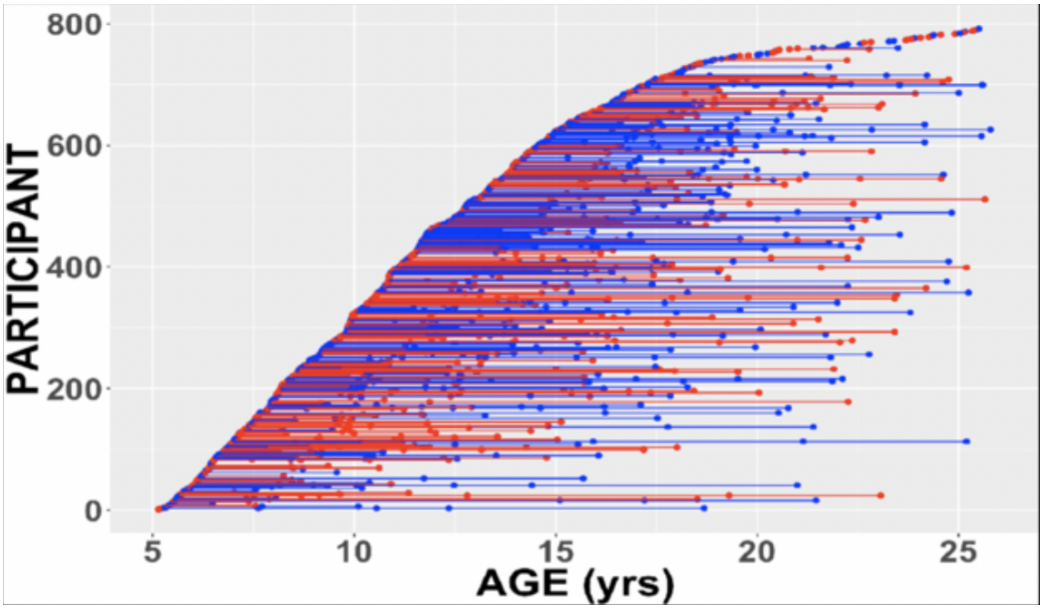


Figure 3.2: **NIH**. Dot and line plot of distribution of scans of each participant by age and sex. Female participants are labeled red and male participants blue.

Characteristic	All	Male	Female
Number of Individuals	1113	507	606
Age Bins (years)			
22 — 25	231	147	84
26 — 30	486	221	265
31 — 35	383	135	248
36 and above	13	4	9

Table 3.3: **Human Connectome Project**. Adult Crossectional Cohort.

3.3 Surface Area Scaling in the Cortex

To generate a reference map of areal scaling in the cortex, local surface area associated was measured at each of approximately 80,000 cortical points per processed sMRI scan (henceforth "vertex area") using CIVET, an automated image-processing pipeline [56]. Semiparametric generalized additive models [90] were then used to estimate vertex-specific scaling as the log-log regression coefficient for total cortical area as a predictor of vertex area. For a more detailed description of the statistical modeling procedure performed, please refer to Chapter 2, Section 4.

Our results supported estimation of a single scaling map for each of the two developmental cohorts examined, which did not vary as a function of age and sex. In all cohorts, scaling relationships between vertex area and total cortical area varied across the cortical sheet (Fig 3.3) in a manner that was symmetric and reproducible (Table 3.4).

Inter-vertex differences in scaling were highly correlated between PNC and NIH cohorts (Pearson r = 0.7), at levels above chance in a spatial permutation procedure that relies upon random surface-based rotation of cortical maps (henceforth "spins"; i.e., pSPIN <0.001, Methods, Fig 3.4, Table 3.5).

Testing for statistically-significant deviation from 1 of vertex scaling coefficients and correcting for multiple comparisons across vertices defined two distributed domains of statistically-significant, non-linear areal scaling in each cohort (Fig 3.5).

Across cohorts, we observed regions of positive areal scaling in prefrontal, lateral temporo-parietal, and medial parietal cortex, and negative areal scal-

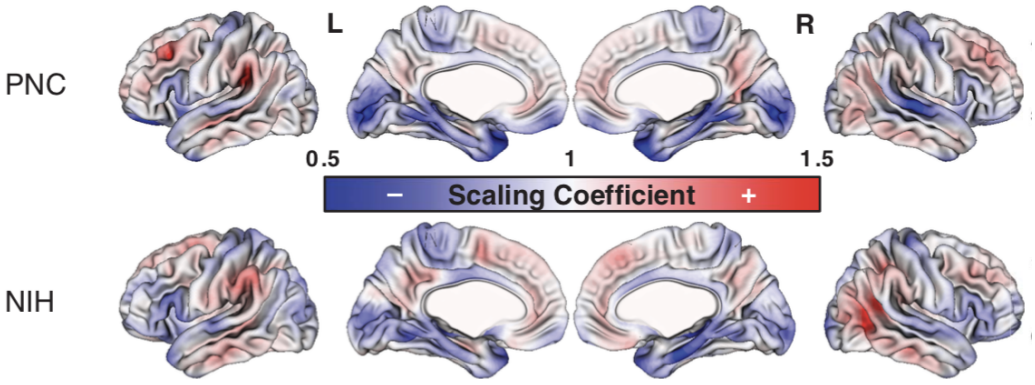


Figure 3.3: **Areal Scaling Map**. Un-thresholded vertex maps showing local surface area scaling with naturally-occurring variations in total cortical area. **Red** denotes relative expansion in larger cortices ("positive scaling") and **blue** denotes relative contraction ("negative scaling").

COMPARISON MAP	REFERENCE SCALING MAP			
	PNC asymmetry		NIH asymmetry	
	observed r	p_{SPIN}	observed r	p_{SPIN}
PNC asymmetry				
left	-	-	0.34	0.001
HCP asymmetry				
left	0.19	<0.01	r=0.01	0.5

Table 3.4: **Cortical Asymmetry of Area Scaling Across Cohorts**. Pearson's R of correlation of surface area scaling asymmetry across cohorts.

COMPARISON MAP	REFERENCE SCALING MAP			
	PNC		NIH	
	observed r	p_{SPIN}	observed r	p_{SPIN}
PNC				
bilateral	-	-	0.69	<0.001
left	-	-	0.65	<0.001
right	-	-	0.72	<0.001
HCP - FreeSurfer 5mm smoothing				
bilateral	0.35	0.001	0.28	0.001
left	0.32	0.003	0.23	0.006
right	0.38	0.002	0.33	0.002
HCP - FreeSurfer 10mm smoothing				
bilateral	0.37	0.001	0.3	0.001
left	0.34	0.004	0.25	0.007
right	0.4	0.003	0.35	0.002
HCP - FreeSurfer 20mm smoothing				
bilateral	0.38	0.002	0.31	0.001
left	0.38	0.002	0.25	0.009
right	0.41	0.003	0.37	0.002
HCP - FreeSurfer 30mm smoothing				
bilateral	0.37	0.003	0.3	0.004
left	0.33	0.013	0.24	0.016
right	0.4	0.003	0.37	0.003
HCP - FreeSurfer 40mm smoothing				
bilateral	0.35	0.006	0.29	0.005
left	0.31	0.017	0.22	0.024
right	0.38	0.003	0.35	0.003
PNC - permuting scans across people				
bilateral	0.01	0.42	-0.02	0.61
PNC - scaling in over 18 year olds only				
bilateral	0.8	<0.001	-	-
left	0.8	<0.001	-	-
right	0.8	<0.001	-	-
NIH - scaling in over 18 year olds only				
bilateral	-	-	0.78	<0.001
left	-	-	0.76	<0.001
right	-	-	0.79	<0.001

Table 3.5: **Scaling Map Correlations**. Pearson's R for correlation of scaling metrics across cohorts and permutations

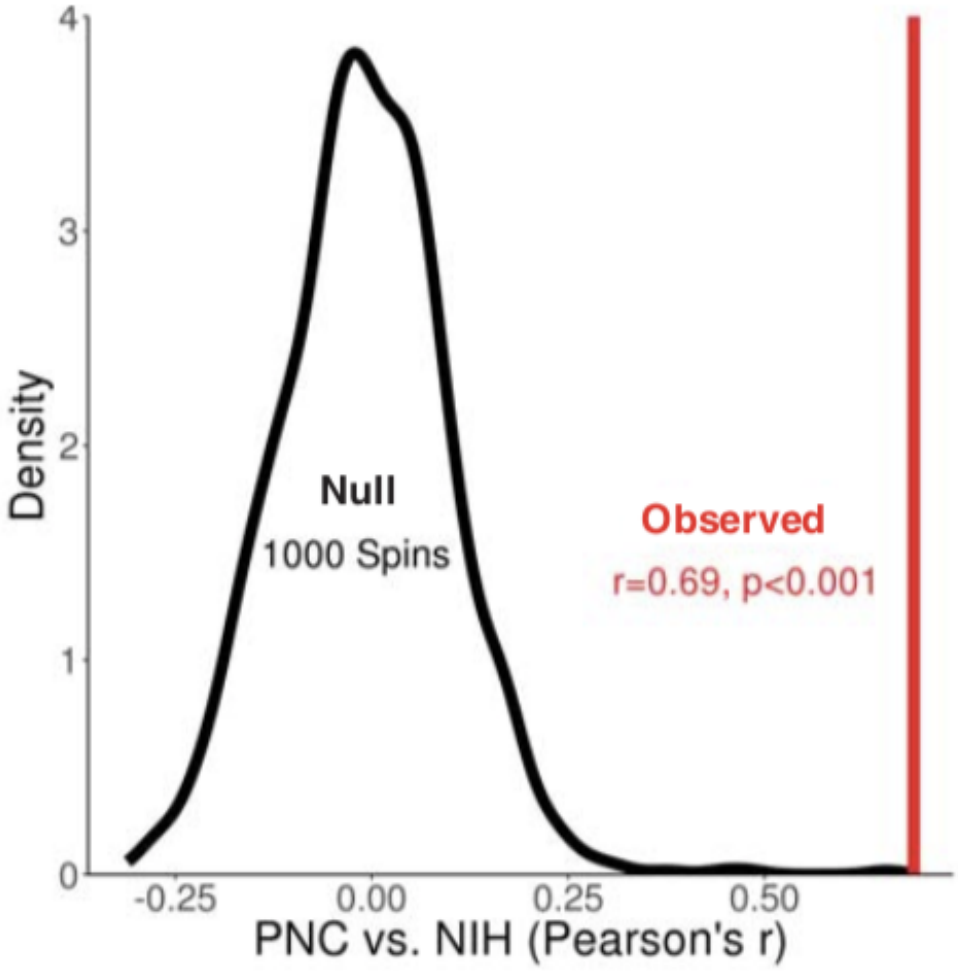


Figure 3.4: **Spatial Similarity of Scaling between NIH and PNC cohorts**. The observed cross-vertex correlation in scaling between PNC/NIH cohorts is greater than that in 1000 surface-based rotations of the NIH scaling map (i.e. pSPIN <0.001, density plot).

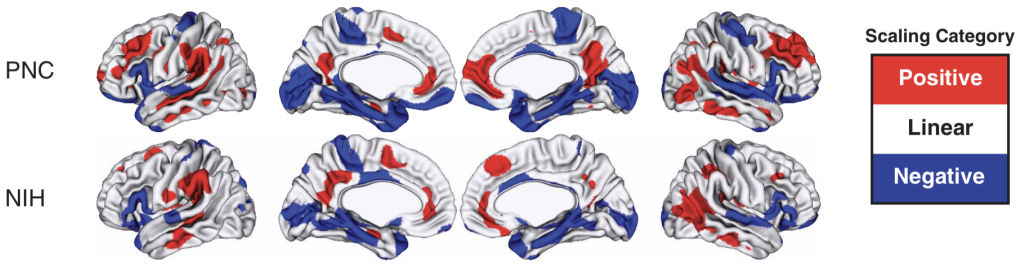


Figure 3.5: **Regions of Categorical Positive and Negative Surface Area Scaling in the Human Brain**. Categorical scaling maps showing regions of statistically-significant positive and negative areal scaling after correction for multiple comparisons across vertices.

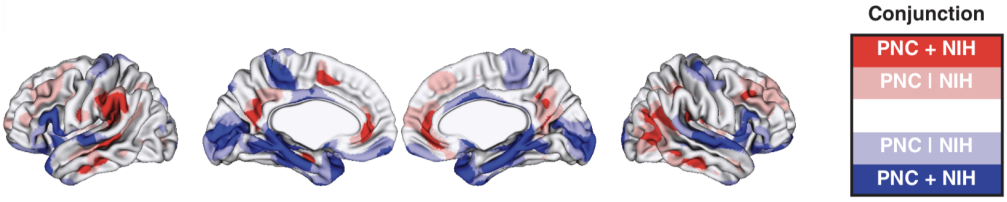


Figure 3.6: **Overlap between Maps of Thresholded Scaling**. Conjunction of PNC and NIH maps

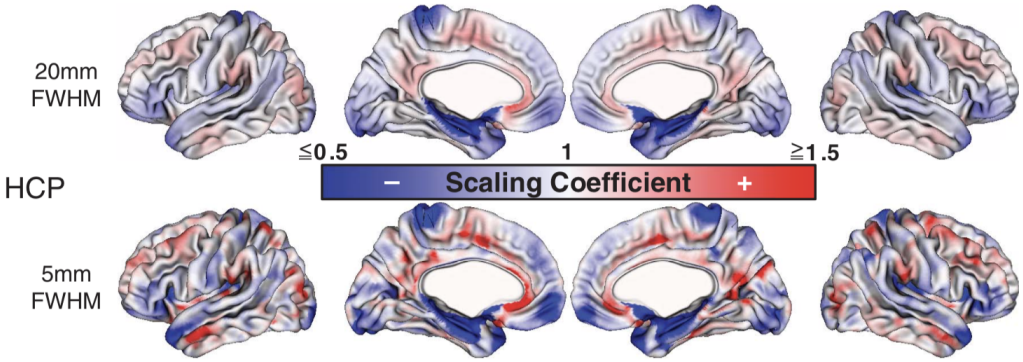


Figure 3.7: **Scaling in Human Connectome Project at Different Smoothing Kernels**. Regional scaling in a third independent dataset (Human Connectome Project, n=1113), across 2 different smoothing kernels

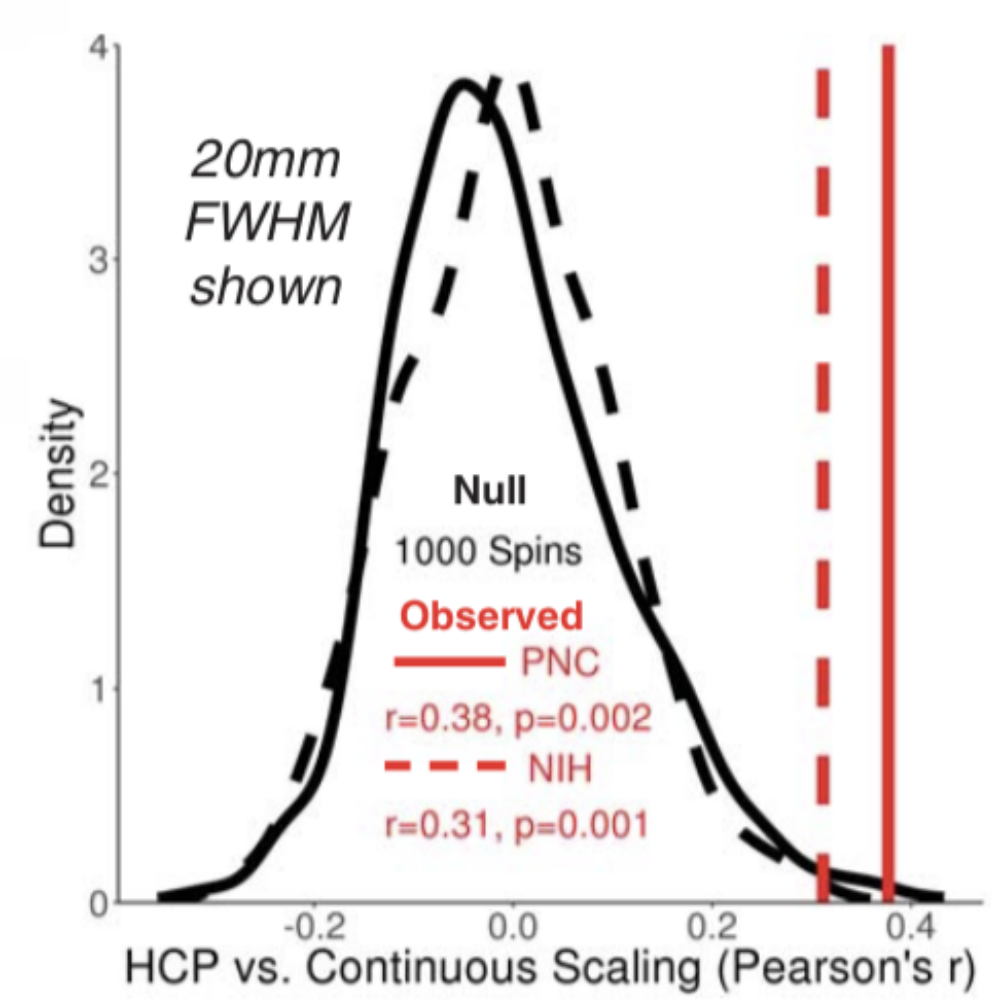


Figure 3.8: **Spatial Overlap** Density plot of permutation test for spatial similarity between HCP and NIH/PNC scaling maps.

ing in limbic, primary visual and primary sensorimotor regions (Fig 3.6).

The reproducibility of areal scaling across cohorts was unlikely to reflect intrinsic methodological artifacts from a shared cortical analysis pipeline because these scaling patterns were (i) lost after permuting scans across individuals in the PNC cohort, and (ii) seen after processing a third independent MRI dataset from the Human Connectome Project (HCP, n=1113) with a different computational pipeline (FreeSurfer), at varying smoothing kernels (Fig 3.7, Table 3.5). The density plot (Fig 3.8) shows that the observed alignment of HCP scaling with PNC(solid)/NIH(dashed) ($r > 0.3$) exceeds chance (pSPINS < 0.002).

Thus, log-log regression analysis revealed regionally-specific patterns of non-linear areal scaling in the human cortex which were broadly reproducible across three study cohorts, three image-acquisition platforms, two image processing pipelines and a range of smoothing kernels.

3.4 Surface Area Scaling Across 5 Subcortical Nuclei

To assess if regional differences in areal scaling were unique to the cortical sheet we mapped areal scaling across five non-neocortical (henceforth "subcortical") structures (thalamus, pallidum, striatum, hippocampus and amygdala) using recently-developed algorithms for automated subcortical shape analysis (MAGeT Brain, Methods). This approach provided a homogeneous surface-based framework for quantification and visualization of areal scaling

gradients across the cortex and subcortex (Methods).

Vertex-level areal scaling coefficients varied within each subcortical structure examined (e.g. positive scaling in hippocampal head vs. negative scaling in tail, Fig 3.9), revealing that size-related shifts in human brain shape are not restricted to the cortex.

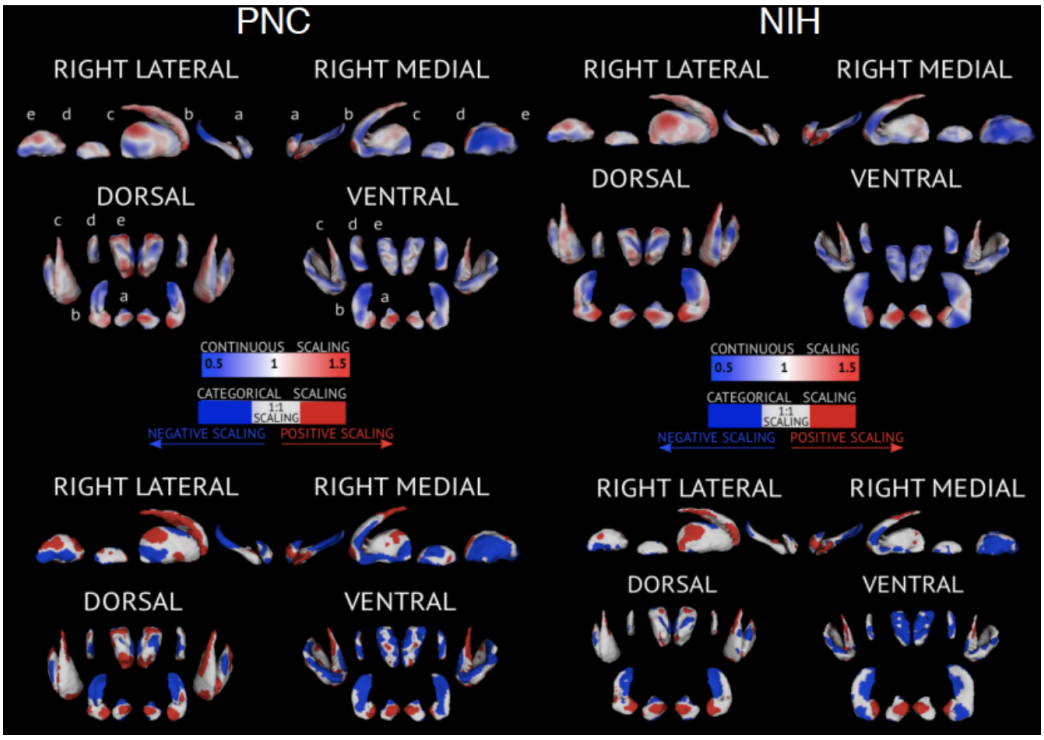


Figure 3.9: **Subcortical Scaling in Amygdala, Globus Pallidus, Hippocampus, Striatum, and Thalamus** Un-thresholded maps show how surface area at each subcortical vertex scales with naturally-occurring variations in total subcortical area: reddening indicates relative expansion in larger cortices ("positive scaling"), and blueing indicates relative contraction ("negative scaling"). Note the close correspondence between PNC and NIH scaling maps, and the tendency for neighboring facets of different subcortical structures to show similar scaling coefficients. (a) amygdala, (b) hippocampus, (c) striatum, (d) pallidum, (e) thalamus. Categorical scaling maps showing regions of statistically-significant positive and negative areal scaling (i.e. H_o: scaling coefficient=1 rejected) after correction for multiple comparisons across vertices. Subcortical patterns of non-linear areal scaling were invariant across age and sex.

Chapter 4

Assessing the Biological Significance of Cortical Areal Scaling via Spatial Permutation

4.1 Abstract

Brain size variation over primate evolution and human development is associated with coordinated changes in the proportions of different brain regions [74]. Using in vivo neuroimaging data from over 3,000 individuals, we find that larger human brains show greater areal expansion in distributed fronto-parietal cortical networks and related subcortical regions than in limbic, sensory and motor systems. This areal redistribution recapitulates cortical remodeling across evolution, manifests by early childhood in humans, and is linked to multiple markers of heightened metabolic cost and neuronal connectivity. Thus, human brain shape is systematically coupled to

naturally-occurring variations in brain size through a scaling map that integrates spatiotemporally diverse aspects of neurobiology.

4.2 Scaling and Evolution and Development

To assess the biological significance of spatially-patterned areal scaling within the human brain, we compared regional differences in cortical scaling to several independent assays of cortical organization. We first tested if patterns of cortical area redistribution as a function of normative brain size variation in humans (Fig 3.3) aligned with those that accompany evolutionary and developmental changes in primate brain size [74]. Inter-vertex scaling variations in PNC and NIH cohorts (Fig 3.3) were positively correlated with those seen in evolution and development (Figs 4.1, 4.3 Table 3.5). Original data sourced with permission from Hill et al, 2010, PNAS [74] and re-projected onto the ICBM-152 atlas surface as described in sections 2.9 and 2.10.

All three sources of primate brain size disparity (evolution, development, and naturally occurring size variation) involved disproportionate areal expansion within anterior cingulate, angular gyrus, superior parietal lobule, and lateral temporal cortex.

4.3 Scaling and Functional Networks and Cytoarchitecture

We next asked if regional differences in human cortical scaling were related to functional and microstructural topography of the human cortex. Us-

]

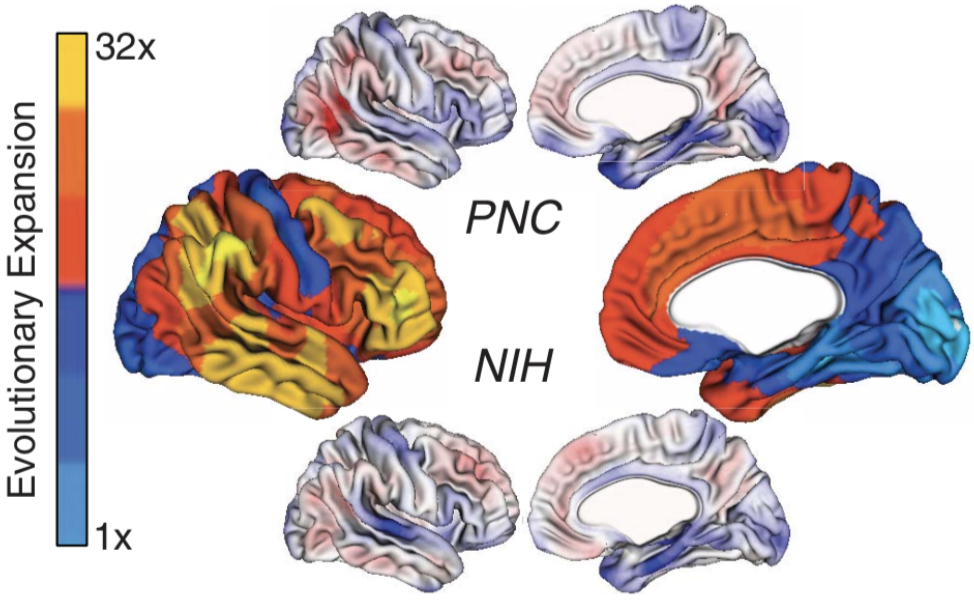


Figure 4.1: **Positive Scaling vs Focal Surface Area Changes over Evolution** Comparison of Surface Area in humans relative to macaques with PNC/NIH scaling maps for comparison. Original data sourced with permission from Hill et al, 2010, PNAS [74] and re-projected onto the ICBM-152 atlas surface as described in section 2.9.

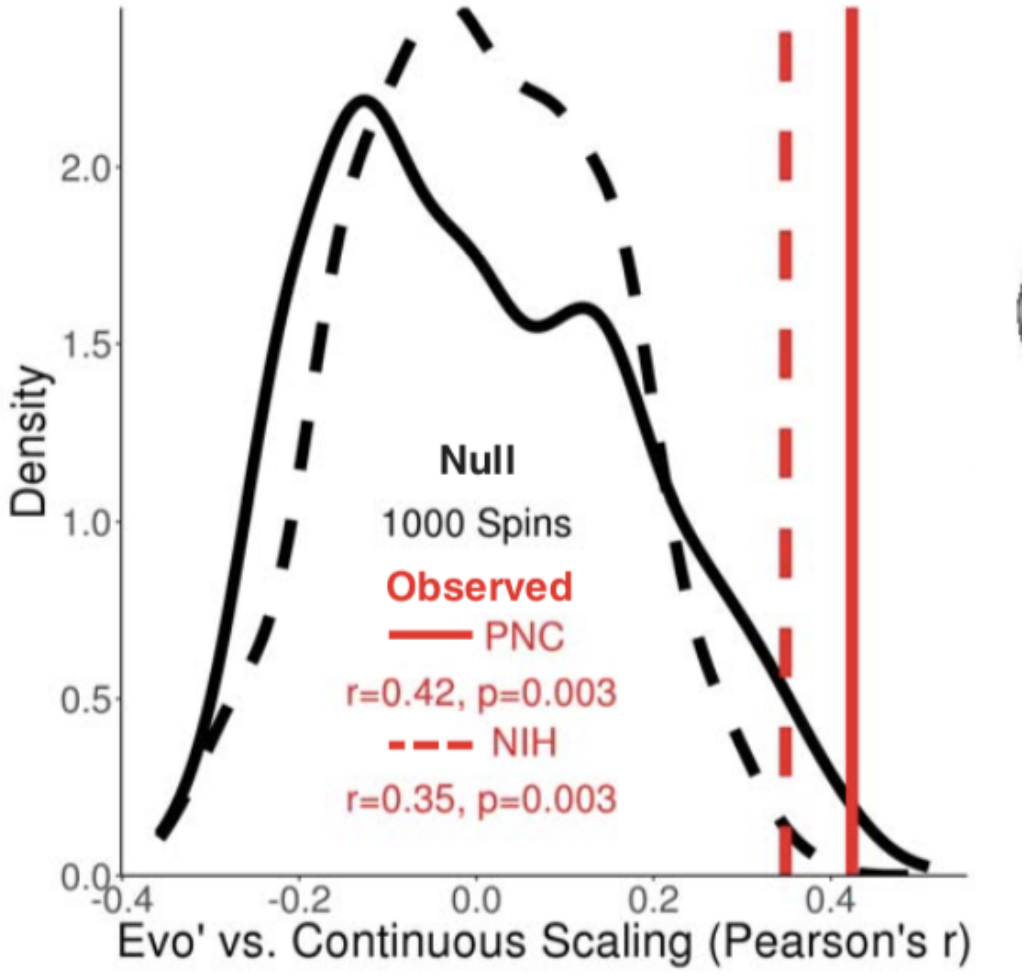


Figure 4.2: **Permutation Testing for Overlap Between Positive Scaling and Evolutionary Expansion** Density plot of permutation test for spatial similarity between positive scaling and evolutionary expansion and NIH/PNC scaling maps.

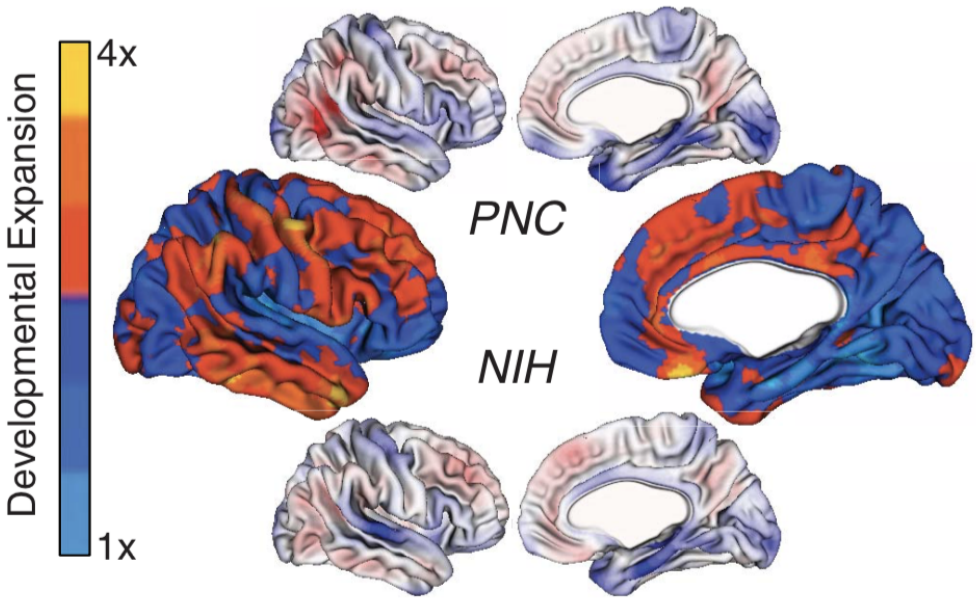


Figure 4.3: **Positive Scaling vs Focal Surface Area Changes over Development** Comparison of Surface Area in adults relative to infants with PNC/NIH scaling maps for comparison. Original data sourced with permission from Hill et al, 2010, PNAS [74] and re-projected onto the ICBM-152 atlas surface as described in section 2.10.

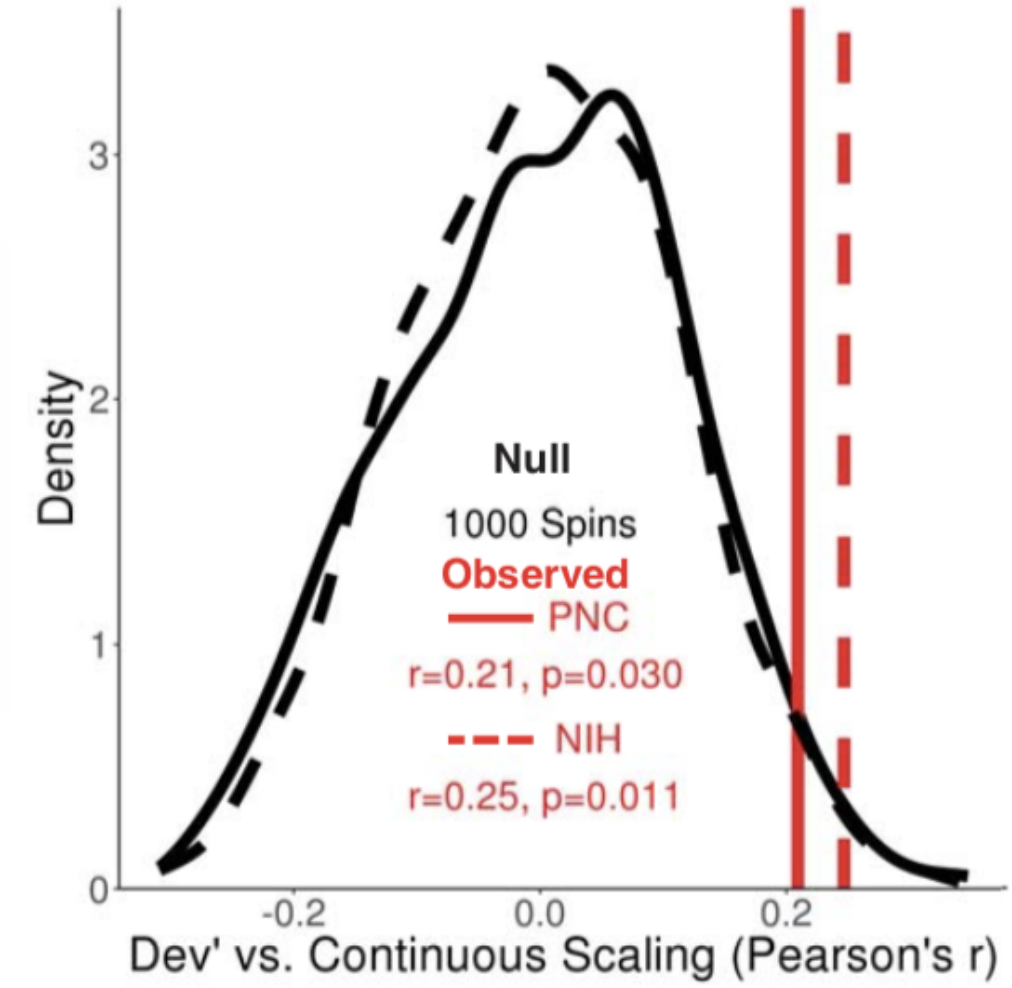


Figure 4.4: **Permutation Testing for Overlap Between Positive Scaling and Developmental Expansion** Density plot of permutation test for spatial similarity between positive scaling and developmental expansion.

ing a previously-published parcellation of the cortical sheet into 7 canonical resting-state functional connectivity networks [76], we found that (i) regions of positive scaling were concentrated within association cortices including the default mode (DMN), dorsal attention and fronto-parietal networks (p_{SPIN} = 0.001 for DMN), whereas (ii) regions of negative scaling were over-represented (p_{SPIN}= 0.007) within the limbic network (Fig 4.5). Original data sourced with permission from Yeo et al, 2011, Jnl Neurophysiology [76] and re-projected onto the ICBM-152 atlas surface as described in section 2.11.

These associations were replicated using a finer-grained functional parcellation of the human cortex [76], and indicated that larger human brains show preferential areal expansion within regions of association cortex that sit at the apex of a functional network hierarchy [91, 92] and provide high-level integration across lower systems [93]. This theme was reinforced by comparison of scaling maps with a classical parcellation of the cortex into 7 cytoarchitectonic "types" with differing laminar organizations [10]: regions of positive areal scaling were over-represented within "von Economo Type 3" cortices (Fig 4.6) that bear cytoarchitectonic specializations for long-range cortico-cortical connectivity (e.g. thickening of supragranular layers II/III). Data sourced with permission from Whitaker et al, PNAS, 2016 [77] and re-projected onto the ICBM-152 atlas surface as described in section 2.12.

Thus, regions of preferential areal expansion in larger vs. smaller human brains appeared to be both functionally and microstructurally suited to operate as hubs of information integration.

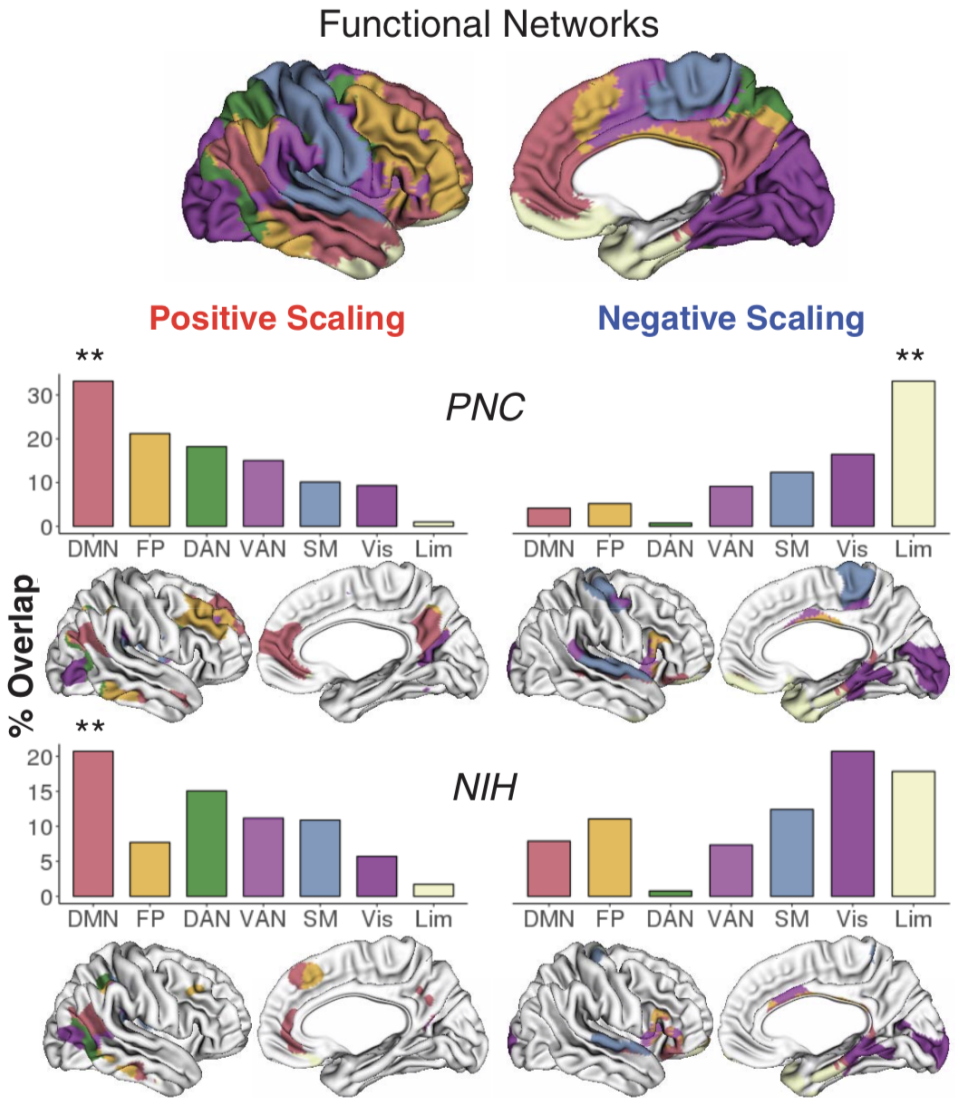


Figure 4.5: **Scaling and Function** Parcellation of cortex into 7 canonical resting state functional connectivity networks, with bar plots and conjunction maps showing differential representation of positive vs. negative scaling in each network (** p_{SPIN} <0.001, * p_{SPIN} <0.05). Regions of positive scaling localize to the default mode networks (DMN), and regions of negative scaling to the limbic network (Lim). Original data sourced with permission from Yeo et al, 2011, Jnl Neurophysiology [76] and re-projected onto the ICBM-152 atlas surface as described in section 2.11.

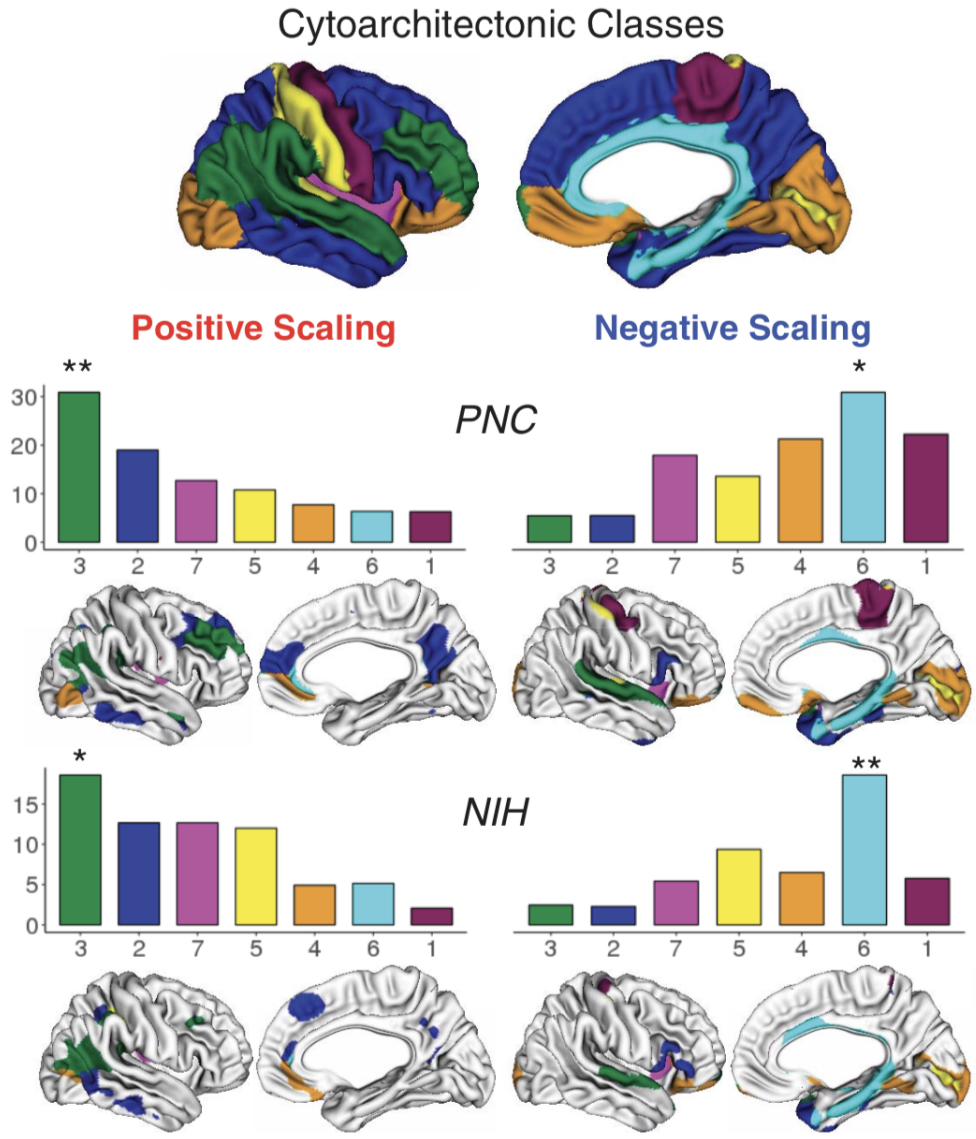


Figure 4.6: **Scaling and Cytoarchitecture** Cortical parcellation into 7 different laminar types according to a classical cytoarchitectonic atlas [10] with bar plots and conjunction maps showing that regions of positive scaling localize to von Economo Type 3 cortices, and negative to Type 6 (** p_{SPIN} <0.001, * p_{SPIN} <0.05). Data sourced with permission from Whitaker et al, PNAS, 2016 [77] and re-projected onto the ICBM-152 atlas as described in section 2.12.

4.4 Scaling, Genetics, and Metabolism

To next probe potential molecular correlates of regional differences in cortical scaling, we used a shared stereotaxic coordinate system to assign an areal scaling coefficient (Fig 3.3) to each of approximately 1940 spatially-distributed and transcriptomically-characterized cortical samples from an independent cohort of 6 adult human donors provided by the Allen Institute for Brain Science (AIBS, [28], Methods, Fig 4.7).

This data alignment allowed us to rank approximately 16,000 genes by the spatial correspondence between their expression and cortical scaling gradients in PNC and NIH cohorts — with expression of the high-ranking genes being most positively correlated with scaling. Rank-based gene ontology (GO) analysis (Methods, [85]) revealed high-ranking genes were significantly enriched for mitochondrial and synaptic GO annotations (Fig 4.8), and related processes of oxidative phosphorylation and transmembrane K+ transport.

Observed gene ranks were robust to randomly excluding up to 70% of samples per donor, and the high-rank of genes associated with mitochondrial and synaptic GO terms was lost after permutation of scaling values across AIBS samples (Methods). The positive association between areal scaling and postmortem expression of mitochondria-related genes (Fig 4.8) suggested that cortical regions which are preferentially expanded in larger vs. smaller human brains may possess a distinct energy metabolism profile.

This hypothesis was supported by convergent evidence for a statistically-significant positive association between regional differences in cortical areal scaling and regional differences in two different neuroimaging proxies for cor-

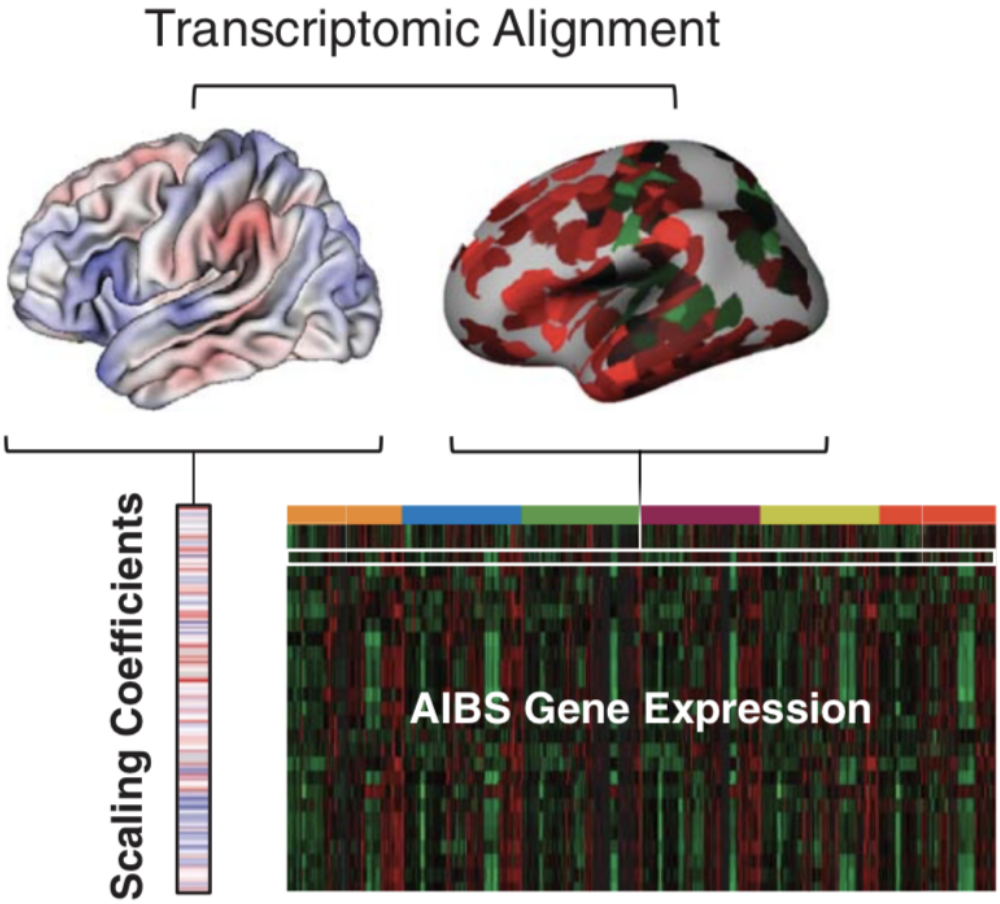


Figure 4.7: **Scaling and Genetics** Vertex scaling coefficients from PNC and NIH maps (Fig. 3.3) were uniquely assigned to each of approximately 2k cortical samples from the Allen Institute for Brain Sciences (AIBS)) by spatial proximity, allowing ranking of the approximately 16k genes measured across all AIBS samples by their spatial correlation with areal scaling.

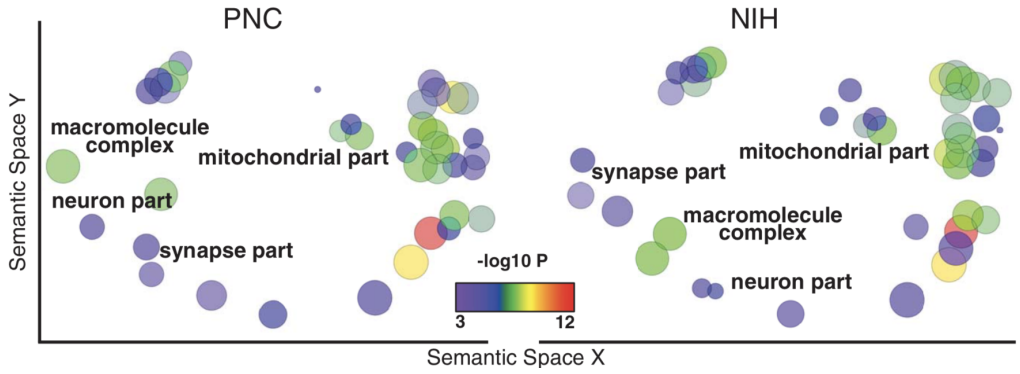


Figure 4.8: **GO Cellular Component** GO cellular component terms in semantic space showing statistically-significant enrichment of mitochondria- and synapse-related terms amongst top-ranking genes.

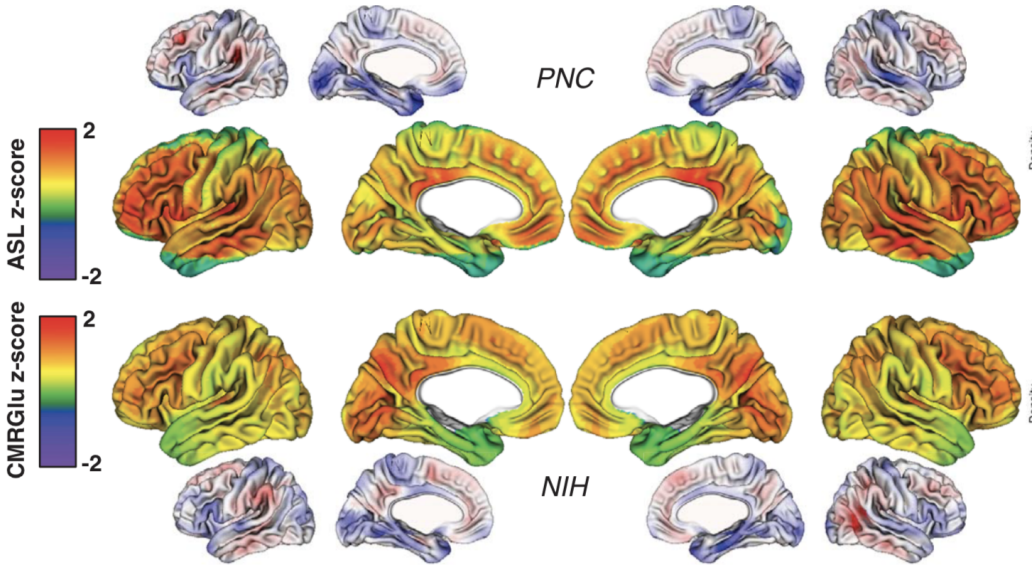


Figure 4.9: **Positive Scaling v. Glucose Metabolism and Blood Flow** Areal scaling is positively correlated with two neuroimaging-based proxies for cortical energy consumption at rest - arterial spin labeling (ASL) measures of arterial blood flow, and positron emission tomography measures of glucose uptake (CMRGlu). Data sourced with permission from Vishnavi et al, 2010, PNAS and Glasser et al, 2014, Neuroimage [78, 79] and re-projected onto the ICBM-152 atlas as described in section 2.14

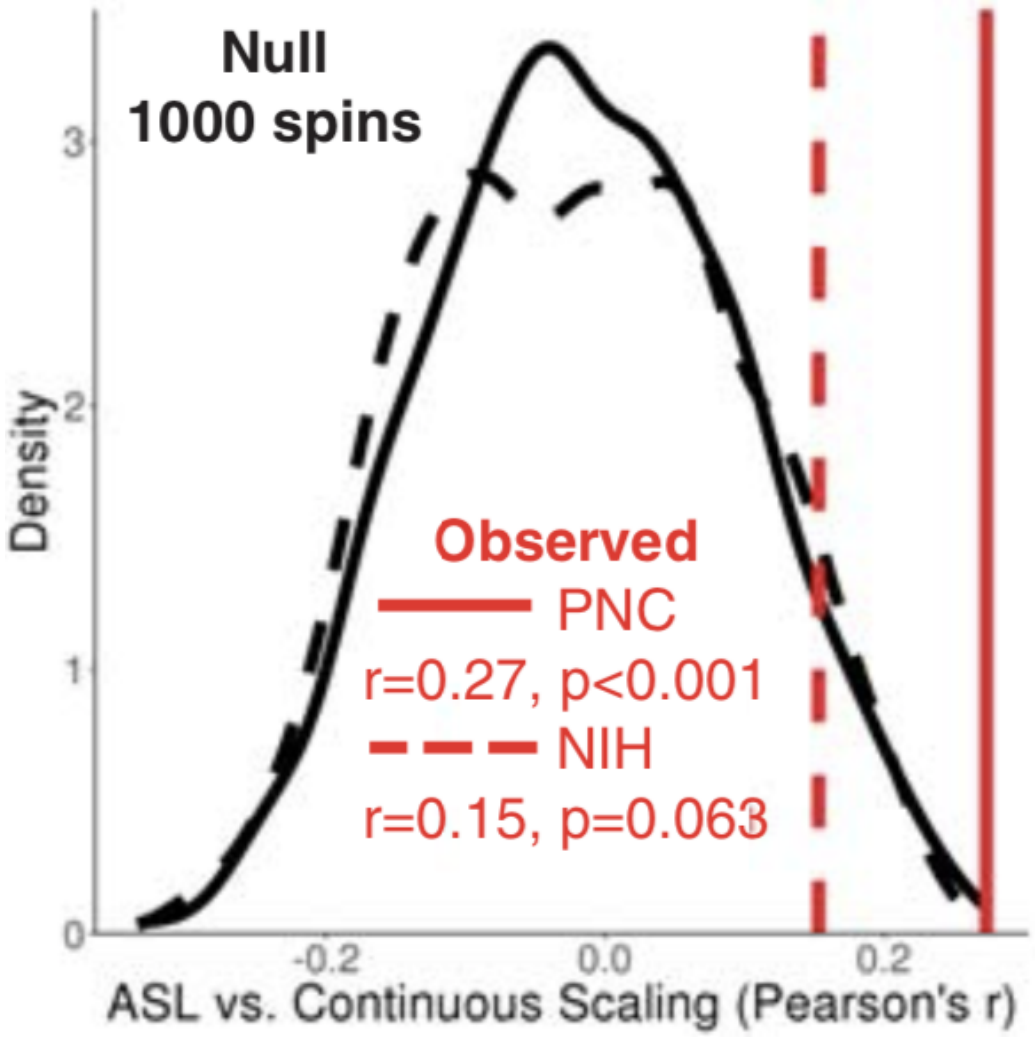


Figure 4.10: **Density Plot of Permuted Positive Scaling v. Blood Flow** PNC solid, NIH dashed, black null, red observed. Data sourced with permission Satterthwaite et al, 2014, PNAS [51] and re-projected onto the ICBM-152 atlas as described in section 2.13

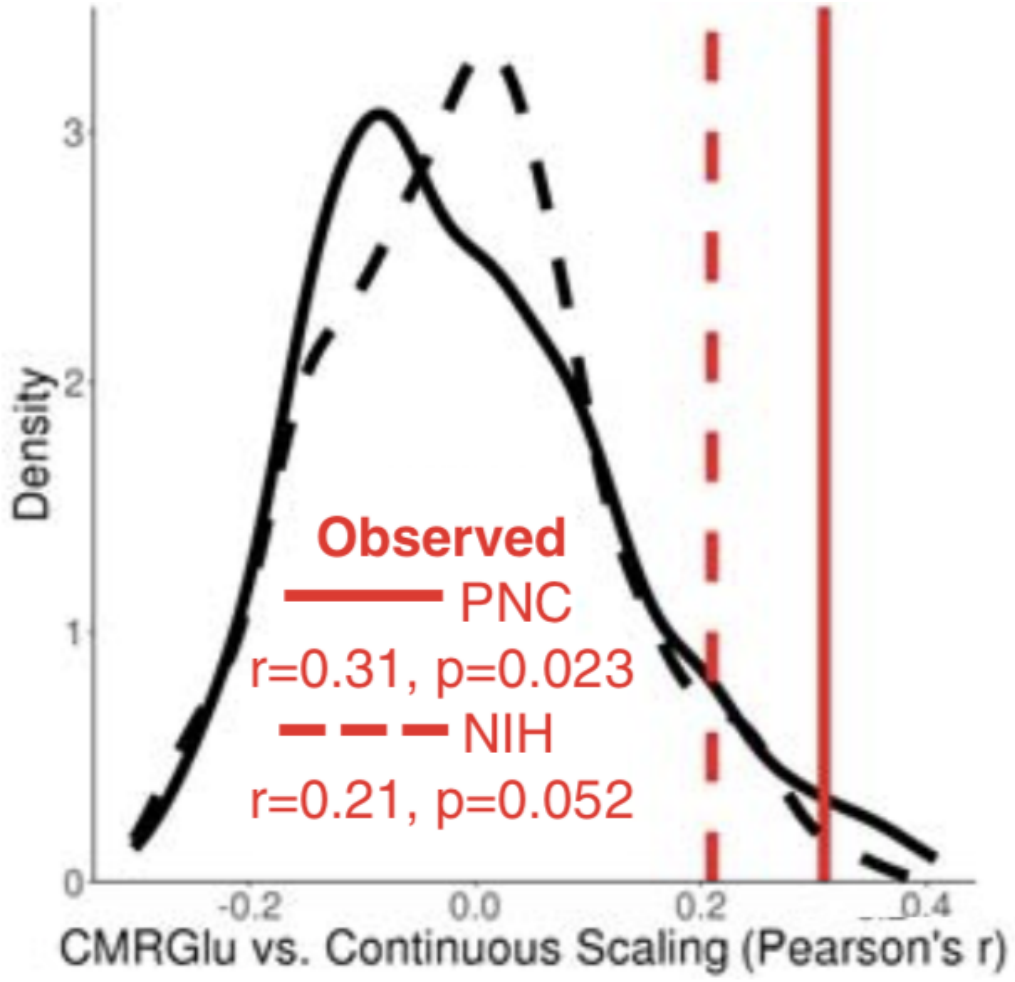


Figure 4.11: **Density Plot of Positive Scaling v. Glucose Metabolism** PNC solid, NIH dashed, black null, red observed

tical energy consumption at rest ([51, 79]; Figs 4.9 4.10, 4.11).

Our findings illuminate several aspects of cortical patterning. First, the spatial convergence of areal scaling maps across all three major axes of primate brain size variation (Figs 4.1, 4.3, 3.3) – evolution, development, and standing inter-individual variation – implies shared mechanisms for size-dependent patterning of the primate cortical sheet. These mechanisms presumably link variation in early progenitor cell proliferation to: (i) the genesis of regional differences in cellular composition during prenatal corticogenesis [94, 95], or (ii) the subsequent emergence of regional differences in cellular morphology and neuropil composition [75]. Second, the anabolic costs of tissue growth [96], and the overlap of positive areal scaling with diverse markers of biological investment (Figs 4.9), show that cortical regions that overlap with the association cortex (e.g., DMN) scale supra-linearly with overall brain volume.

Chapter 5

Scaling, Sex Differences, and Sex Chromosome Aneuploidy: Subcortical Volumes

5.1 Abstract

This chapter presents analyses on volumetric scaling amongst several adolescent patient groups — with matched controls — carrying different sex chromosome complement variations. It presents morphometric analysis of the striatum, pallidum and, thalamus — three subcortical structures salient to the coordination of movement, reward, and attention and implicated in a diverse suite of psychiatric disorders that emerge in youth and are epidemiologically enriched in individuals with supernumerary sex chromosomes. The study sample includes a large cohort of typically developing youth and multiple patient cohorts with single or multiple supernumerary sex chromosomes.

The morphometric data and sample permit both observational dissection of normative sex differences in the volume and shape of these structures in adolescence and statistical modeling of the dose-wise effect of either supernumerary sex chromosome on both sexes' subcortical neuroanatomy.

5.2 Sample Characteristics

The sample for this study included 354 individuals representing a range of karyotypes: 120 XX, 134, XY, 38 XXY, 23 XXX, 19 XYY, 15 XXYY, and 5 XXXXY. A subsample of individuals with normative sex chromosome complements (33 XX and 37 male) aged 12—14 years was excluded from statistical analysis of sex difference or sex chromosome dosage effect to construct descriptive allometric scaling norms for subcortical volume and shape at the mean age of our core sample (Table 5.1).

Continuous (e.g. age at scan) and categorical (e.g. Tanner stage — a proxy for pubertal development, see Table 5.2 [97, 98]) characteristics were compared across karyotype groups in our core sample and across sex in our non-overlapping sample of typically developing participants using omnibus Analysis of Variance (ANOVA) F-tests and Chi-squared tests respectively.

CHARACTERISTIC	CORE SAMPLE							SAMPLE FOR ALLOMETRIC ANALYSES
	XX	XY	XXX	XXY	XYY	XXYY	XXXXY	
Sample Size	87	97	23	38	19	15	5	70 (33 FEMALE / 37 MALE)
Age [yrs]								
Mean	12.75	12.94	12.98	14.15	13.56	14.98	12.85	13.04
Std Dev	4.40	4.10	6.00	4.8	5.1	5.7	4.8	0.6
Range	5.16-25.13	5.57-25.50	5.02-24.78	5.89-25.97	6.45-23.05	5.07-22.96	7.66-17.17	12.02 -13.99
Mean IQ								
Full Scale*	113.50	118.00	95.04	97.05	87.19	82.93	55.67	115.7 (12.7)
Verbal *	114.40	115.40	95.26	95.30	83.19	77.14	60.67	113.9(12.5)
Performance*	111.80	115.60	95.57	99.22	94.38	92.93	56.00	113.7 (12.5)
Social Economic Status								
Mean*	53	73	42	56	59	46	69	35.5
TANNER STAGE+								
1	19	16	5	9	6	5	2	2
2	10	16	3	6	2	2	1	8
3	17	28	6	9	6	2	1	25
4	25	16	5	6	3	5	1	29
5	13	15	4	7	2	1	0	2
Not Known	3	6	4	1	0	0	1	4

Table 5.1: **Demographics** P values reported for omnibus test of significant variation across groups in core sample. NB: p value of 0.03 for chi-squared test for non-random distribution of tanner stage between sexes in allometric sample. Females in allometric sample show an expected pubertal advancement relative to males as reflected by the distribution of Tanner stages by sex.

Tanner Scale Stages of Physical Development

Stage	Males	Females
Stage 1	Prepubertal	Prepubertal
Stage 2	Testicular volume 1.6 to 6ml; Pigmentation of scrotal sack; Downy pubic hair	Breast buds form with areolar hyperplasia ; downy pubic hair
Stage 3	Testicular volume 6 to 12ml; coarse pubic hair	Breast Tissue palpable outside areola; coarse hair
Stage 4	Testicular volume between 12 and 20ml; coarse, curly pubic hair; development of axillary hair	Areola and nipple form secondary mound; menarche begins; coarse, curly pubic hair
Stage 5	Testicular volume greater than 20ml; facial hair may appear; coarse, curly pubic hair	Breasts with single contour; coarse, curly pubic hair

Table 5.2: **Tanner Stages** Phenotypic changes associated with stages in puberty as defined by Marshall and Tanner [97, 98].

5.3 Statistical Modeling of Scaling, Sex, and Chromosome Dosage Effects on Subcortical Structure Volume

Sex and Sex Chromosome Dosage Effects on Subcortical Volume

The mean striatal, pallidal and thalamic volumes in each karyotype group within our core sample were calculated. For each structure, karyotype effects on volume were first quantified using omnibus F-tests. For structures showing a significant omnibus effect of group, follow-up post-hoc pairwise t-tests were used to clarify the pattern of volumetric group-differences. We explicitly tested for, and ruled out, significant interactions between (i) X aneuploidy status (no aneuploidy vs. supernumerary X) and gonadal sex (male vs. female), and (ii) X aneuploidy and Y aneuploidy status, using linear models in relevant subsets of our sample [(XY, XXY, XX, XXX), and (XY, XXY, XYY, XXYY) respectively].

To facilitate comparison across structures, mean structure volumes (+/- 95% CI) were plotted by karyotype group as effect-size deviations relative to volume distributions in typically developing females (XY and XXX relative to XX) or males (XX, XXY, XYY, XXYY, and XXXXY relative to XY).

Allometry of Subcortical Volumes

An independent sample of 70 typically developing individuals was used to calculate normative allometric relationships between total brain volume and the volume of each subcortical structure. For each subcortical structure, normative scaling laws were estimated using the following equation (using thalamic volume as an example):

$\log_{10}$ (Bilateral Thalamic Volume) $\sim$ ß$_0$(Intercept) + ß$_1$($\log_{10}$(TBV)) [1]

Here, ß$_1$ provides the estimated scaling coefficient linking variation in thalamic volume to variation in total brain volume. A ß$_1$ value of 1 indicates linear scaling (i.e. proportional thalamic volume remains unchanged with variations in brain size). A ß$_1$ values less than 1 denotes hypoallometric scaling (i.e. proportional thalamic volume becomes smaller with increasing brain size). Lastly, ß$_1$ values greater than 1 indicate hyperallometric scaling (i.e. proportional thalamic volume becomes larger with increasing brain size). For all three structures examined, the linear model design summarized by [1] was used after first establishing the absence of significant interactions between sex and logarithmically normalized total brain volume measurements for explaining the variance of subcortical structure volume in the study sample. For the pallidum, sex was retained as a main effect given evidence for a total brain volume invariant increase in mean pallidal volume amongst males relative to females. Next, having estimated these normative scaling laws for each subcortical structure to construct a normative framework for structure volume given a particular brain size, it was tested if the subcortical volumes observed in each karyotype group fell within the normative range

derived from the non-overlapping sample of individuals with XX and XY 23^{rd} chromosome complements. The normative framework derived from typical scaling of subcortical volumes with total brain volume was also leveraged to test if subcortical volumes in individuals with non XX and XY 23^{rd} chromosome complements in our sample represented a statistically significant disruption of the normative relationship between structure volume and total brain volume. A significant deviation from the allometrically informed normative framework was operationalized as a lack of overlap between the 95% confidence intervals for the observed and predicted mean structure volume in each karyotype group. As a comparison for these allometric analyses, we also modeled sex and sex chromosome effects on subcortical volume using the two traditional (non-allometric) approaches to accounting for brain size when studying regional brain volumes: expressing regional volumes as a ratio of TBV, and including the linear effect of total brain size as a covariate in regression analyses.

Tests for Effects of Demographic, Pubertal and Cognitive Factors

For all analyses of sex chromosome dosage effects on subcortical anatomy within our core sample, we ran additional models that confirmed robustness of our findings to inclusion of SES as a covariate. We did not co-vary for IQ in analyses of sex chromosome aneuploidy effects because (i) IQ reductions are central to the sex chromosome aneuploidy phenotype, and (ii) inclusion of IQ as a nuisance variable in regression analyses assumes the presence of

a linear relationship between IQ and brain anatomy that is invariant across karyotype groups.

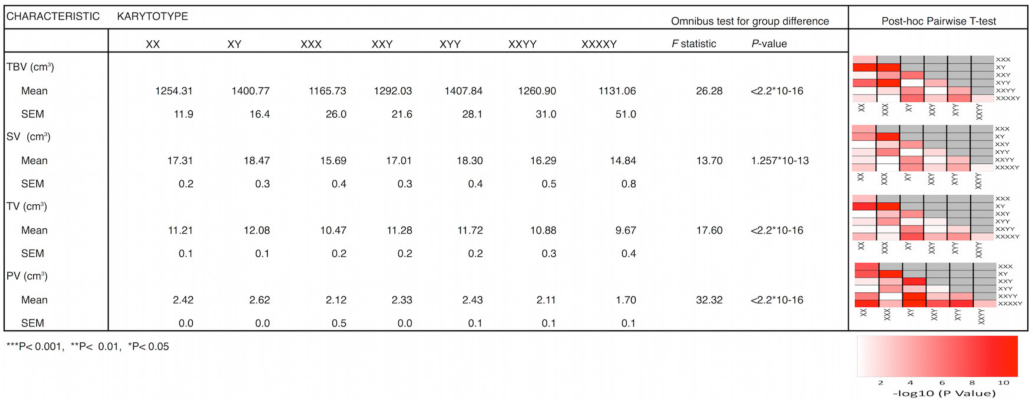
Within our non-overlapping normative sample, we ran additional models that confirmed robustness of all reported sex differences in subcortical allometry to inclusion of Tanner stage, IQ and SES as covariates.

Sex and Sex Chromosome Dosage Effects on Subcortical Volumes

Mean striatal, pallidal and thalamic volume each differed significantly across karyotype groups, as did total brain volume (Fig 5.1).

Relative to females with an XX 23^{rd} chromosome complement, males with an XY 23^{rd} chromosome complement showed increased total brain volume in addition to increased striatal, pallidal, and thalamic volumes. The effects-size for male-female differences in total brain volume was greater than the effect sizes for male-female differences in all three subcortical volumes (Figs 5.2, and 5.3).

Sex chromosome aneuploidies in individuals with both testes and ovaries were associated with large-effect size reductions in total brain, striatal, pallidal and thalamic volume (Figs 5.2, and 5.3), with the sole exception of the XYY karyotype which only resulted in a statistically significant reduction of thalamic and pallidal volume relative to XY males. Across all sex chromosome aneuploidies, effect sizes for absolute pallidal volume loss outstripped those seen in the striatum and thalamus. Supplementary analyses established



CHARACTERISTIC	KARYOTYPE							Omnibus test for group difference		Post-hoc Pairwise T-test
	XX	XY	XXX	XXY	XYY	XXYY	XXXXY	*F* statistic	*P*-value	
TBV (cm^3)										
Mean	1254.31	1400.77	1165.73	1292.03	1407.84	1260.90	1131.06	26.28	<2.2*10-16	
SEM	11.9	16.4	26.0	21.6	28.1	31.0	51.0			
SV (cm^3)										
Mean	17.31	18.47	15.69	17.01	18.30	16.29	14.84	13.70	1.257*10-13	
SEM	0.2	0.3	0.4	0.3	0.4	0.5	0.8			
TV (cm^3)										
Mean	11.21	12.08	10.47	11.28	11.72	10.88	9.67	17.60	<2.2*10-16	
SEM	0.1	0.1	0.2	0.2	0.2	0.3	0.4			
PV (cm^3)										
Mean	2.42	2.62	2.12	2.33	2.43	2.11	1.70	32.32	<2.2*10-16	
SEM	0.0	0.0	0.5	0.0	0.1	0.1	0.1			

Figure 5.1: **Nucleus Volumes In Core Sample** Group mean values, estimates of error, and omnibus test statistics for each anatomical metric were determined using $ß_1$ coefficients from the following model: nucleus volume intercept + $ß_1$(karyotype group). Color bar encodes level of statistical significance for the cross-tabulated post-hoc pairwise comparisons.

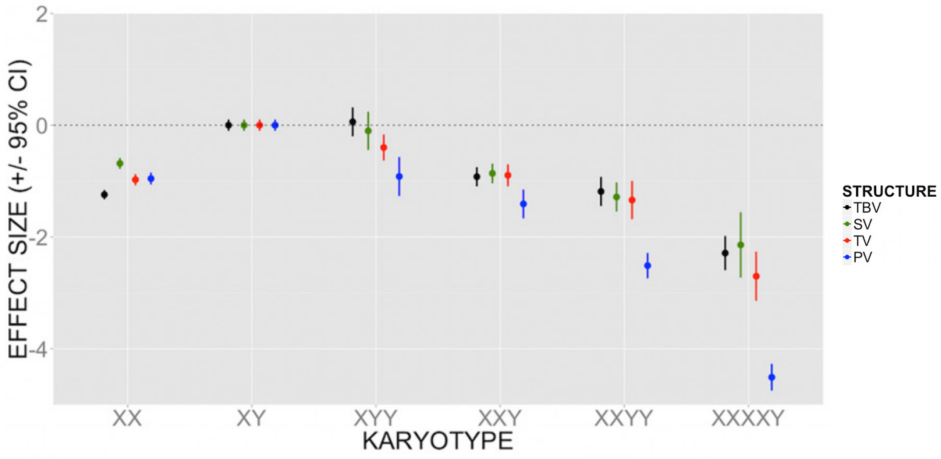


Figure 5.2: **Subcortical Nuclei Volumes across Aneuploidy Karyotypes vs Individuals with XY 23rd Comment Chromosome Complement** Total brain volume, striatal volume, thalamic volume, and pallidal volume in karyotype groups expressed as mean (with 95% confidence intervals) effect-size deviations according to observed distribution in males

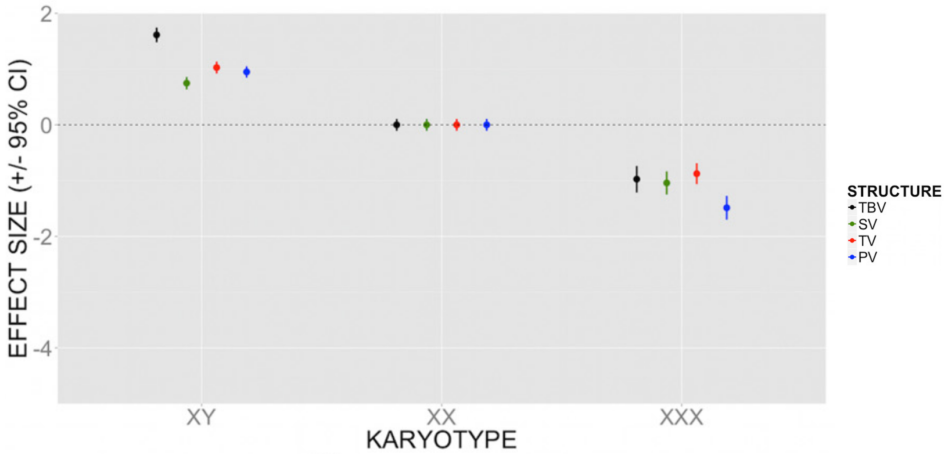


Figure 5.3: **Subcortical Nuclei Volumes across Aneuploidy Karyotypes vs Individuals with XX 23rd Comment Chromosome Complement** Total brain volume, striatal volume, thalamic volume, and pallidal volume in karyotype groups expressed as mean (with 95% confidence intervals) effect-size deviations according to observed distribution in females

that the effects of X-chromosome aneuploidy were not modified by gonadal sex (p values for global and regional anatomy were all greater than 0.6 for the interaction between X-chromosome supernumeracy and sex using the XX, XXX, XY, XXY participant subset), or Y-chromosome aneuploidy (p values for global and regional anatomy contrasts were all greater than 0.2 for the interaction between X-chromosome and Y-chromosome supernumeracy using the XY, XXY, XYY, XXYY subset).

Our findings replicate previous reports that typically-developing males show greater mean total brain, striatal, pallidal and thalamic volume than females [39, 40], and further establish that the effect-size magnitude of these volume differences is greatest for total brain volume, intermediate for thalamic volume and pallidal volume, and least for striatal volume.

Supernumerary X- and Y-chromosomes were both associated with subcortical volume reductions. This observation contrasts with the divergent supernumerary X- and Y-chromosome effects on cortical volume [45], and suggests that normative sex-differences in subcortical volume are unlikely to arise through differential X- and Y-chromosome complement. Consistent with this inference, the profile of total brain volume, striatal volume, pallidal volume and thalamic volume change seen in individuals with supernumerary X- or Y-chromosomes does not recapitulate the profile of volume differences seen across these structures between typically-developing males and females.

5.4 Allometry of Subcortical Volumes

Our models of normative subcortical volume scaling revealed that striatal, pallidal and thalamic volume all show hypoallometric scaling with total brain volume in health (Table 5.3) meaning that across individuals, larger brains have proportionally smaller subcortical volumes than smaller brains. The magnitude of this hypoallometric scaling was significantly more marked for pallidal volume compared with thalamic and striatal volume. None of the three structures studied showed sexually-dimorphic scaling with total brain volume, although males showed a statistically significant "offset" (increase) in pallidal volume relative to females.

Comparison of observed subcortical volumes in individuals with supernumerary sex chromosomes relative to the predictions of normative brain allometry (Fig 5.4) indicated that the extent of pallidal volume reduction in all sex chromosome aneuploidies significantly outstripped what would be predicted from changes in brain size alone.

On the other hand striatal and thalamic volume reductions showed a trend towards being disproportionately large in XYY (thalamus), XXYY (thalamus and striatum) and XXXXY (thalamus and striatum) groups relative to observed changes in total brain volume without reaching statistical significance (Figs 5.6, 5.5).

In keeping with our observation that the volume of all three subcortical structures studied scaled in a non-linear fashion with total brain volume, we found that classical methods of "controlling for" total brain volume differences — which both assume linear scaling between regional volumes and total

STRUCTURE	NORMATIVE SCALING COEFFICIENTS	
	Allometric Coefficient (+/-95%CI)	Male Intercept Offset (+/-95%CI)
Striatum	0.74 (+/-0.188)**	-------
Pallidum	0.37 (+/- 0.2231)***	0.022 (+/- 0.019)*
Thalamus	0.77 (+/- 0.119)***	-------

***P< 0.001, **P< 0.01, *P< 0.05

Table 5.3: **Normative scaling of subcortical volumes in health**. Allometric coefficients, male-related intercept offset, and associated P values for the scaling of each subcortical nucleus volume with TBV as significantly different from 1.

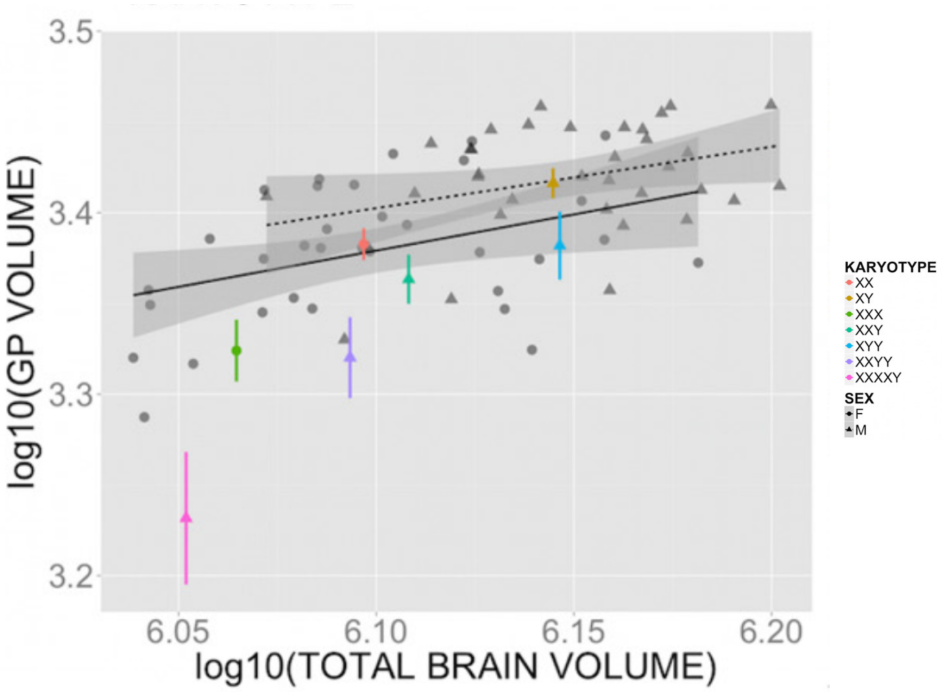


Figure 5.4: **Normative Globus Pallidus Scaling and the Effect of Sex Chromosome Aneuploidy** Globus Pallidus volume in our core sample in the context of normative brain allometry. Gray points and fit-lines (see Table 5.3 for associated coefficients) show the log-log relationship between total brain volume and pallidal volume in an independent sample of typically-developing males and females. Super-imposed points show observed distributions of pallidal volume at mean total brain size for each karyotype group within our core sample.

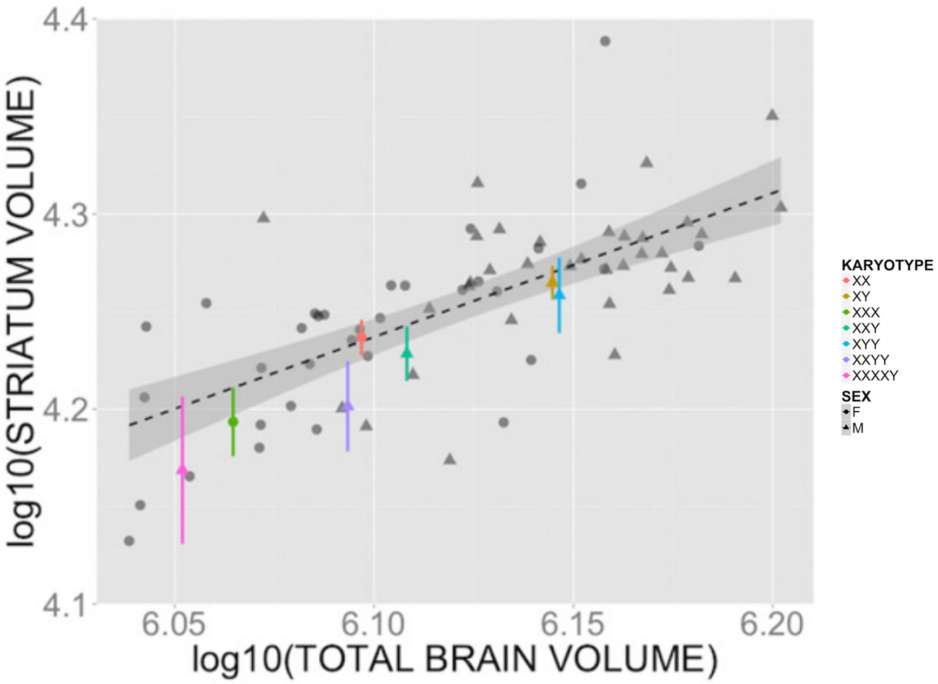


Figure 5.5: **Normative Striatum Scaling and the Effect of Sex Chromosome Aneuploidy** Striatum volume in our core sample in the context of normative brain allometry. Gray points and fit-lines (see Table 5.3 for associated coefficients) show the log-log relationship between total brain volume and pallidal volume in an independent sample of typically-developing males and females. Super-imposed points show observed distributions of striatal volume at mean total brain size for each karyotype group within our core sample.

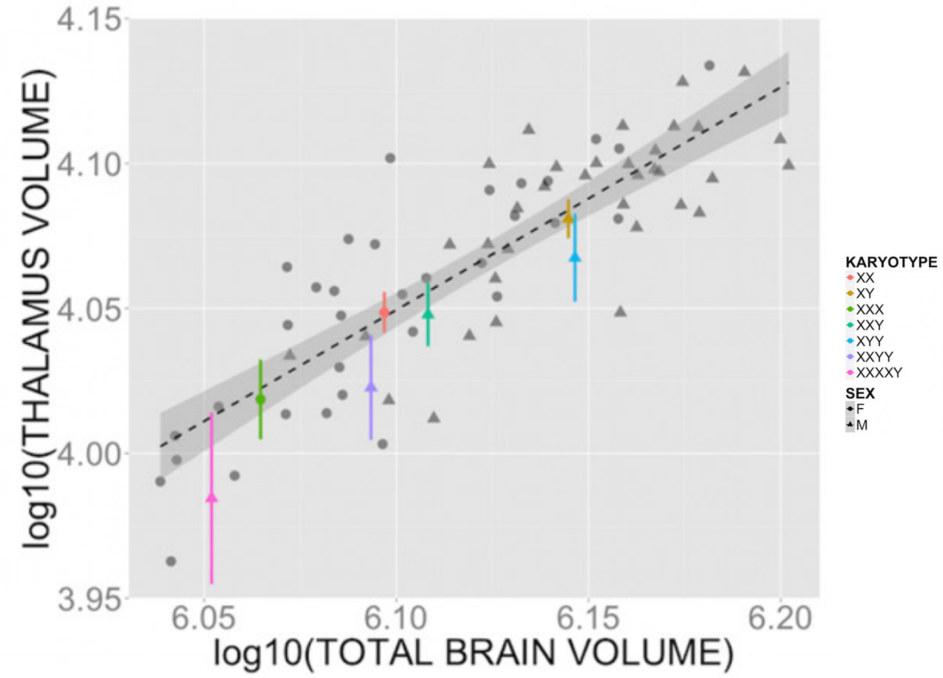


Figure 5.6: **Normative Thalamus Scaling and the Effect of Sex Chromosome Aneuploidy** Thalamus volume in our core sample in the context of normative brain allometry. Gray points and fit-lines (see Table 5.3 for associated coefficients) show the log-log relationship between total brain volume and pallidal volume in an independent sample of typically-developing males and females. Super-imposed points show observed distributions of thalamic volume at mean total brain size for each karyotype group within our core sample.

brain volume — conflated the effects of non-linear scaling with the effects of sex and sex chromosome aneuploidy on subcortical anatomy.

	vs. XX		vs. XY			
	XY	XXX	XXY	XYY	XXYY	XXXXY
STRIATUM						
Normalization	↓	-	-	-	-	-
Covarying	-	↓	-	-	↓	-
Allometry	-	-	-	-	-	-
THALAMUS						
Normalization	↓	-	-	↓	-	-
Covarying	-	-	-	↓	↓	↓
Allometry	-	-	-	-	-	-
PALLIDUM						
Normalization	↓	↓	↓	↓	↓	↓
Covarying	↑	↓	↓	↓	↓	↓
Allometry	↑	↓	↓	↓	↓	↓

Table 5.4: **Comparing different methods of controlling for brain size in analysis of subcortical volume**. Subcortical volumes were compared between each SCA group and their "gonadal control" using three different methods to control for total brain size variation: Normalizing by total brain volume, co-varying by total brain volume, and using our new allometric framework. Arrows indicate presence and direction of statistically significant group difference in the volume of each structure at $p < 0.05$.

Chapter 6

Scaling, Sex Differences, and Sex Chromosome Aneuploidy: Subcortical Surface Area

6.1 Abstract

In this chapter, normative scaling rules are leveraged to normalize for differences in brain and structure size in the analysis of group-wise focal surface area differences in the striatum, globus pallidus, and thalamus among sex chromosome aneuploidy karyotypes. Expansion or contraction in focal surface area of a structure is interpreted here as a change in structural shape. All analyses were performed in the same cohort as before, viz. 354 youth with varying karyotypes (XX, XY, XXX, XXY, XYY, XXYY, XXXXY). Large effect-size differences in the shape of all three structures are detected as a function of sex and sex chromosome dosage — namely, supernumer-

ary X- and Y-chromosomes are associated with coordinated deformations of striato-pallidal shape.

6.2 Statistical Modeling of Scaling, Sex, and Chromosome Dosage Effects on Subcortical Structure Shape

Normative sex-differences in subcortical shape between the XX and XY participants in the sample were estimated by testing for sex differences in surface area at all subcortical vertices using the following model:

Vertex Area $\sim$ ß$_0$(Intercept) + ß$_1$(age – mean age) + ß$_2$(Sex) [1]

Regions showing significant sex-differences in subcortical shape were visualized by projecting vertex-wise ß$_2$ coefficients from the above model onto subcortical surfaces after applying a False Discovery Rate correction for multiple comparisons [99] with q (the expected proportion of falsely rejected null hypotheses) set at 0.05. Model design equation [1] was applied at all vertices after first testing for and ruling out statistically significant interactions between age and sex in predicting vertex area.

To provide an independent yet complementary view of sex differences in subcortical shape that accounts for sex differences in the overall size of each structure, the following vertex-wise analysis was performed within our non-overlapping allometric sample of typically-developing controls (using the striatum as an example):

Log_{10}(vertex area) $\sim$ ß$_0$(Intercept) + ß$_1$($\log_{10}$(Total Bilateral Striatal Sur-

face Area) + ß$_2$(Sex) [2]

The ß$_2$ coefficient was visualized after correction for multiple comparisons, and identified regional sex differences in subcortical shape that exist above and beyond sex differences on overall subcortical size.

Next, to map the areal sensitivity of subcortical shape to sex chromosome dosage effects, vertices were grouped and defined based on the condition that they shared a common pattern of areal response to the variations in X- and Y-chromosome dosage in our sample. To achieve this, mean vertex-wise SA measures in each SCA group were re-expressed as effect-size deviations from SA distributions at homologous vertices in the appropriate gonadally-matched control group (i.e. XXX mean against the XX distribution / XXY, XYY, XXYY, and XXXXY means against the XY distribution). These steps resulted in a matrix of 21156 rows (all subcortical vertices) and 5 columns (effect-size for SA in each SCA group vs. its gonadal control). This matrix was then submitted to a k-means partitioning algorithm [‘”kmeans” function in the R language and environment for statistical computing [68] (with iter.max and nstart set at 100)], and an optimal 4-cluster solution was indicated by visual inspection of a scree-plot charting reduction in the mean within-partition sums of squares against increasing partition number. Vertex-wise cluster designations according to this four-class solution were visualized on exemplar subcortical surfaces using color codes. A Chi-squared analysis was used to quantitatively describe the non-random distribution of clusters across subcortical nuclei.

The above approach was adopted to provide an integrated picture of SCA effects on subcortical anatomy. Supplementary vertex-wise group contrasts

between each SCA and their gonadal control (using an identical approach to that detailed in model equation [2] above) identified statistically significant effects of each separate SCA on regional subcortical anatomy that corroborated the integrated summary provided by k-means analysis.

6.2.1 Allometry of Subcortical Shape

The same independent sample of 70 typically developing controls used to model normative allometry of subcortical volume was used to estimate structure-specific allometric scaling laws for all four subcortical partitions defined by k-means analysis above. These normative scaling laws were estimated in a step-wise manner for each unique cluster-structure pairing. Significant sex-differences in normative allometry were tested for by using the following equation:

$\log_{10}$ (K cluster area) $\sim$ Intercept + ß$_1$($\log_{10}$(Total Bilateral Surface Area)) + ß$_2$(SEX) + ß$_3$(SEX*$\log_{10}$(Total Bilateral Surface Area)) [4]

For cluster-structure pairings where the ß$_3$ terms failed to reach statistical significance, model design was developed by the backward selection procedure by stepping-down to the following equations, depending on the presence/absence (equation [5]) / equation [6] respectively) of a statistically significant main effect of sex:

$\log_{10}$ (K cluster area) $\sim$ Intercept + ß$_1$($\log_{10}$(Total Bilateral Surface Area)) + ß$_2$(SEX) [5]

$\log_{10}$ (K cluster area) $\sim$ Intercept + ß$_1$($\log_{10}$(Total Bilateral Surface Area)) [6]

Finally, in a manner analogous to that used for subcortical volumes, we assessed if observed cluster areas in each group of individuals with supernumerary sex chromosomes were congruent with what would be expected given the observed change in the overall size (Total Bilateral Surface Area) of each subcortical structure and the cluster-specific allometric relationships defined above.

6.3 Sex and Sex Chromosome Dosage Effects on Subcortical Shape

Vertex-wise analyses of sex-differences in local subcortical surface area indicated that the subcortical volumetric increases observed in males with an XY 23^{rd} chromosome complement relative to females with an XX 23^{rd} chromosome complement were not associated with even areal expansion throughout each subcortical structure studied (Fig 6.1).

A set of bilaterally symmetric subcortical regions failed to show significant areal expansion in males relative to females, including rostromedial facets of the caudate body, the rostral putamen, rostral pallidum, and both para-ventricular and dorsal facets of the thalamus. Conversely, regions of statistically-significant subcortical areal expansion in males relative to females were not homogeneous in the observed magnitude of areal sex-differences: notable "hotspots" of areal expansion in males vs. females included the ventral striatum and dorso-caudal putamen, dorsal pallidum and ventral thalamus. Reanalyzing sex differences in subcortical shape while ac-

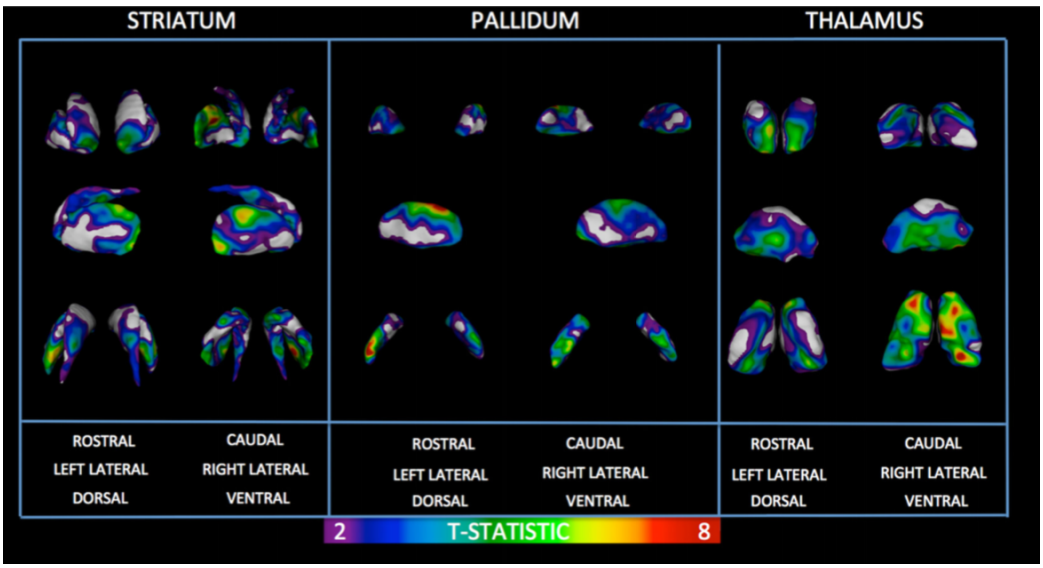


Figure 6.1: **Normative Sex Differences in Striatal, Pallidal and Thalamic Shape** Colored regions denote significant areal expansion in males relative to females after FDR correction for multiple comparisons. Warmer colors denote more pronounced areal expansion in males. Grey regions denote regions of statistical areal equivalence between males and females. There were no regions of significant areal contraction in males relative to females.

counting for sex differences in subcortical size within our non-overlapping sample of typically-developing controls (Fig 6.2) identified (i) regions of relative areal expansion in males that overlapped with several "hotspots" where absolute subcortical area was most dramatically increased in males vs. females within our core sample, and (ii) regions of relative areal expansion in females that overlapped with areas where absolute surface area did not differ between males and females in our core sample despite significant sex differences in overall subcortical size.

The k-means partitioning algorithm used to map sex chromosome effects on subcortical shape identified four spatially distributed yet bilaterally symmetric subcortical domains with different anatomical responses to changes in X- and Y-chromosome dosage (Fig. 6.3, 6.4). The "blue cluster" — spanning the caudate tail and dorsal thalamus — exhibited significant areal expansion in SCA groups relative to their gonadally matched controls. In contrast the "cyan cluster" — spanning the caudate body, nucleus accumbens and ventromedial thalamus — showed a smaller and less consistent areal response to changes in X- and Y-chromosome dosage across groups. All remaining subcortical regions fell within yellow and red clusters.

Both these clusters showed robust areal contraction in all sex chromosome aneuploidy groups relative to gonadal controls, but these reductions were most pronounced within the red cluster, which encompassed rostroventral regions of the striatum, neighboring facets of the pallidum and the lateral thalamus. These four clusters were not evenly distributed across all three subcortical structures: the blue cluster was relatively enriched in the striatum and completely absent from the pallidum; the cyan cluster was enriched

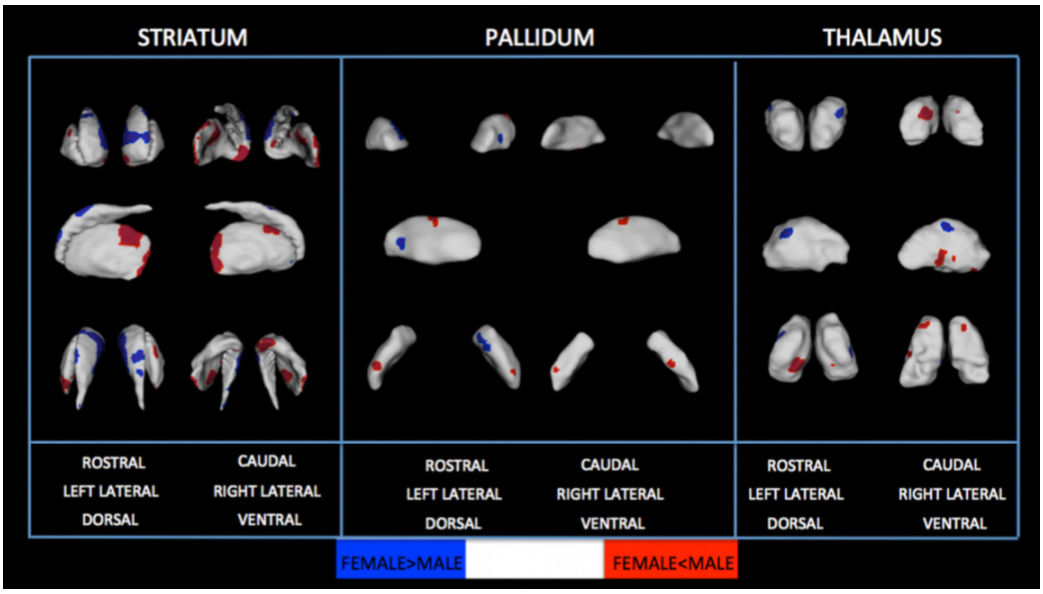


Figure 6.2: **Normative Sex Differences Accounting for Allometry** Red regions denote significant local expansion in males relative to females given overall nucleus size changes after FDR correction for multiple comparisons. Blue regions denote significant local expansion in females relative to males given overall nucleus size changes after FDR correction.

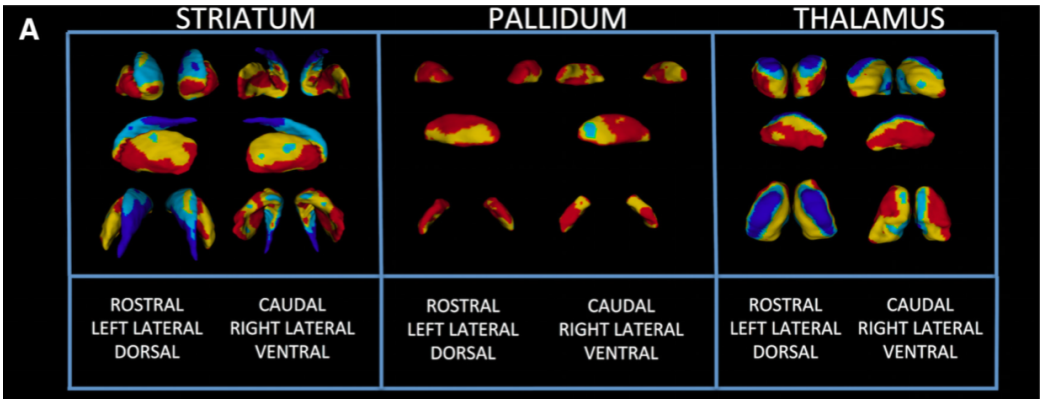


Figure 6.3: **Sex Chromosome Dosage Effects on Striatal, Pallidal and Thalamic Shape** Vertex-wise maps vertex color distinguishes four spatially-distributed subcortical domains with differing patterns of shape-change in response to sex chromosome aneuploidy. Blue domains are regions that show areal expansion in all SCA groups relative to their respective gonadal control groups. The Cyan domain shows smaller and less consistent areal changes with SCA. Remaining subcortical facets fall into a Yellow domain of intermediate areal contraction with SCA or a Red domain of more marked areal contraction with SCA.

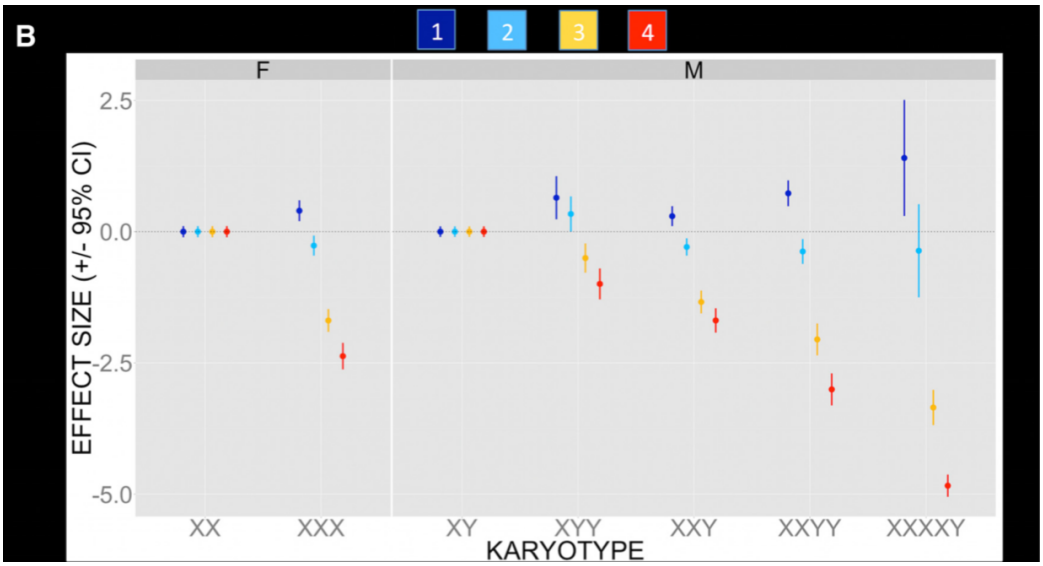


Figure 6.4: **Point Range Plot of Surface Area for Each Domain by SCA Group** The mean area of each color-coded domain in each SCA group – expressed as a standard deviation relative to that domain's area in controls.

in the striatum and thalamus but underrepresented in the pallidum; while the yellow and red cluster were relatively enriched within the thalamus and pallidum (Table 6.1).

6.4 Allometry of Subcortical Shape

Given the significant effects of sex and supernumerary sex chromosome dose on the overall size of each subcortical structure (Figs 5.2, 5.3), the regionally specific effects of these factors on subcortical shape (Fig 6.4) could potentially be wholly reflective of regional differences in the normative allometry of each subcortical nucleus. To examine this possibility, we constructed normative scaling laws to describe how the relative size of each k-means cluster varied with the total size of each subcortical structure in health (Fig 6.5). Comparison of the observed effects of supernumerary sex chromosome dose on regional subcortical area with regional areal changes predicted from normative allometry revealed that only a subset of regional SCA effects on subcortical shape reflected unexpected deviations from what would be predicted by normative allometry alone: XXX, XXY, XXYY and XXXXY effects on the area of blue and red domains within the striatum and thalamus.

Our models of normative allometry within each k-means cluster also pointed towards regionally heterogeneous scaling of subcortical shape in health (Table 6.2). For example, blue and cyan clusters within the striatum and thalamus all showed disproportionate areal expansion with increasing structure size. In contrast, red clusters in the striatum and thalamus became proportionally smaller with increasing structure size. We also noted that nor-

STRUCTURE	CLUSTER			
	BLUE	CYAN	YELLOW	RED
Striatum	8.34	15.01	-8.14	-9.39
Pallidum	-17.54	-22.83	-0.57	29.62
Thalamus	3.25	-0.79	9.2	-10.57

Table 6.1: **Standardized Residuals for Vertex Counts in Each Pairing of Structure and K-means Cluster**. The Striatum is enriched for blue and cyan clusters, the thalamus is enriched for blue and yellow clusters, and the pallidum is enriched for the red cluster

mative scaling relationships within cyan and red clusters of the thalamus were sexually dimorphic such that the observed deviations from isometric scaling within these regions were less pronounced in males than females. Finally, our sample of typically-developing males and females showed baseline differences in the proportional size of each cluster within the striatum: blue and cyan clusters were relatively smaller in males than females across all striatal sizes, whereas yellow and red clusters were proportionally larger in males.

6.5 Sex and Sex Chromosome Effects on Local Subcortical Anatomy

These vertex-wise analyses show that greater striatal volume, thalamic volume, and pallidal volume in males relative to females are not associated with evenly-distributed sex differences in subcortical surface area. Specifically, subcortical regions of areal sex-equivalence include the caudate head, ventral putamen, neighboring rostral facets of the lateral and medial pallidum, and dorso-medial regions of the thalamus; whereas, regions of prominent areal expansion in males include the ventral striatum, the mid-tail of the caudate, dorsal putamen and pallidum, as well as rostral and ventral facets of the thalamus. It is notable that striato-thalamic regions that are statistically indistinguishable between males and females share functional associations with orbitofrontal and lateral prefrontal cortices, whereas regions of pronounced areal increase in males vs. females show strongest functional connectivity with cingulo-opercular and motor cortices [100, 101].

CLUSTER	STRUCTURE		
	Striatum		
	Allometric Coefficient(+/-95%CI)	Male Intercept Offset (+/-95%CI)	Male Slope (+/-95%CI)
Blue	1.53 (+/- 0.224)***	-0.02 (+/- 0.014)**	-------
Cyan	1.38 (+/- 0.139)***	-0.02 (+/- 0.008)***	-------
Yellow	0.77 (+/- 0.071)***	0.01 (+/- 0.004)***	-------
Red	0.79 (+/- 0.107)***	0.01 (+/- 0.007)**	-------
	GP		
	Allometric Coefficient(+/-95%CI)	Male Intercept Offset (+/-95%CI)	Male Slope (+/-95%CI)
Blue	-------	-------	-------
Cyan	1.17 (+/- 0.382)	-------	-------
Yellow	0.95 (+/- 0.072)	-------	-------
Red	1.03 (+/- 0.040)	-------	-------
	Thalamus		
	Allometric Coefficient(+/-95%CI)	Male Intercept Offset (+/-95%CI)	Male Slope (+/-95%CI)
Blue	1.24 (+/- 0.456)	-------	-------
Cyan	1.27 (+/- 0.224)*	-------	0.85 (+/- 0.370)*
Yellow	0.98 (+/- 0.153)	-------	-------
Red	0.78 (+/- 0.142)**	-------	1.09 (+/- 0.233)*

* P <0.05, **P<0.01, ***P<0.001

Table 6.2: **Scaling of Regional Subcortical Area with Overall Structure Size in Health**. Allometric coefficients for each unique structure-cluster pairing show how regional surface areas change with the overall size of each subcortical structure. Additional coefficients are provided for clusters that show a statistically significant fixed male intercept offset (+/- 95% CI) or allometrically-varying male slope (+/- 95% CI) sex-difference in size.

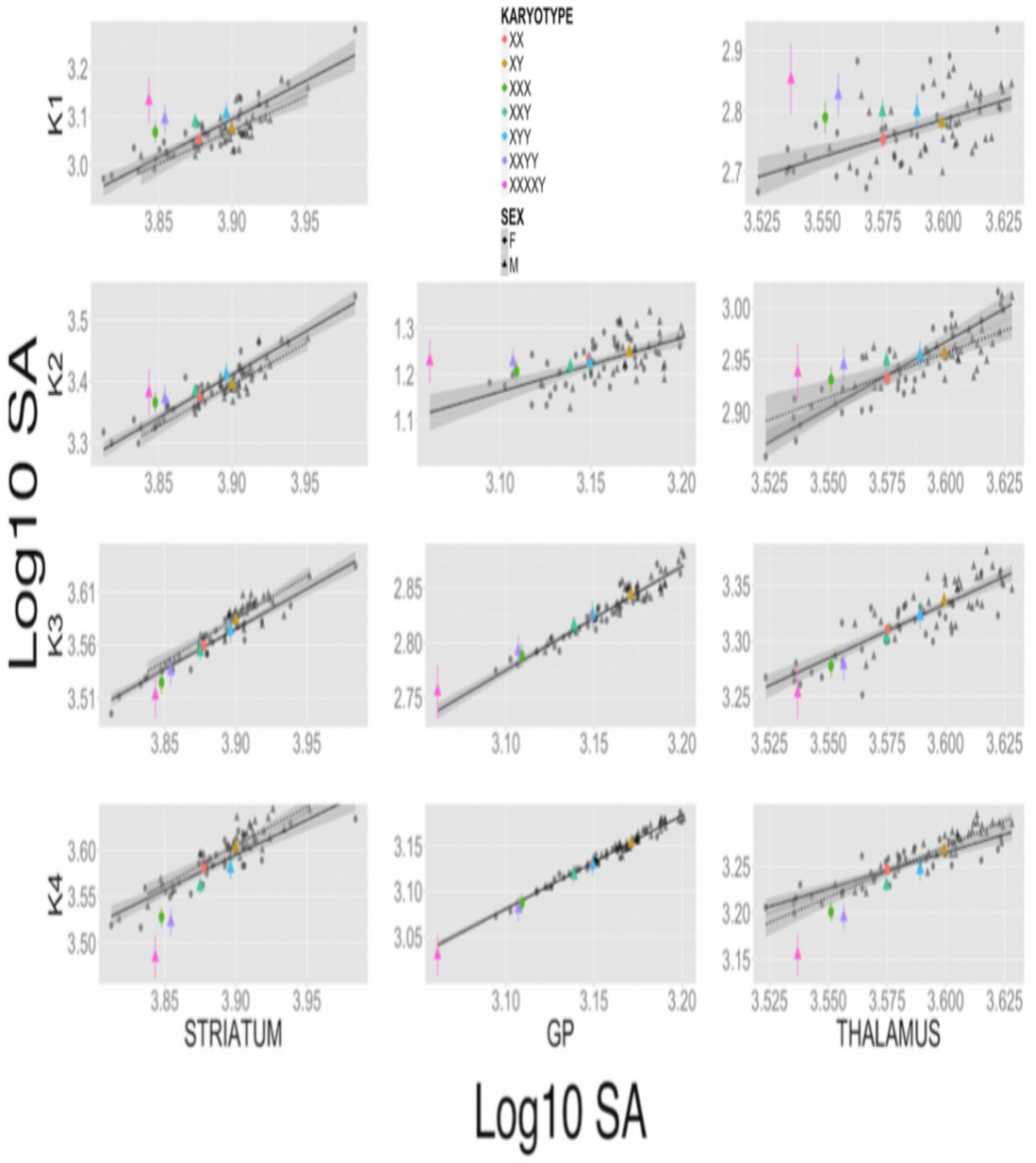


Figure 6.5: **Regional Allometry of Subcortical Shape by K-means Clusters** These scatterplots display observed distributions of regional k-means group surface area (SA) relative to total SA of its respective nucleus for all karyotypes within our core sample (color-coded), relative to scaling relationships observed in an independent sample of typically developing controls (sex shape coded) with annotations for sex-effect in intercept and slope.

K-means partitioning of effect size differences among groups with atypical sex chromosome complements also demonstrates regionally specific supernumerary sex-chromosome dosage effects on subcortical shape. Using a fully data-driven method, four subcortical domains may be distinguished with differing responses to supernumerary sex chromosome dose. Without any a priori spatial constraints, the subcortical domains detected by our method (i) show striking bilateral symmetry, (ii) integrate neighboring facets across different structures (e.g. blue domains in caudate tail and dorsal thalamus, see Fig. 6.1) and (iii) define a ventro-dorsal gradient of X- and Y-chromosome dose effects on striatal and thalamic surface area that recapitulates a major topographic axis of cortico-striato-thalamic connectivity [102, 103, 100].

X- and Y-chromosome dose have similar areal effects to each other within blue, yellow and red subcortical domains — with greater sex-chromosome dose imparting greater anatomical changes in each domain. Thus, in keeping with our previous study of cortical anatomy in SCA [45], the present study identifies convergent X- and Y-chromosome effects on regional subcortical anatomy. Our data hint at a possible alignment between the spatial patterning of SCA effects on cortical and subcortical anatomy. For example, available maps of functional connectivity between the human caudate and cortex [100, 101] pair subcortical and cortical regions which we find have shared anatomical vulnerability (anterior cingulate, caudate head or resilience (dorsolateral prefrontal cortex , caudate body) to SCA effects. Coherence between the spatial patterning of SCA effects within and between cortical and subcortical structures provides a candidate systems-level framework for investigating the functional anatomy of documented changes in mo-

tor development, language, attention, and mood that can accompany SCA [104, 105, 106, 49].

Chapter 7

Limitations and Future Directions for Imaging-Genetics in Neuroimaging

This thesis leverages automated brain registration algorithms in addition to large normative and clinical cohorts to detect a previously undescribed feature of brain morphometry. As a consequence, this thesis also presents a new parcellation in the cortex and subcortex. This parcellation is based on how brain regions, both defined by *a priori* past neuroanatomical atlases and by *a posteriori* unconstrained data-driven and registration methods, scale with variation in overall brain size. Through multi-modal analysis of publicly available maps of the cortical sheet and five subcortical nuclei, this thesis shows that regions of positive scaling (proportional expansion) overlap with a diverse set of physiological properties of the normal brain. These features include increased glucose metabolism, increased blood flow, enrichment for

areas subserving the default mode and which expand dynamically in evolution and development. Areas of negative scaling (proportional contraction) are shown to coincide with regions subserving motor and sensory processing. Taken together, these regions represent a new feature of primate brain morphology, one which illuminates how the two-fold variation in brain size amongst healthy humans is constructed based on regional expansion of the cortical sheet and subcortical volumes. The insights gained from utilizing a normative framework informed by nonlinear scaling are more dramatic in analyses of subcortical volumes in demographic and clinical groups. This thesis shows that a brain scaling framework is required to increase the specificity of biomarker discovery for subcortical sex differences and sex chromosome dosage biomarkers — with a particular emphasis on the globus pallidus, a deep grey matter nucleus salient to the coordination of motor control amongst other behaviors. While the findings of this thesis are strengthened by its replication in multiple study designs, cohorts, and age ranges, there are several important limitations that need to be flagged. The true measure of the significance of this new parcellation will be whether it enables more sensitive demarcation of disease from control groups for the applicability of cortical scaling in the analysis of disease and behavior and inferences about the mechanistic underpinning of scaling based on this observational study design.

7.1 Cortical Scaling

It can not be overstated that all the study designs presented here are fundamentally observational in their character. While methods for the quantification of the observations made herein are advances over previous observational studies, it is inappropriate to assign a causal function to scaling in the absence of an experimental paradigm with appropriate interventions, controls, and cross over conditions. With that caveat, it is worth stating explicitly the drawbacks to the current cortical analysis presented here.

First, it is unclear whether scaling-informed cortical morphometry offers any additional value over traditional statistical analyses of neuroimaging data for comparing patient and control groups at the vertex level in the cortex. While the results chapters of this thesis show that scaling-informed analyses improve the specificity of regional volume-based biomarker discovery for distinguishing disease and demographic cohorts, it is unclear at what granularity scaling-informed normative frameworks provide additional value. This is a crucial question for anatomical-based biomarker discovery. Are groupwise differences most informatively detected on the level of structures identified in previous neuroanatomical atlases or is the data-driven approach offered here more informative? Put more provactively, do scaling-informed vertex maps of the cortical sheet provide any additional insights into the neuroanatomical differences between controls and individuals with sex chromosome complement variations? It is impossible to answer this question without undertaking an analysis of clinical cohorts. This is a striking omission in this work given the access to disease cohorts within the NIH data available for analysis

but not included herein [45]. One can only speculate as to the reasons for this omission or whether such analyses were undertaken and not reported. Bracketing this at the moment, it is import to pause to recognize the loss this represents to the field given the suggestive findings presented here. A vertex-level analysis of the effect of supernumerary sex chromosome dose on the cortex would provide an ideal testing ground to prove the value of allometrically-informed frameworks for increasing the specificity of potential neuroanatomical biomarkers derived from imaging data. In particular, it would be valuable to compare scaling-informed maps of groupwise differences between groups of individuals with non XX/XY 23^{rd} chromosome complements and maps derived using either proportionalization or regression-based co-varying normalization methods. Validating the biological meaning of this parcellation for the understanding of disease must await future analyses for the time being.

Second, it is unclear if there is a reproducible link between nonlinear scaling and behavior. While positive scaling in the NIH data has been linked to a quantifiable behavioral phenotype of Intelligence Quotient in the NIH cohort as assessed through the Wechsler Intelligence Scales, no further analysis is reported as having been undertaken in the Philadelphia Neurodevelopmental Cohort. This may be due to several factors. First, intelligence was not assessed by the Wechsler Intelligence Scales in the Philadelphia Neurodevelopmental Cohort but instead through a series of computerized cognitive batteries. In particular, individuals in the Philadelphia Neurodevelopmental Cohort were quantitatively assessed with the computerized neurocognitive battery, which was designed for large-scale studies [107]. With a computer-

ized interface, the Philadelphia Neurodevelopmental Cohort's computerized neurocognitive battery swiftly generates measures of executive control, memory, complex cognitive processing, social cognition, and sensory and motor speed. Importantly, these measures do not yield a direct estimate of IQ or general cognitive ability [108, 109]. Thus, while many of the observations in this thesis are replicated across both National Institutes of Health and Philadelphia Neurodevelopmental Cohort groups, it was decided that it was not necessary to replicate an association with cognitive ability with the given measures in these samples before publication. As a result, the behavioral significance of nonlinear scaling has yet to be reproducibly established.

7.2 Subcortical Scaling in Disease

This thesis' work on subcortical volume demonstrates how neglecting normative brain allometry can distort conclusions regarding sex effects on potential neuroanatomical biomarkers. Before discussing the insights gained from accounting for brain scaling, it is necessary to address the limitations of the study design.

First, the cross-sectional study sample cannot be appropriately used to model how age might alter sex, sex chromosome dosage, and total brain volume effects on subcortical anatomy. The rarity of sex chromosome aneuploidies — and their ascertainment — is a challenge for the generation of cohorts needed for such longitudinal analyses. As a result, this thesis is unable to address whether supernumerary sex chromosome dosage alters the trajectory of striatal, thalamic, or pallidal development in volume or shape,

as assessed by vertex-level surface area. This is crucial as these trajectories themselves may be potential biomarkers for the development of more severe behavioral phenotypes amongst individuals with supernumerary sex chromosomes and could provide clinicians with the data to appropriately offer anticipatory guidance in cases where a more severe behavioral disorder may emerge in this genetic context.

Second, as an observational study, this work is limited in its ability to provide causal and mechanistic explanations for the anatomical differences detected amongst aneuploidy groups. The differences detected here must first be replicated in other groups to confirm the validity of the observations herein. Once the reliability of these observations is established, it will be possible to rule out the potential for these findings to be an artefact of the particular cohort, study design, and data acquisition strategy that underpin the findings reported here. Until proper experimental models are constructed, neuroimaging may only appropriately speculate how these striking morphological changes arise in humans with differences iin sex chromosome complement.

Third, the cellular bases for our neuroimaging results remain unclear and could only be studied indirectly here. Animal models are required to assess the possibility of any causal relationship between sex chromosome aneuploidy and subcortical morphology. The cellular consequences of sex chromosome aneuploidy in humans must await study in any *post-mortem* analyses of patient neurons and brain regions or through *in vitro* models. In this context, neuroimaging is understood as a hypothesis generating procedure and any causal inference based on observational imaging data must be understood as

speculative without an appropriate experimental paradigm. In particular, the advent of induced pleuripotent stem-cell-derived cortical neurons as a model for querying the cellular basis of neuroimaging phenotypes is incredibly promising.

As iPSC technologies mature, it is an alluring promise that hypotheses generated from imaging modalities may be directly tested with these in vitro model systems with patient-derived tissue. For the purposes of this thesis, it is possible to base speculation around the genetic content of the X and Y chromosome as the source of the divergent thalamic, striatal, and pallidal volumes and shapes. Given the largely divergent gene content of human X- and Y-chromosomes, convergent supernumerary X- and Y-chromosome effects on subcortical anatomy may presumably reflect either: i) increased dose of the few homologous X-Y gene pairs ([110, 111], or ii) increased nuclear chromatin dosage. Direct studies of gene expression from patient samples will be required to test these hypotheses and the degree to which sex chromosome dosage variation in aneuploidy fully recapitulates the effects of normative sex chromosome dosage differences between males with an XY 23^{rd} chromosome complement and females with an XX 23^{rd} chromosome complement.

Fourth, future studies will be required to test the phenotypic relevance of the focal variations in subcortical anatomy that are linked in this sample to sex, sex chromosome dosage and normative variation in brain size. While the work in this thesis identifies clear neuroanatomical markers of sex chromosome variations in the subcortex, it is an open question which of the markers presented here or in cortical and subcortical regions presented elsewhere are the most informative biomarkers for disease. The behavioral and

neurological pathologies associated with sex chromosome aneuploidy may be best anticipated based on the appearance of markers not addressed in this study — such as changes in cortical thickness or surface area.

Moreover, sex chromosome aneuploidies themselves show a remarkably diverse set of behavioral presentations. In a recent population-level study of residents in the United Kingdom, many individuals with trisomy X and Turner's Syndrome were identified based on DNA microarray genotyping and had not previously presented for clinical care [112]. This has striking implications for inferences based on our data for the neurobiological etiology of many of the disorders associated with sex chromosome aneuploidy. Given that many individuals with non-standard sex chromosome complements do not present for clinical care, there are other genomic or environmental factors that contribute to either the neuroanatomical features described here or the symptoms seen in this clinical population.

7.2.1 Subcortical Surface Area in Disease

The allometrically-informed analysis of normative sex-differences in subcortical volumes presented here shows that (i) the striatum and thalamus are proportionally smaller in males due to brain size alone, but (ii) the pallidum is proportionally larger in males irrespective of sex-differences in overall brain size. In contrast, analysis of the sample data presented here using two classical corrections for total brain volume effects — which both fail to account for non-linear relationships between subcortical volume and total brain volume — conclude that male sex imparts smaller striatal, thalamic and pallidal vol-

umes (normalization by total brain volume through proportionalization), or smaller striatal and thalamic volumes, alongside larger pallidal volume (covarying for total brain volume with linear regression models). Our analyses using these classical corrections recapitulate previous findings of normative sex-differences in subcortical volume using normalization by or covariation for total brain volume [113, 41].

The allometrically-informed analysis of supernumerary sex chromosome dosage effects on subcortical volumes presented here highlights the special vulnerability of pallidal volume to supernumerary X- and Y-chromosome dosage (Table 5.4). While a mechanistic explanation for this lies outside of the remit of this thesis and the study design, it is possible to speculate that the neurons of the globus pallidus possess a special vulnerability to sex chromosome aneuploidy because of their function in the coordination of motor behavior. In particular, this vulnerability could reflect the sensitivity of pallidal neurons to oxidative stress [114], given that aneuploidy states are known to modify the expression of genes related to oxidative stress [115].

In addition to framing analysis of sex and sex-chromosome dosage effects, the allometric analyses presented here also establish for the first time that striatal volume, pallidal volume and thalamic volume all scale sub-linearly with total brain volume in humans. This feature of brain scaling in health aligns with established sub-linear scaling of the putamen and diencephalon with increasing total brain volume across diverse species [116]. Thus, both within humans and across species, the disproportionate expansion of cortical volume with greater total brain volume [23, 45] does not require commensurate increases in subcortical nuclei volume.

7.2.2 Allometry of Subcortical Shape in Sex Chromosome Aneuploidy

The work in this thesis on neuroanatomy in individuals with supernumerary sex chromosomes demonstrates that regional subcortical allometry in health provides a critical framework for the study of supernumerary sex chromosome effects on subcortical shape. For example, an allometric framework reveals that whereas supernumerary X- and Y-chromosome dose preserves pallidal shape (despite dramatically impacting pallidal volume), it distorts striatal and thalamic shape. Intriguingly, these distortions counter the shape changes predicted by supernumerary sex chromosome dosage effects on striatal and thalamic volume assuming normative brain allometry. Surface area domains in the striatum and thalamus that should show disproportionate areal contraction as striatal volume and thalamic volume decrease with mounting X- and Y-chromosome dose, actually show an increase in their absolute size. Conversely, hypoallometric domains in these same nuclei, which should show the least areal contraction with reducing striatal volume and thalamic volume, are actually the subcortical regions that show the greatest areal loss with mounting X- and Y-chromosome dose. Thus, these allometric perspectives indicate that supernumerary sex chromosome dose actively changes the differential regional growth patterns that regulate normative relationships between striato-thalamic shape and nucleus size.

Although our study analyzes the normative allometry of subcortical shape using a parcellation defined by supernumerary sex chromosome dose effects, these analyses yield several novel insights into the organization of subcor-

tical shape in health. First, they show that amongst typically developing youth, the striatum and thalamus change their shape with increasing size, while the pallidum does not. With increasing structure size, the caudate body/tail and the dorsal thalamus become proportionately larger, whereas the putamen and latero-ventral facets of the thalamus become proportionately smaller. Size-related variations in subcortical shape point towards local differences in the regulation of subcortical growth. An important area for future work will be examining if and how regional differences in subcortical allometry correspond to candidate anatomical (e.g. proximity of hyperallometric regions to fluid-filled ventricles [117]), and/or connectivity-based (e.g a topographical mirroring in the subcortex of regional differences in cortical expansion [74]) regulators of subcortical growth.

7.3 Last Thoughts

Automated brain registration algorithms made it possible for this thesis to interrogate for the first time the relationship between brain scaling and local neuroanatomical morphometry. Consequently it presents a new perspective of surface area analysis of regions of interest in both the cortex and the subcortex. It provides a necessary lens through which to appreciate any groupwise biomarker identified by neuroanatomical structural neuroimaging studies going forward. Moreover, by presenting both *a priori* and hypothesis-free scaling maps at multiple resolutions, this thesis shows that scaling holds at multiple resolutions within the brain. As such, it provides the first step in the assessment of local neuroanatomical biomarkers in a scaling-informed

normative framework that takes into account the interdependence of the neuroanatomy at a systems level. It is the hope of this author that it contributes, one day, to the improvement of the detection and treatment of disease in youth and adults.

Bibliography

[1] Jay N. Giedd, Jonathan Blumenthal, Neal O. Jeffries, F. X. Castellanos, Hong Liu, Alex Zijdenbos, Tomáš Paus, Alan C. Evans, and Judith L. Rapoport. Brain development during childhood and adolescence: a longitudinal MRI study. *Nature Neuroscience*, 2(10):861–863, October 1999.

[2] Galileo Galilei. *Dialogues Concerning Two New Sciences*. Macmillan, 1914. Google-Books-ID: fdnPAAAAMAAJ.

[3] Katherine E. Willmore. The Body Plan Concept and Its Centrality in Evo-Devo. *Evolution: Education and Outreach*, 5(2):219–230, June 2012.

[4] Ernst Haeckel. *Generelle Morphologie der Organismen. Allgemeine Grundzüge der organischen Formen-Wissenschaft, mechanisch begründet durch die von C. Darwin reformirte Descendenz-Theorie, etc*, volume 2. 1866.

[5] Ernst Heinrich Philipp August Haeckel. *Anthropogenie: oder, Entwickelungsgeschichte des menschen, Keimes-und stammesgeschichte*. W. Engelmann, 1877.

[6] Karl Zilles. Brodmann: a pioneer of human brain mapping—his impact on concepts of cortical organization. *Brain*, 141(11):3262–3278, November 2018.

[7] Korbinian Brodmann. Feinere anatomie des grosshirns. In *Handbuch der Neurologie*, pages 206–307. Springer, 1910.

[8] Korbinian Brodmann. Neuere forschungsergebnisse der großhirnrindenanatomie mit besonderer berücksichtigung anthropologischer fragen. *Naturwissenschaften*, 1(46):1120–1122, 1913.

[9] Korbinian Brodmann. *Brodmann's: Localisation in the cerebral cortex*. Springer Science & Business Media, 2007.

[10] Constantin Freiherr von Economo and Georg N Koskinas. *Die cytoarchitektonik der hirnrinde des erwachsenen menschen*. J. Springer, 1925.

[11] Yasemin Kaya, Hilmi Uysal, Gokhan Akkoyunlu, and Levent Sarikcioglu. Constantin von economo (1876–1931) and his legacy to neuroscience. *Child's Nervous System*, 32(2):217–220, 2016.

[12] Donald W McRobbie, Elizabeth A Moore, Martin J Graves, and Martin R Prince. *MRI from Picture to Proton*. Cambridge university press, 2017.

[13] Arno Klein, Satrajit S. Ghosh, Forrest S. Bao, Joachim Giard, Yrjö Häme, Eliezer Stavsky, Noah Lee, Brian Rossa, Martin Reuter,

Elias Chaibub Neto, and Anisha Keshavan. Mindboggling morphometry of human brains. *PLOS Computational Biology*, 13(2):e1005350, February 2017.

[14] Arno Klein and Jason Tourville. 101 Labeled Brain Images and a Consistent Human Cortical Labeling Protocol. *Frontiers in Neuroscience*, 6, 2012.

[15] D. Louis Collins, Peter Neelin, Terrence M. Peters, and Alan C. Evans. Automatic 3d Intersubject Registration of MR Volumetric Data in Standardized Talairach Space. *Journal of Computer Assisted Tomography*, 18(2):192–205, April 1994.

[16] M. A. Balafar, A. R. Ramli, M. I. Saripan, and S. Mashohor. Review of brain MRI image segmentation methods. *Artificial Intelligence Review*, 33(3):261–274, March 2010.

[17] Arno Klein, Jesper Andersson, Babak A Ardekani, John Ashburner, Brian Avants, Ming-Chang Chiang, Gary E Christensen, D Louis Collins, James Gee, Pierre Hellier, et al. Evaluation of 14 nonlinear deformation algorithms applied to human brain mri registration. *Neuroimage*, 46(3):786–802, 2009.

[18] Verne S Caviness Jr, James Meyer, Nikos Makris, and David N Kennedy. Mri-based topographic parcellation of human neocortex: an anatomically specified method with estimate of reliability. *Journal of Cognitive Neuroscience*, 8(6):566–587, 1996.

[19] Mark Jenkinson, Peter Bannister, Michael Brady, and Stephen Smith. Improved Optimization for the Robust and Accurate Linear Registration and Motion Correction of Brain Images. *NeuroImage*, 17(2):825–841, October 2002.

[20] Schmidt-Nielsen. *Scaling: Why Is Animal Size So Important?* Cambridge University Press, Cambridge ; New York, first printing. edition edition, January 2008.

[21] Julian Sorell Huxley. Constant differential growth-ratios and their significance. *Nature*, 114(2877):895–896, 1924.

[22] WENTWORTH THOMPSON D'ARCY et al. *On Growth and Form.* Cambridge university press, 2010.

[23] Finlay, Barabra L. and Darlington, Richard B. Linked Regularities in the Development and Evolution of Mamalian Brains. *Science*, 268(5217):1578–1584, 1995.

[24] Michael P Sanfilipo, Ralph H. B Benedict, Robert Zivadinov, and Rohit Bakshi. Correction for intracranial volume in analysis of whole brain atrophy in multiple sclerosis: the proportion vs. residual method. *NeuroImage*, 22(4):1732–1743, August 2004.

[25] Kiho Im, Jong-Min Lee, Oliver Lyttelton, Sun Hyung Kim, Alan C. Evans, and Sun I. Kim. Brain Size and Cortical Structure in the Adult Human Brain. *Cerebral Cortex*, 18(9):2181–2191, September 2008.

[26] Josephine Barnes, Gerard R. Ridgway, Jonathan Bartlett, Susie M.D.

Henley, Manja Lehmann, Nicola Hobbs, Matthew J. Clarkson, David G. MacManus, Sebastien Ourselin, and Nick C. Fox. Head size, age and gender adjustment in MRI studies: a necessary nuisance? *NeuroImage*, 53(4):1244–1255, December 2010.

[27] Laura W. de Jong, Jean-Sébastien Vidal, Lars E. Forsberg, Alex P. Zijdenbos, Thaddeus Haight, Sigurdur Sigurdsson, Vilmundur Gudnason, Mark A. van Buchem, Lenore J. Launer, and For the Alzheimer's Disease Neuroimaging Initiative. Allometric scaling of brain regions to intra-cranial volume: An epidemiological MRI study: Allometric Scaling of Brain Regions. *Human Brain Mapping*, August 2016.

[28] Michael J. Hawrylycz, Ed S. Lein, Angela L. Guillozet-Bongaarts, Elaine H. Shen, Lydia Ng, Jeremy A. Miller, Louie N. van de Lagemaat, Kimberly A. Smith, Amanda Ebbert, Zackery L. Riley, Chris Abajian, Christian F. Beckmann, Amy Bernard, Darren Bertagnolli, Andrew F. Boe, Preston M. Cartagena, M. Mallar Chakravarty, Mike Chapin, Jimmy Chong, Rachel A. Dalley, Barry David Daly, Chinh Dang, Suvro Datta, Nick Dee, Tim A. Dolbeare, Vance Faber, David Feng, David R. Fowler, Jeff Goldy, Benjamin W. Gregor, Zeb Haradon, David R. Haynor, John G. Hohmann, Steve Horvath, Robert E. Howard, Andreas Jeromin, Jayson M. Jochim, Marty Kinnunen, Christopher Lau, Evan T. Lazarz, Changkyu Lee, Tracy A. Lemon, Ling Li, Yang Li, John A. Morris, Caroline C. Overly, Patrick D. Parker, Sheana E. Parry, Melissa Reding, Joshua J. Royall, Jay Schulkin, Pedro Adolfo Sequeira, Clifford R. Slaughterbeck, Simon C. Smith, Andy J. Sodt, Su-

san M. Sunkin, Beryl E. Swanson, Marquis P. Vawter, Derric Williams, Paul Wohnoutka, H. Ronald Zielke, Daniel H. Geschwind, Patrick R. Hof, Stephen M. Smith, Christof Koch, Seth G. N. Grant, and Allan R. Jones. An anatomically comprehensive atlas of the adult human brain transcriptome. *Nature*, 489(7416):391–399, September 2012.

[29] H. Meltzer, R. Gatward, R. Goodman, and T. Ford. The mental health of children and adolescents in Great Britain: Summary Report. Technical report, 2000. Times cited: 1.

[30] M. Rutter, A. Caspi, and T. E. Moffitt. Using sex differences in psychopathology to study causal mechanisms: unifying issues and research strategies. [Review] [219 refs]. *Journal of Child Psychology & Psychiatry & Allied Disciplines.44(8):1092-115*, 2003. Times cited: 1.

[31] David R. Roalf, Raquel E. Gur, Kosha Ruparel, Monica E. Calkins, Theodore D. Satterthwaite, Warren B. Bilker, Hakon Hakonarson, Lauren Julius Harris, and Ruben C. Gur. Within-individual variability in neurocognitive performance: age- and sex-related differences in children and youths from ages 8 to 21. *Neuropsychology*, 28(4):506–518, July 2014. Times cited: 1.

[32] John L. Bradshaw and Dianne M. Sheppard. The Neurodevelopmental Frontostriatal Disorders: Evolutionary Adaptiveness and Anomalous Lateralization. *Brain and Language*, 73(2):297–320, June 2000.

[33] Jessica A. Grahn, John A. Parkinson, and Adrian M. Owen. The

cognitive functions of the caudate nucleus. *Progress in Neurobiology*, 86(3):141–155, November 2008.

[34] Dae-Jin Kim, Bumhee Park, and Hae-Jeong Park. Functional connectivity-based identification of subdivisions of the basal ganglia and thalamus using multilevel independent component analysis of resting state fMRI. *Human Brain Mapping*, 34(6):1371–1385, June 2013.

[35] Armin Raznahan, William Cutter, Francois Lalonde, Dene Robertson, Eileen Daly, Gerard S. Conway, David H. Skuse, Judith Ross, J. P. Lerch, Jay N. Giedd, and Declan D. G. M. Murphy. Cortical anatomy in human X monosomy. *NeuroImage*, 49(4):2915–2923, February 2010.

[36] J. N. Giedd, A. Raznahan, A. Alexander-Bloch, E. Schmitt, N. Gogtay, and J. L. Rapoport. Child Psychiatry Branch of the National Institute of Mental Health Longitudinal Structural Magnetic Resonance Imaging Study of Human Brain Development. *Neuropsychopharmacology*, September 2014. Times cited: 2.

[37] Sergio Escorial, Francisco J. Román, Kenia Martínez, Miguel Burgaleta, Sherif Karama, and Roberto Colom. Sex differences in neocortical structure and cognitive performance: A surface-based morphometry study. *NeuroImage*, 104:355–365, January 2015. Times cited: 1.

[38] Elizabeth R Sowell, Doris A Trauner, Anthony Gamst, and Terry L Jernigan. Development of cortical and subcortical brain structures in childhood and adolescence: a structural MRI study. *Developmental Medicine & Child Neurology*, 44(1):4–16, January 2002.

[39] Ylva Østby, Christian K. Tamnes, Anders M. Fjell, Lars T. Westlye, Paulina Due-Tønnessen, and Kristine B. Walhovd. Heterogeneity in Subcortical Brain Development: A Structural Magnetic Resonance Imaging Study of Brain Maturation from 8 to 30 Years. *The Journal of Neuroscience*, 29(38):11772–11782, September 2009.

[40] Brain Development Cooperative Group. Total and regional brain volumes in a population-based normative sample from 4 to 18 years: the NIH MRI Study of Normal Brain Development. *Cerebral Cortex (New York, N.Y.: 1991)*, 22(1):1–12, January 2012. Times cited: 2.

[41] Mark Rijpkema, Daphne Everaerd, Carline van der Pol, Barbara Franke, Indira Tendolkar, and Guillén Fernández. Normal sexual dimorphism in the human basal ganglia. *Human Brain Mapping*, 33(5):1246–1252, May 2012.

[42] E. Lentini, M. Kasahara, S. Arver, and I. Savic. Sex Differences in the Human Brain and the Impact of Sex Chromosomes and Sex Hormones. *Cerebral Cortex*, 23(10):2322–2336, October 2013.

[43] Lara Wierenga, Marieke Langen, Sara Ambrosino, Sarai van Dijk, Bob Oranje, and Sarah Durston. Typical development of basal ganglia, hippocampus, amygdala and cerebellum from age 7 to 24. *NeuroImage*, 96:67–72, August 2014.

[44] Christina Corre, Miriam Friedel, Dulcie A. Vousden, Ariane Metcalf, Shoshana Spring, Lily R. Qiu, Jason P. Lerch, and Mark R. Palmert. Separate effects of sex hormones and sex chromosomes on brain struc-

ture and function revealed by high-resolution magnetic resonance imaging and spatial navigation assessment of the Four Core Genotype mouse model. *Brain Structure and Function*, pages 1–20, December 2014.

[45] A. Raznahan, N. R. Lee, D. Greenstein, G. L. Wallace, J. D. Blumenthal, L. S. Clasen, and J. N. Giedd. Globally Divergent but Locally Convergent X- and Y-Chromosome Influences on Cortical Development. *Cerebral Cortex*, August 2014.

[46] D. M. Bryant, F. Hoeft, S. Lai, J. Lackey, D. Roeltgen, J. Ross, and A. L. Reiss. Neuroanatomical Phenotype of Klinefelter Syndrome in Childhood: A Voxel-Based Morphometry Study. *Journal of Neuroscience*, 31(18):6654–6660, May 2011.

[47] Daniel M Bryant, Fumiko Hoeft, Song Lai, John Lackey, David Roeltgen, Judith Ross, and Allan L Reiss. Sex chromosomes and the brain: a study of neuroanatomy in XYY syndrome: Neuroanatomical Variation in XYY Syndrome. *Developmental Medicine & Child Neurology*, 54(12):1149–1156, December 2012.

[48] D. S. Hong, F. Hoeft, M. J. Marzelli, J.-F. Lepage, D. Roeltgen, J. Ross, and A. L. Reiss. Influence of the X-Chromosome on Neuroanatomy: Evidence from Turner and Klinefelter Syndromes. *Journal of Neuroscience*, 34(10):3509–3516, March 2014.

[49] David S. Hong and Allan L. Reiss. Cognitive and neurological aspects of sex chromosome aneuploidies. *The Lancet Neurology*, 13(3):306–318, 2014.

[50] Roberto Toro, Marie Chupin, Line Garnero, Gabriel Leonard, Michel Perron, Bruce Pike, Alain Pitiot, Louis Richer, Suzanne Veillette, Zdenka Pausova, and Tomáš Paus. Brain volumes and Val66met polymorphism of the BDNF gene: local or global effects? *Brain Structure and Function*, 213(6):501–509, February 2009.

[51] Theodore D. Satterthwaite, Russell T. Shinohara, Daniel H. Wolf, Ryan D. Hopson, Mark A. Elliott, Simon N. Vandekar, Kosha Ruparel, Monica E. Calkins, David R. Roalf, Efstathios D. Gennatas, Chad Jackson, Guray Erus, Karthik Prabhakaran, Christos Davatzikos, John A. Detre, Hakon Hakonarson, Ruben C. Gur, and Raquel E. Gur. Impact of puberty on the evolution of cerebral perfusion during adolescence. *Proceedings of the National Academy of Sciences*, 111(23):8643–8648, June 2014.

[52] Thomas M. Achenbach. The Child Behavior Checklist and related instruments. In *The use of psychological testing for treatment planning and outcomes assessment, 2nd ed*, pages 429–466. Lawrence Erlbaum Associates Publishers, Mahwah, NJ, US, 1999.

[53] P. Shaw, D. Greenstein, J. Lerch, L. Clasen, R. Lenroot, N. Gogtay, A. Evans, J. Rapoport, and J. Giedd. Intellectual ability and cortical development in children and adolescents. *Nature*, 440(7084):676–679, March 2006.

[54] August B Hollingshead. Four factor index of social status. 1975.

[55] Kathleen K Bucholz, Remi Cadoret, C Robert Cloninger, Stephen H

Dinwiddie, VM Hesselbrock, JI Nurnberger Jr, T Reich, I Schmidt, and Marc A Schuckit. A new, semi-structured psychiatric interview for use in genetic linkage studies: a report on the reliability of the ssaga. *Journal of studies on alcohol*, 55(2):149–158, 1994.

[56] Y Ad-Dab'bagh, O Lyttelton, JS Muehlboeck, C Lepage, D Einarson, K Mok, O Ivanov, RD Vincent, J Lerch, and E Fombonne. The CIVET image-processing environment: a fully automated comprehensive pipeline for anatomical neuroimaging research. page 2266. Florence, Italy, 2006.

[57] J. G. Sled, A. P. Zijdenbos, and A. C. Evans. A nonparametric method for automatic correction of intensity nonuniformity in MRI data. *IEEE transactions on medical imaging*, 17(1):87–97, February 1998.

[58] June Sic Kim, Vivek Singh, Jun Ki Lee, Jason Lerch, Yasser Ad-Dab'bagh, David MacDonald, Jong Min Lee, Sun I. Kim, and Alan C. Evans. Automated 3-D extraction and evaluation of the inner and outer cortical surfaces using a Laplacian map and partial volume effect classification. *NeuroImage*, 27(1):210–221, August 2005.

[59] David MacDonald, Noor Kabani, David Avis, and Alan C. Evans. Automated 3-D Extraction of Inner and Outer Surfaces of Cerebral Cortex from MRI. *NeuroImage*, 12(3):340–356, September 2000.

[60] Matthew F. Glasser, Timothy S. Coalson, Emma C. Robinson, Carl D. Hacker, John Harwell, Essa Yacoub, Kamil Ugurbil, Jesper Andersson, Christian F. Beckmann, Mark Jenkinson, Stephen M. Smith, and

David C. Van Essen. A multi-modal parcellation of human cerebral cortex. *Nature*, 536(7615):171–178, August 2016.

[61] Oliver C. Lyttelton, Sherif Karama, Yasser Ad-Dab'bagh, Robert J. Zatorre, Felix Carbonell, Keith Worsley, and Alan C. Evans. Positional and surface area asymmetry of the human cerebral cortex. *NeuroImage*, 46(4):895–903, July 2009.

[62] Chi-Hua Chen, Matthew S. Panizzon, Lisa T. Eyler, Terry L. Jernigan, Wes Thompson, Christine Fennema-Notestine, Amy J. Jak, Michael C. Neale, Carol E. Franz, Samar Hamza, Michael J. Lyons, Michael D. Grant, Bruce Fischl, Larry J. Seidman, Ming T. Tsuang, William S. Kremen, and Anders M. Dale. Genetic Influences on Cortical Regionalization in the Human Brain. *Neuron*, 72(4):537–544, November 2011.

[63] S. N. Vandekar, R. T. Shinohara, A. Raznahan, D. R. Roalf, M. Ross, N. DeLeo, K. Ruparel, R. Verma, D. H. Wolf, R. C. Gur, R. E. Gur, and T. D. Satterthwaite. Topologically Dissociable Patterns of Development of the Human Cerebral Cortex. *Journal of Neuroscience*, 35(2):599–609, January 2015.

[64] Chris A Cocosco, Alex P Zijdenbos, and Alan C Evans. A fully automatic and robust brain mri tissue classification method. *Medical image analysis*, 7(4):513–527, 2003.

[65] M. Mallar Chakravarty, Patrick Steadman, Matthijs C. van Eede, Rebecca D. Calcott, Victoria Gu, Philip Shaw, Armin Raznahan, D. Louis Collins, and Jason P. Lerch. Performing label-fusion-based segmenta-

tion using multiple automatically generated templates: MAGeT Brain: Label Fusion Segmentation Using Automatically Generated Templates. *Human Brain Mapping*, 34(10):2635–2654, October 2013.

[66] A. Raznahan, P. W. Shaw, J. P. Lerch, L. S. Clasen, D. Greenstein, R. Berman, J. Pipitone, M. M. Chakravarty, and J. N. Giedd. Longitudinal four-dimensional mapping of subcortical anatomy in human development. *Proceedings of the National Academy of Sciences*, 111(4):1592–1597, January 2014.

[67] M. Mallar Chakravarty, Gilles Bertrand, Charles P. Hodge, Abbas F. Sadikot, and D. Louis Collins. The creation of a brain atlas for image guided neurosurgery using serial histological data. *NeuroImage*, 30(2):359–376, April 2006.

[68] R Core Team. *R: A language and environment for statistical computing*. R Foundation for Statistical Computing, Vienna, Austria, 2017.

[69] Simon N Wood. Fast stable restricted maximum likelihood and marginal likelihood estimation of semiparametric generalized linear models. *Journal of the Royal Statistical Society: Series B (Statistical Methodology)*, 73(1):3–36, 2011.

[70] Pierre Jolicoeur. 193. note: the multivariate generalization of the allometry equation. *Biometrics*, 19(3):497–499, 1963.

[71] Anders M Dale, Bruce Fischl, and Martin I Sereno. Cortical surface-based analysis: I. segmentation and surface reconstruction. *Neuroimage*, 9(2):179–194, 1999.

[72] Bruce Fischl, Martin I Sereno, and Anders M Dale. Cortical surface-based analysis: Ii: inflation, flattening, and a surface-based coordinate system. *Neuroimage*, 9(2):195–207, 1999.

[73] Daniel Marcus, John Harwell, Timothy Olsen, Michael Hodge, Matthew Glasser, Fred Prior, Mark Jenkinson, Timothy Laumann, Sandra Curtiss, and David Van Essen. Informatics and Data Mining Tools and Strategies for the Human Connectome Project. *Frontiers in Neuroinformatics*, 5, 2011.

[74] Jason Hill, Terrie Inder, Jeffrey Neil, Donna Dierker, John Harwell, and David Van Essen. Similar patterns of cortical expansion during human development and evolution. *Proceedings of the National Academy of Sciences*, 107(29):13135–13140, July 2010.

[75] Guy N Elston and Ichiro Fujita. Pyramidal cell development: postnatal spinogenesis, dendritic growth, axon growth, and electrophysiology. *Frontiers in neuroanatomy*, 8:78, 2014.

[76] B T Thomas Yeo, Fenna M Krienen, Jorge Sepulcre, Mert R Sabuncu, Danial Lashkari, Marisa Hollinshead, Joshua L Roffman, Jordan W Smoller, Lilla Zöllei, Jonathan R Polimeni, Bruce Fischl, Hesheng Liu, and Randy L Buckner. The organization of the human cerebral cortex estimated by intrinsic functional connectivity. *Journal of Neurophysiology*, 106(3):1125–1165, September 2011.

[77] Kirstie J. Whitaker, Petra E. Vértes, Rafael Romero-Garcia, František Váša, Michael Moutoussis, Gita Prabhu, Nikolaus Weiskopf, Mar-

tina F. Callaghan, Konrad Wagstyl, Timothy Rittman, Roger Tait, Cinly Ooi, John Suckling, Becky Inkster, Peter Fonagy, Raymond J. Dolan, Peter B. Jones, Ian M. Goodyer, the NSPN Consortium, Edward T. Bullmore, Ian Goodyer, Edward Bullmore, Raymond Dolan, Peter Fonagy, Peter Jones, Paul Fletcher, John Suckling, Nikolaus Weiskopf, Pasco Fearon, Becky Inkster, Gita Prabhu, David Bernal-Casas, Eran Eldar, Taposhri Ganguly, Tobias Hauser, Konstantinos Ioannidis, Gemma Lewis, Alda Mita, Michael Moutoussis, Sharon Neufeld, Ela Polek-MacDaeid, Rafael Romero-Garcia, Michelle St Clair, Roger Tait, Umar Toseeb, Anne-Laura van Harmelen, Petra Vértes, Kirstie Whitaker, Geert-Jan Will, Gabriel Ziegler, Jorge Zimbron, Joost Haarsma, Sian Davies, Juliet Griffin, Michael Hart, František Váša, Konrad Wagstyl, Cinly Ooi, Barry Widmer, Ayesha Alrumaithi, Sarah Birt, Kalia Cleridou, Hina Dadabhoy, Ashlyn Firkins, Sian Granville, Elizabeth Harding, Alexandra Hopkins, Daniel Isaacs, Janchai King, Clare Knight, Danae Kokorikou, Christina Maurice, Cleo McIntosh, Jessica Memarzia, Harriet Mills, Ciara O'Donnell, Sara Pantaleone, Jennifer Scott, Alison Stribling, Junaid Bhatti, Neil Hubbard, Natalia Ilicheva, Michael Kentell, Ben Wallis, and Laura Villis. Adolescence is associated with genomically patterned consolidation of the hubs of the human brain connectome. *Proceedings of the National Academy of Sciences*, 113(32):9105–9110, August 2016.

[78] S. Neil Vaishnavi, Andrei G. Vlassenko, Melissa M. Rundle, Abraham Z. Snyder, Mark A. Mintun, and Marcus E. Raichle. Regional

aerobic glycolysis in the human brain. *Proceedings of the National Academy of Sciences*, 107(41):17757–17762, October 2010.

[79] Matthew F. Glasser, Manu S. Goyal, Todd M. Preuss, Marcus E. Raichle, and David C. Van Essen. Trends and properties of human cerebral cortex: Correlations with cortical myelin content. *NeuroImage*, 93:165–175, June 2014.

[80] Aaron F Alexander-Bloch, Haochang Shou, Siyuan Liu, Theodore D Satterthwaite, David C Glahn, Russell T Shinohara, Simon N Vandekar, and Armin Raznahan. On testing for spatial correspondence between maps of human brain structure and function. *NeuroImage*, 178:540–551, 2018.

[81] J. Richiardi, A. Altmann, A.-C. Milazzo, C. Chang, M. M. Chakravarty, T. Banaschewski, G. J. Barker, A. L. W. Bokde, U. Bromberg, C. Buchel, P. Conrod, M. Fauth-Buhler, H. Flor, V. Frouin, J. Gallinat, H. Garavan, P. Gowland, A. Heinz, H. Lemaitre, K. F. Mann, J.-L. Martinot, F. Nees, T. Paus, Z. Pausova, M. Rietschel, T. W. Robbins, M. N. Smolka, R. Spanagel, A. Strohle, G. Schumann, M. Hawrylycz, J.-B. Poline, M. D. Greicius, IMAGEN consortium, L. Albrecht, C. Andrew, M. Arroyo, E. Artiges, S. Aydin, C. Bach, T. Banaschewski, A. Barbot, G. Barker, N. Boddaert, A. Bokde, Z. Bricaud, U. Bromberg, R. Bruehl, C. Buchel, A. Cachia, A. Cattrell, P. Conrod, P. Constant, J. Dalley, B. Decideur, S. Desrivieres, T. Fadai, H. Flor, V. Frouin, J. Gallinat, H. Garavan, F. G. Briand, P. Gowland, B. Heinrichs, A. Heinz, N. Heym, T. Hubner, J. Ireland, B. Itter-

mann, T. Jia, M. Lathrop, D. Lanzerath, C. Lawrence, H. Lemaitre, K. Ludemann, C. Macare, C. Mallik, J.-F. Mangin, K. Mann, J.-L. Martinot, E. Mennigen, F. Mesquita de Carvahlo, X. Mignon, R. Miranda, K. Muller, F. Nees, C. Nymberg, M.-L. Paillere, T. Paus, Z. Pausova, J.-B. Poline, L. Poustka, M. Rapp, G. Robert, J. Reuter, M. Rietschel, S. Ripke, T. Robbins, S. Rodehacke, J. Rogers, A. Romanowski, B. Ruggeri, C. Schmal, D. Schmidt, S. Schneider, M. Schumann, F. Schubert, Y. Schwartz, M. Smolka, W. Sommer, R. Spanagel, C. Speiser, T. Spranger, A. Stedman, S. Steiner, D. Stephens, N. Strache, A. Strohle, M. Struve, N. Subramaniam, L. Topper, R. Whelan, S. Williams, J. Yacubian, M. Zilbovicius, C. P. Wong, S. Lubbe, L. Martinez-Medina, A. Fernandes, and A. Tahmasebi. Correlated gene expression supports synchronous activity in brain networks. *Science*, 348(6240):1241–1244, June 2015.

[82] Janine Arloth, Daniel M. Bader, Simone Röh, and Andre Altmann. Re-Annotator: Annotation Pipeline for Microarray Probe Sequences. *PLOS ONE*, 10(10):e0139516, October 2015.

[83] Peter H Westfall and S Stanley Young. *Resampling-based multiple testing: Examples and methods for p-value adjustment*, volume 279. John Wiley & Sons, 1993.

[84] Yoav Benjamini and Yosef Hochberg. Controlling the false discovery rate: a practical and powerful approach to multiple testing. *Journal of the royal statistical society. Series B (Methodological)*, pages 289–300, 1995.

[85] Eran Eden, Roy Navon, Israel Steinfeld, Doron Lipson, and Zohar Yakhini. GOrilla: a tool for discovery and visualization of enriched GO terms in ranked gene lists. *BMC Bioinformatics*, 10:48, 2009.

[86] Fran Supek, Matko Bošnjak, Nives Škunca, and Tomislav Šmuc. REVIGO Summarizes and Visualizes Long Lists of Gene Ontology Terms. *PLOS ONE*, 6(7):e21800, July 2011.

[87] Catherine Mankiw, Min Tae M. Park, P. K. Reardon, Ari M. Fish, Liv S. Clasen, Deanna Greenstein, Jay N. Giedd, Jonathan D. Blumenthal, Jason P. Lerch, M. Mallar Chakravarty, and Armin Raznahan. Allometric Analysis Detects Brain Size-Independent Effects of Sex and Sex Chromosome Complement on Human Cerebellar Organization. *The Journal of Neuroscience: The Official Journal of the Society for Neuroscience*, March 2017.

[88] Paul Kirkpatrick Reardon, Liv Clasen, Jay N. Giedd, Jonathan Blumenthal, Jason P. Lerch, M. Mallar Chakravarty, and Armin Raznahan. An Allometric Analysis of Sex and Sex Chromosome Dosage Effects on Subcortical Anatomy in Humans. *The Journal of Neuroscience*, 36(8):2438–2448, February 2016.

[89] Theodore D. Satterthwaite, Mark A. Elliott, Kosha Ruparel, James Loughead, Karthik Prabhakaran, Monica E. Calkins, Ryan Hopson, Chad Jackson, Jack Keefe, Marisa Riley, Frank D. Mentch, Patrick Sleiman, Ragini Verma, Christos Davatzikos, Hakon Hakonarson, Ruben C. Gur, and Raquel E. Gur. Neuroimaging of the Philadel-

phia Neurodevelopmental Cohort. *NeuroImage*, 86:544–553, February 2014.

[90] Simon Wood. *Generalized additive models: an introduction with R*. CRC press, 2006.

[91] Olaf Sporns. Network attributes for segregation and integration in the human brain. *Current opinion in neurobiology*, 23(2):162–171, 2013.

[92] Daniel S. Margulies, Satrajit S. Ghosh, Alexandros Goulas, Marcel Falkiewicz, Julia M. Huntenburg, Georg Langs, Gleb Bezgin, Simon B. Eickhoff, F. Xavier Castellanos, Michael Petrides, Elizabeth Jefferies, and Jonathan Smallwood. Situating the default-mode network along a principal gradient of macroscale cortical organization. *Proceedings of the National Academy of Sciences*, 113(44):12574–12579, November 2016.

[93] John D Medaglia, Mary-Ellen Lynall, and Danielle S Bassett. Cognitive network neuroscience. *Journal of cognitive neuroscience*, 27(8):1471–1491, 2015.

[94] Isabel Reillo, Camino de Juan Romero, Miguel Ángel García-Cabezas, and Víctor Borrell. A role for intermediate radial glia in the tangential expansion of the mammalian cerebral cortex. *Cerebral Cortex*, 21(7):1674–1694, 2010.

[95] Diarmuid J Cahalane, Christine J Charvet, and Barbara L Finlay. Systematic, balancing gradients in neuron density and number across the primate isocortex. *Frontiers in neuroanatomy*, 6, 2012.

[96] Christopher W Kuzawa, Harry T Chugani, Lawrence I Grossman, Leonard Lipovich, Otto Muzik, Patrick R Hof, Derek E Wildman, Chet C Sherwood, William R Leonard, and Nicholas Lange. Metabolic costs and evolutionary implications of human brain development. *Proceedings of the National Academy of Sciences*, 111(36):13010–13015, 2014.

[97] William A Marshall and James M Tanner. Variations in pattern of pubertal changes in girls. *Archives of disease in childhood*, 44(235):291, 1969.

[98] William A Marshall and James M Tanner. Variations in the pattern of pubertal changes in boys. *Archives of disease in childhood*, 45(239):13–23, 1970.

[99] Christopher R. Genovese, Nicole A. Lazar, and Thomas Nichols. Thresholding of Statistical Maps in Functional Neuroimaging Using the False Discovery Rate. *Neuroimage*, 15(4):870–878, 2002. Times cited: 1.

[100] E. Y. Choi, B. T. T. Yeo, and R. L. Buckner. The organization of the human striatum estimated by intrinsic functional connectivity. *Journal of Neurophysiology*, 108(8):2242–2263, October 2012.

[101] Deanna J. Greene, Timothy O. Laumann, Joseph W. Dubis, S. Katie Ihnen, Maital Neta, Jonathan D. Power, John R. Pruett, Kevin J. Black, and Bradley L. Schlaggar. Developmental Changes in the Organization of Functional Connections between the Basal Ganglia and

Cerebral Cortex. *The Journal of Neuroscience*, 34(17):5842–5854, April 2014.

[102] P. Voorn, L. J. Vanderschuren, H. J. Groenewegen, T. W. Robbins, and C. M. Pennartz. Putting a spin on the dorsal-ventral divide of the striatum. *Trends in Neurosciences*, 27(8):468–74, August 2004. Times cited: 1.

[103] Bogdan Draganski, Ferath Kherif, Stefan Klöppel, Philip A. Cook, Daniel C. Alexander, Geoff J. M. Parker, Ralf Deichmann, John Ashburner, and Richard S. J. Frackowiak. Evidence for Segregated and Integrative Connectivity Patterns in the Human Basal Ganglia. *The Journal of Neuroscience*, 28(28):7143–7152, July 2008.

[104] Nicole Tartaglia, Shanlee Davis, Alison Hench, Sheela Nimishakavi, Renee Beauregard, Ann Reynolds, Laura Fenton, Lindsey Albrecht, Judith Ross, Jeannie Visootsak, Robin Hansen, and Randi Hagerman. A new look at XXYY syndrome: Medical and psychological features. *American Journal of Medical Genetics Part A*, 146A(12):1509–1522, June 2008.

[105] Nancy Raitano Lee, Gregory L. Wallace, Elizabeth I. Adeyemi, Katherine C. Lopez, Jonathan D. Blumenthal, Liv S. Clasen, and Jay N. Giedd. Dosage effects of X and Y chromosomes on language and social functioning in children with supernumerary sex chromosome aneuploidies: implications for idiopathic language impairment and

autism spectrum disorders. *Journal of Child Psychology and Psychiatry*, 53(10):1072–1081, October 2012.

[106] Jonathan D. Blumenthal, Eva H. Baker, Nancy Raitano Lee, Benjamin Wade, Liv S. Clasen, Rhoshel K. Lenroot, and Jay N. Giedd. Brain morphological abnormalities in 49,XXXXY syndrome: A pediatric magnetic resonance imaging study. *NeuroImage: Clinical*, 2:197–203, 2013.

[107] Ruben C Gur, J Daniel Ragland, Paul J Moberg, Travis H Turner, Warren B Bilker, Christian Kohler, Steven J Siegel, and Raquel E Gur. Computerized neurocognitive scanning:: I. methodology and validation in healthy people. *Neuropsychopharmacology*, 25(5):766–776, 2001.

[108] Ruben C Gur, Jan Richard, Paul Hughett, Monica E Calkins, Larry Macy, Warren B Bilker, Colleen Brensinger, and Raquel E Gur. A cognitive neuroscience-based computerized battery for efficient measurement of individual differences: standardization and initial construct validation. *Journal of neuroscience methods*, 187(2):254–262, 2010.

[109] Ruben C. Gur, Jan Richard, Monica E. Calkins, Rosetta Chiavacci, John A. Hansen, Warren B. Bilker, James Loughead, John J. Connolly, Haijun Qiu, Frank D. Mentch, Patrick M. Abou-Sleiman, Hakon Hakonarson, and Raquel E. Gur. Age group and sex differences in performance on a computerized neurocognitive battery in children age 8–21. *Neuropsychology*, 26(2):251–265, March 2012.

[110] Sarah P. Otto, John R. Pannell, Catherine L. Peichel, Tia-Lynn Ash-

man, Deborah Charlesworth, Adam K. Chippindale, Lynda F. Delph, Rafael F. Guerrero, Samuel V. Scarpino, and Bryant F. McAllister. About PAR: The distinct evolutionary dynamics of the pseudoautosomal region. *Trends in Genetics*, 27(9):358–367, September 2011.

[111] Daniel W. Bellott, Jennifer F. Hughes, Helen Skaletsky, Laura G. Brown, Tatyana Pyntikova, Ting-Jan Cho, Natalia Koutseva, Sara Zaghlul, Tina Graves, Susie Rock, Colin Kremitzki, Robert S. Fulton, Shannon Dugan, Yan Ding, Donna Morton, Ziad Khan, Lora Lewis, Christian Buhay, Qiaoyan Wang, Jennifer Watt, Michael Holder, Sandy Lee, Lynne Nazareth, Jessica Alföldi, Steve Rozen, Donna M. Muzny, Wesley C. Warren, Richard A. Gibbs, Richard K. Wilson, and David C. Page. Mammalian Y chromosomes retain widely expressed dosage-sensitive regulators. *Nature*, 508(7497):494–499, April 2014. Times cited: 1.

[112] Marcus A Tuke, Katherine S Ruth, Andrew R Wood, Robin N Beaumont, Jessica Tyrrell, Samuel E Jones, Hanieh Yaghootkar, Claire LS Turner, Mollie E Donohoe, Antonia M Brooke, et al. Mosaic turner syndrome shows reduced penetrance in an adult population study. 2018.

[113] R. Laila Ahsan, Richard Allom, Ioannis S. Gousias, Helai Habib, Federico E. Turkheimer, Samantha Free, Louis Lemieux, Ralph Myers, John S. Duncan, David J. Brooks, Matthias J. Koepp, and Alexander Hammers. Volumes, spatial extents and a probabilistic atlas of the human basal ganglia and thalamus. *NeuroImage*, 38(2):261–270, November 2007. Times cited: 1.

[114] Michael V. Johnston. Excitotoxicity in neonatal hypoxia. *Mental retardation and developmental disabilities research reviews*, 7(4):229–234, 2001.

[115] Jason M. Sheltzer, Eduardo M. Torres, Maitreya J. Dunham, and Angelika Amon. Transcriptional consequences of aneuploidy. *Proceedings of the National Academy of Sciences*, 109(31):12644–12649, July 2012.

[116] B. L. Finlay and R. B. Darlington. Linked regularities in the development and evolution of mammalian brains. *Science (New York, N.Y.)*, 268(5217):1578–1584, June 1995. Times cited: 2.

[117] H. M. Duvernoy. *The Human Brain*. Springer, Vienna, 1999. Times cited: 1.